# Design, Analysis, and Validation of a Custom Planetary Gearbox for a Formula SAE Hub Motor

A thesis
submitted in fulfilment
of the requirements for the degree
of

**Master of Engineering in Mechanical Engineering**

at

**The University of Waikato**

by

**Mark Hies**

THE UNIVERSITY OF
WAIKATO
*Te Whare Wānanga o Waikato*

2026

## Abstract

This thesis presents the analysis, design, manufacture, and validation of a custom in-hub planetary gearbox for use within a Formula Student electric vehicle powertrain. This work establishes a baseline for the transition from an inboard single power unit into a dual motor rear wheel drive architecture.

Existing commercial transmission solutions were unsuitable for direct integration into a Formula Student platform due to their packaging limitations, excessive mass, and lack of optimisation for the specific operating case. The limited availability of documented Formula SAE specific solutions justify the development and validation of a custom gearbox solution.

The gearbox was developed with consideration for manufacturability, packaging requirements, and future team integration. A stepped planetary configuration is used, achieving a gear ratio of 14:1. The design process focuses on the gear geometry selection, powertrain integration, as well as the stresses experienced through critical components under peak loading conditions.

Experimental testing demonstrated that the gearbox was capable of operating under the predicted torque input of 8 Nm. The custom planetary gearbox was able to complete a full endurance length of 22 km fatigue test without structural failure or significant wear. A post-test inspection of the gearbox identified minor surface wear present on the gear faces with no evidence of any other damage to supporting components throughout the system.

The developed prototype serves as an early stage foundation for future in-hub powertrain development within the Formula Student platform. With the gearbox validated, opportunities remain for improvement, particularly in the area of mass reduction, optimisation and long term durability validation.

## Acknowledgements

Thank you to the supervisors of the project Ben McGuinness and Mark Lay for their guidance and support throughout the project, which made the concept become a reality.

Thank you to the engineering technical team, with special thanks to Stephan Gwerder. Their assistance during manufacture to turn drawings into a completed work was essential to the success of the project.

Appreciation is given to the team at Waikato Bearings who were so gracious for their support and sponsorship of the bearings used.

Thank you to my friends and family for the encouragement throughout the year. Their ongoing support and patience are not unnoticed.

A final thank you to everyone else who contributed to the project either directly or simply by listening to me rant.

# Contents

## List of Figures

## List of Tables

# 1 Introduction

## 1.1 Background

Formula SAE (FSAE) is an international motorsport competition established in 1981 in which universities design, manufacture and compete with open-wheel race cars [1]. In recent years, a trend towards fully Electric Vehicles (EV) has emerged, with most cars now running fully electric powertrains. Waikato Engineering Student Motorsport Organisation (WESMO) is the University of Waikato's Formula SAE team. Until the 2024 vehicle, WESMO has run Internal Combustion Engines (ICE) making it part of the minority of teams still using this configuration. At the 2024 Australasian event, only four teams competed in the ICE class compared to the 22 in the EV class [2]. The transition to electric was a major decision for the team but a necessary one. Internationally, there is a clear trend towards phasing out ICE classes entirely, as demonstrated by Formula Student Germany in 2022, with the Australasian competition expected to follow a similar direction in the near future [3].

When switching from ICE to EV, many subsystems on the car remain vastly the same, such as the suspension, steering, and pedal box. However, major changes are required within the powertrain. The introduction of a large, heavy accumulator (battery pack) is required for energy storage, along with an electric motor that offers significantly higher power density compared to an ICE. The transmission of power from the motor to the wheels must meet the demands of the car like an ICE transmission but with differences due to the instant torque an electric motor can provide. During the competition there are four dynamic events, each of them having their own unique demands from the car. Acceleration, skidpad, auto cross and endurance requiring balance between torque, speed and efficiency. Each dynamic event is assigned a specific number of points, and in order to score, the vehicle must complete the event. The endurance event has the most points associated with it and has the most non finishers throughout all dynamic events. Finishing endurance is an important stage to an FSAE vehicle and a larger emphasis is placed on this.

Figure 1 and Figure 2 show the differences between the latest ICE-powered car (W-FS23) and the latest EV-powered car (W-FS24). While many subsystems change, the overall vehicle architecture remains similar, with a single motor driving a chain and differential setup much like the ICE configuration. This represents a natural transition from ICE to EV for first-year teams. However, the single-motor configuration caused significant packaging issues at the rear of the chassis. Integrating the accumulator, motor, inverter, cooling system, and other associated components led to considerable space constraints and layout challenges, therefore motivating the need to investigate other powertrain configurations.


Figure 1. W-FS23


Figure 2. W-FS24

There are multiple approaches to implementing the power unit, with each team adopting its own design philosophy. Due to the motorsport application, the transmission must be lightweight yet robust, while remaining compact to satisfy packaging constraints and comply with Formula SAE regulations. A common progression from single-motor systems is the adoption of hub motor configurations, where compact in-wheel motors are paired with a reduction gearbox to achieve the required gear ratio. More competitive teams typically favour this approach due to its advantages in packaging efficiency and overall system performance. Planetary gearboxes are commonly used in these systems due to their high torque density and coaxial input–output arrangement, making them well suited to the spatial constraints of wheel-mounted drivetrains.

## 1.2 Problem Statement

While planetary gearboxes are available for purchase off the shelf, those for the specific application of Formula Student (FS) racing are very niche. These commercially available gearboxes are typically very large and often oversized for the application required for a small EV vehicle such as a FS vehicle. Thus, FS teams will design and manufacture their own gearboxes, often with help or sponsorship from gear manufacturers or larger race teams. When these teams develop their own gearboxes detailed design, design iterations, design validation and data are rarely published.

While there are a few kits available for purchase such as the Humbel they are expensive upwards of €2,000 (~4,000 NZD) per set for each wheel, as well as having a set ratio which cannot be ideal for every situation and vehicle setup.

As WESMO operates through fourth-year engineering final year project often the team has little to no prior knowledge coming into the year. Additionally, previous team members have graduated and no longer present as full time students. This causes significant amounts of knowledge transfer issues, combined with the workload of designing and manufacturing a car from scratch there is often not enough time in the year to validate, and incorporate any necessary changes. Having a major component such as the transmission already designed and validated ready for integration streamlines the development process of the new vehicle.

These reinforce the clear gap requirements for a FS electric powertrain solution by addressing this gap and creating a documented and validated formula student specific resource for others to use and develop further rather than requiring redevelopment each year.

## 1.3 Aim

The aim of this project is to design, manufacture, and validate a planetary gearbox for use in a Formula SAE vehicle, ensuring it meets performance, packaging, reliability, and manufacturability requirements, while also delivering a physical prototype that can be validated and supporting documentation to enable reproducibility and future team development.

## 1.4 Thesis Structure

This thesis is structured as follows. Chapter 2 presents a literature review covering Formula SAE, planetary gearboxes, and relevant background theory. Chapter 3 defines the system requirements, including transmission selection, tyre data and capacity, and the implications of motor selection on the gearbox design. Chapter 4 details the gearbox design process. Chapter 5 outlines the manufacturing methods and associated constraints. Chapter 6 describes the design and development of the test rig and the validation testing procedure. It presents the results and analysis, including gearbox performance evaluation and post-testing inspection of the system. Finally, Chapter 7 presents the conclusions and recommendations for future work.

# 2 Literature Review

The performance of modern EVs and motorsport applications is effectively governed by how each subcomponent is designed and integrated with respect to each other. The powertrain system is no different. Within the system the powertrain plays a critical role in delivering power to the road and allowing for the vehicle to perform in all situations. Small efficiency losses and design hindsight can reduce the effectiveness of performance. These factors remain critical in a race car.

This literature review consolidates existing research, industry practices and relevant concepts to the design and development of the FSAE powertrain. Focus on identifying established principles and design methodologies that can be used to inform the development. This review covers areas including FSAE powertrain architectures, planetary gearbox system designs and performance characteristics. Fundamental concepts such as gear design theory, manufacturing methods and constraints are also considered.

Attention is given to the efficiency, packaging, mass and manufacturing of each stage of the development as these factors are critical within the student motorsport application. By reviewing existing work this section lays a foundation to support the subsequent design, manufacture and validation of the design.

## 2.1 Configurations/Packaging

Compared to an FSAE utilising an ICE powertrain, the use of an electric motor enables for significantly more flexibility in powertrain configurations and overall vehicle packaging. An electric motor is much more power dense and compact compared to an ICE. For example an Emrax 228, a common electric motor used within FSAE weighs 13.5 kg and a 228 mm diameter and can output over 120 kW [4]. Although electric powertrains require an energy storage system, an accumulator, the compactness of the motors give powertrain design engineers to explore and create flexible solutions. While important in any complex engineering problem it is especially beneficial in FSAE where, packaging, weight distribution, integration, manufacturability and more play important roles to extract every tenth of a second from the car available.

Several common packaging solutions can be seen in Figure 3 highlighting the power source(s) with red blocks and transmission in blue blocks. While these configurations are not an exhaustive list, they are representative of most vehicles seen today.

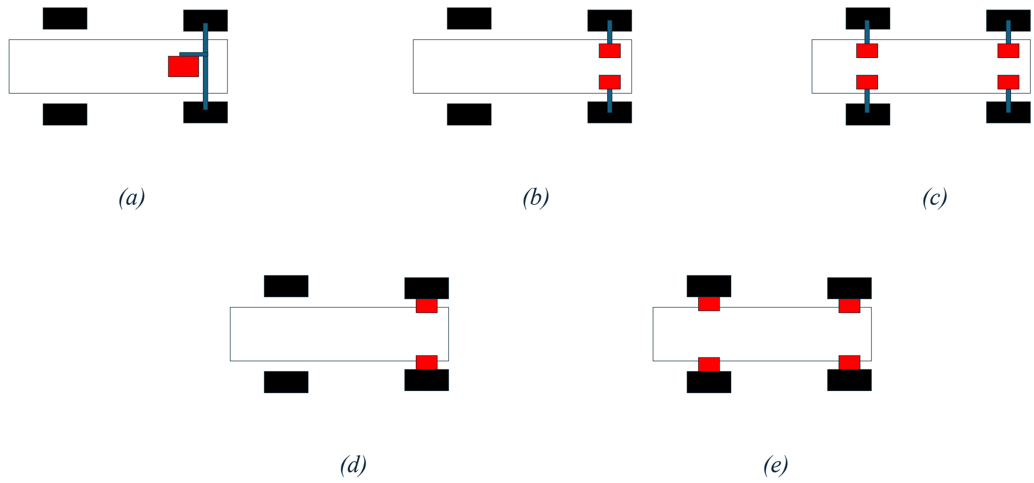


*Figure 3. (a) Single Motor Inboard RWD Configuration, (b) Dual Motor Inboard RWD Configuration, (c) Quad Motor Inboard AWD Configuration, (d) Dual Motor Outboard/In-hub RWD Configuration, (e) Quad Motor Outboard/In-hub AWD Configuration*

### 2.1.1 Single Inboard

The single inboard motor with rear driven wheels illustrated in Figure 3a closely resembles a typical ICE setup, making it an appealing choice for teams transitioning to EV. This layout will often use a chain drive powering a differential which is able to distribute power to the wheels through half shafts. This is why it remains a popular choice for beginning EV teams. Competitive teams such as Monash Motor Sport have used the single inboard motor such as their first EV cars, their M17-E and M18-E [5]. With majority of the components remaining the same and allowing the team to build off known concepts. Utilising only a single power unit allows for simpler integration mechanically and electrically compared to other alternatives. Only a single inverter to pair the motor is needed and thus a single set of high voltage cabling. Similarly cooling only has two components, the motor and inverter to thermally manage.

While mechanically simple, this configuration requires the full system power through a single path. For a given total power output requirement, which is assumed equal among all configurations analysed. The single motor and inverter must handle all electrical demand resulting in high current throughputs. This constraint applies the same for the cooling system, requiring large diameter tubes to increase the throughput to ensure sufficient heat exchange. As observed in the W-FS24 the use of large diameter high voltage cables makes routing difficult due to the large bend radii needed. These factors significantly reduce the configurations ability to create tight and space efficient packaging. An inefficient layout will either require a larger chassis volume and thus chassis, increasing weight of the car or suboptimal weight distribution requiring components to be placed based on the available volume instead of an optimised position. Both of these factors are key for vehicle performance. This was a key design challenge that was experienced on the W-FS24.

Additionally, these packaging constraints have direct effect on the serviceability of the car. A powertrain with a differential and half shafts makes accumulator removal through the rear unobtainable. Rear accumulator removal is a common solution, allowing for the accumulator to slide directly onto a trolley while the vehicle remains on the ground. The alternatives are commonly through the cockpit or through the bottom of the chassis, which was adopted by the W-FS24. Loading through the cockpit requires little modification to the primary structure but introduces difficulty as the heavy accumulator must be removed through a small gap, and it requires removal of the firewall and associated components. Loading through the bottom of the primary structure introduces structural changes requiring a gap in the bottom and requiring the car to be lifted off the ground. These gaps in the primary structure will have sufficient rigidity decreases and affect the performance. While loading an accumulator from the side is an option it remains as an impractical option as the main role hoop must remain a continuous member and removal of an entire corner every time is impractical, as the accumulator is likely to space this length.

*Figure 4. KaRacing Rear Accumulator Loading [6]*

One factor which is important to all configurations is the effect of sprung and unsprung mass. Sprung mass is defined by the mass supported by the suspension, such as the primary structure and any components attached to it. The unsprung mass is naturally any mass not supported by the suspension, typically the wheel assemblies, tyres and includes the suspension itself [7].

An inboard motor and transmission are connected to the primary structure and will contribute to the sprung mass. To achieve the best performance a cars tyre should remain in contact with the road as much as possible, A high unsprung mass increases the inertia causing the unsprung mass to respond slower due to newtons second law of motion [8]. Therefore, having a lower unsprung mass allows for the tyre to follow the road closer and maintain a consistent contact patch. Suspension design criteria are heavily influenced by the ratio of unsprung mass to sprung mass but can be designed to accommodate the ratio [9]. Choosing the optimal unsprung to sprung mass ratio cannot be considered in isolation, depending greatly on different suspension parameters like stiffness. By using the single inboard the unsprung mass can remain low and allows for the best performance abilities.

Vehicle dynamics is an extensive topic and can be studied to great ends. The key conclusion involves making the unsprung mass as light as possible for optimal performance. The single inboard motor configuration is shown to be a simple yet effective solution. Suited greatly for teams in their early years of EV development. It is limited in design freedom but with proper foresight can be optimised and allow for development of a competitive car.

### 2.1.2 RWD Inboard

Figure 3b shows a dual inboard setup, bridging the gap between a single inboard and in-hub motors like that in Figure 3c. Specifics on power transmission are given greater flexibility when using two motors. MUR Motorsport and University of Washington Formula Motorsport show different ways to accomplish the same goal using Emrax 208 and Emrax 188 Motors respectively [10], [11]. While each have their own benefits and drawbacks for packaging, complexity and reliability. Figure 5 shows a planetary gearbox increasing the torque before being coupled with a constant velocity joint and transmitted through the half shaft. It is worth noting that the figure shows only one side of the powertrain, an equal system would be mirrored for the opposite wheel. Figure 6 displays a similar setup, using a chain drive instead of a planetary gearbox.

*Figure 5. Dual Inboard Planetary Drive Setup [11]*

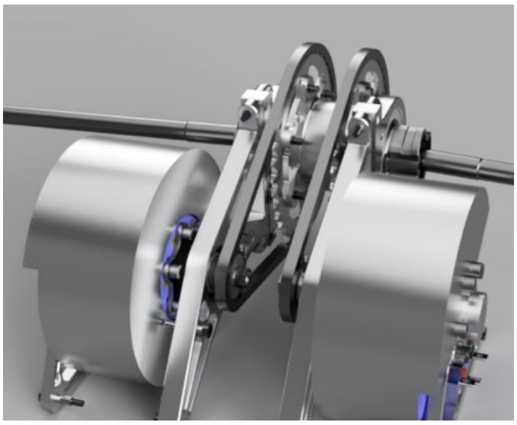

*Figure 6. Dual Inboard Chain Drive Setup [10]*

In each configuration each motor can independently drive each wheel, therefore instead of power being split between the wheels with a mechanical method such as a differential like the previous configuration, the power must now be split electronically. This process is known as torque vectoring, powering each wheel independently while still maximising the power through the wheels to the ground. Torque vectoring is not a required additional but greater increases the performance capabilities of the vehicle. The torque vectoring process includes a base torque dependent on the throttle input and each motor can be adjusted via the torque vectoring control. A torque vectoring algorithm is likely to use sensors that show yaw rate, steering angle, longitudinal speed and acceleration and wheel speeds [12]. Torque vectoring can be simply described as determining the required torque distribution between driven wheels to achieve a desired vehicle yaw response for a given steering input and providing a greater steering response [13]. A vehicle that uses a torque vectoring control has the ability to attain better control by a specific yaw rate compared actively being able to target to a passive solution like that of the mechanical differential.

As the maximum power is determined as 80 kW per the rules using two motors will reduce the power output required of each motor and thus the physical size [14]. By splitting the power between two motors the thermal and electrical demand on each is decreased on each system. Enabling lower current and power requirements, leading to use of smaller inverters. Reducing the diameter of high voltage cabling required compared to the single power unit. By using smaller components packaging options provide flexibility for more optimised distribution, as mentioned in the single inboard motor section.

However, the introduction of a second power unit and transmission increase overall system complexity. By doubling the required components inherently increases the points of potential failure. Additionally, torque vectoring requires feedback from sensors which may have previously been considered non-essential, such as yaw rate sensor. Becoming critical to the vehicle performance now.

As both motors remain inboard parallels lie with the single inboard motor, particularly around the serviceability. The accumulator loading and unloading method remains constrained by the powertrain. Limiting the accumulator to be removed through non optimal bottom or cockpit methods. With each motor remaining inboard the unsprung mass is minimised giving greater vehicle dynamic performance.

### 2.1.3 AWD Inboard

Figure 3c dictates a system architecture with four motors, each powering their own wheel. Expanding on the performance capabilities of the dual inboard setup. Just as with dual motors the torque is distributed among each motor via torque vectoring, with the addition of the front axle. By being able to control the front axle increases the control ability significantly [15].

Distributing the load among four motors further reduces the electrical load on each motor. Enabling even smaller motors, inverters and high voltage wiring. Allowing for more packaging freedom.

While having each wheel powered and minimising the unsprung mass can provide the best performance in theory the practicality of packaging a pair of motors within the primary structure, specifically at the front and adhering to rules such as 100 mm gap between high voltage components and anything conductive is a difficult task [14]. The unsprung mass of the rear corner assemblies is unlikely to change compared to previous configurations. The front unsprung will be likely to increase, requiring tripod housings, bigger bearings to handle dynamic loads and a bigger housing to accommodate. Having a small but noticeable effect on the unsprung mass

However, these benefits come at the cost of significantly increased system complexity. The requirement for four motors, inverters, and associated control systems introduces many components, increasing both design complexity and potential failure points. The control strategy for full torque vectoring is also considerably more complex, requiring accurate modelling of vehicle dynamics and robust sensor integration to ensure stable and predictable behaviour.

Packaging within the front of the vehicle presents a particular challenge. The presence of steering and suspension components limits available space, making integration of front-mounted motors and transmissions difficult. This often results in highly compact and complex packaging solutions, which may impact serviceability and reliability. For these reasons this configuration is impractical and not used by any teams.

### 2.1.4 RWD In-hub

The rear wheel drive in-hub configuration represented in Figure 3d transitions the motors from being a part of the primary structure to integrated directly into the wheel assembly.

The immediate effect of this configuration is removal of the powertrain system from within the primary structure. Components such as differentials, half shafts and transmission are shifted outside of the primary structure, in addition to moving the motors themselves. Removing congestion from the primary structure alleviates the limitations mentioned in previous configurations, specifically those with accumulator placement and loading, inverter integration and cable routing. As a result, greater design freedom can be achieved allowing for optimal component placement and improved serviceability due to the decrease of components. This configuration is the first that allows for the rear removal of an accumulator established to be the most common and effective.

These packaging advantages come by removing the mass from the primary structure and shifting it into the unsprung mass. As discussed above this minimising the unsprung mass has been identified as important. A trade-off between the two must be analysed to assess the importance of each criterion.

Typically, teams would approach an in-hub system with use of a planetary gearbox. This is an ideal solution as planetary gearboxes have their input and output sharing the same axis of rotation. Allowing the motor to be placed within the centre of the wheel. Other approaches include putting the motor off wheel axis and using a simpler configuration of gears, it may introduce an imbalance due to the rotation of the motor rotor off axis creating suspension issues. Although this will be dependent on the mass of the motor rotor and the effect is likely to be minor.

Both these configurations are shown in Figure 7 and Figure 8 below and detail how the motor sits within the wheel hub, showing the required transmission required to achieve power to the wheel. The gear ratio achievable in each of these situations are varied can be altered depending on the gear ratio required.

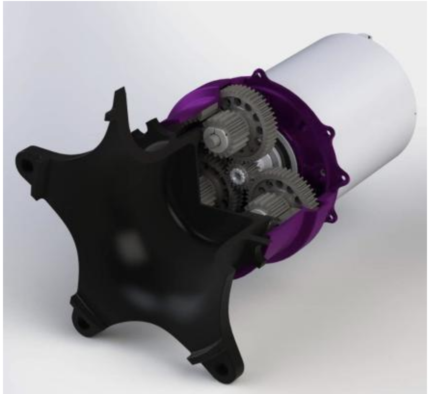

*Figure 7. Stepped Planetary Gearbox [16]*

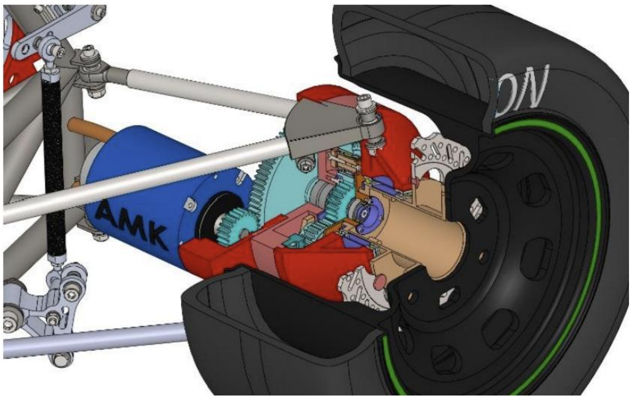

*Figure 8. Off Axis Motor Combined with a Planetary [17]*

By placing the motor off axis, it allows for the introduction of a simple gear pair, reducing the ratio required by the planetary and the planetary gearbox can become more compact. Each solution is feasible to achieve with differing trade-offs, such as the complete planetary remains much more compact into the wheel assembly.

With the inclusion of mounting the motor onto the upright assembly additional rules must be considered, while these are primarily around the high voltage wiring, they are still required to be considered. The rules detailed in EV.4.1.3 are including an interlock which is capable of opening the shutdown circuit, effectively turning the car off [14]. Also included is an arbitrary measurement of reducing the length of any high voltage wiring outside of the primary structure [14].

### 2.1.5 AWD In-hub

The all-wheel drive system represents a further step compared to the rear wheel drive, distributing the power over the front and rear axle. Achieved through integrating a planetary gearbox or similar into the front wheel hub.

Including motors within wheel assemblies which can steer increases complexity, as components become constrains due to the dynamic environment of the rotating wheel assembly. While like the quad inboard the traction potential is much higher due to the increase in motors and complexity to torque vectoring.

While at an advantage it also comes at a disadvantage, increasing the unsprung mass on the front axle as well as the rear. The heavier front axle also increases the steering effort required. As well as the components required as potential failure points.

### 2.1.6 Summary

While there may be other packaging options left unexplored, such as combining inboard and in-hub systems they are not commonly adopted within FS vehicles. This is likely due to the complexity, and component variation requiring separate systems. Teams favour a single consistent architecture to allow for efficient design, validation and testing.

Table 1 summarises the key points discussed within each configuration and assigns a ranking, each ranking is not a final as some parameters may be designed around, such as unsprung mass and suspension design. This assumes the same total power for each configuration.

*Table 1. Summary of Drive Configuration Trade offs*

| Configurations | Acceleration potential | Vehicle Control | Unsprung mass impact | Mechanical Complexity | Packaging Freedom |
|---|---|---|---|---|---|
| Single Inboard (a) | Moderate | Low | Low | Low | Low |
| Dual Inboard (b) | Moderate | Moderate | Low | Moderate | Moderate |
| Quad Inboard (c) | High | High | Moderate | Very High | Low |
| RWD In-Hub (d) | Moderate | Moderate | High | High | Very High |
| AWD In-Hub (e) | High | High | Very High | Very High | High |

Based on the configurations assessed and analysis of existing FS teams implementation of a rear wheel in-hub configuration is to be developed further. In-hub configuration is the most commonly seen throughout the higher-level teams, especially within the Australian competition based on first hand at the 2024 competition.

Initial development focuses on the rear in-hub configuration to establish a validated baseline system while reducing the overall complexity, component count, and cost compared to the all-wheel drive in-hub. The rear wheel configuration provides a platform to begin development of in-hub technology and allows for expansion to an all-wheel drive system in future years if assessed as worthy investment. Restricting power output to two wheels simplifies the integration of a torque vectoring algorithm and ensure complete control before the more complex all-wheel drive system

The choice to implement a planetary gearbox is decided to allow for coaxial power transmission. Due to their high torque capacity and other teams implementing similar solutions, as well as being fit for purpose due to the compact nature of a planetary.

While the unsprung mass of the rear wheels is increased due to the motor, gears and larger wheel assembly. As mentioned, the increase to unsprung mass will reduce the response of the tyre. However, this is something that can be tuned for during suspension design. The advantage of increasing the packaging freedom allows for more optimal component placement and simplifies the integration, allowing more time for the design engineers to optimise each system.

To support the integration and development of the proposed planetary gearbox further literature relating to planetary design and theory is included in the following section.

## 2.2 Planetary Gearboxes

Planetary gearboxes are used for altering the speed of the motor or input and allowing the output to have the same axis of rotation. Known for having high torque transmission ability while remaining compact [18]. Planetary systems can be arranged in multiple ways to achieve the same outcome with different packaging, strength and mass.

The simplest construction is that of the simple planetary gearbox. Consisting of three unique types of gears. The sun gear which is centred, meshing with planet gears held together by a carrier and finally a ring gear surrounding the planets [18]. Figure 9 shows an arrangement of a single stage planetary gear box, where the sun meshes with the planet gear which also mesh with the ring gear. In this depiction the planetary set shows four planets, this can be altered and is not a fixed number. In this situation knowing two of the three gear teeth count fully defines the entire system [19].

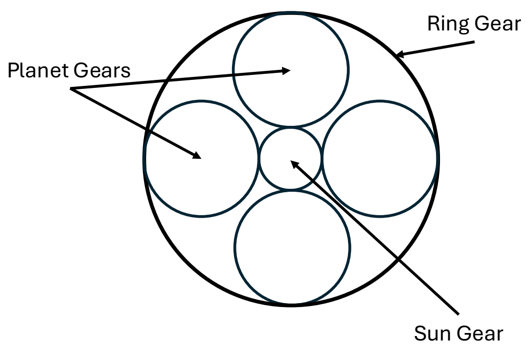


*Figure 9. Simple Planetary Gearbox Layout*

By using a single stage ratios can typically range from 3:1 up to 10:1, due to the geometric constraints about having the sun gear size ratio against the planets [20]. These can be compounded together in multiple stages just like regular parallel shaft gears to increase their ratios.

The simplest multistage planetary gearbox will combine two simple stages end to end, using the output of the first stage as the input to the second. While this approach is effective for compounding the ratio it results in an increase in system length, and the amount of gears required and therefore mass.

An alternative solution is the compound planetary or stepped planetary, acting a hybrid between the two previous. The compound planetary is able to reach the same reductions of a multi stage configuration [19]. While the length of a stepped and multistage will remain similar, the reduced components will decrease the mass comparatively. An example of the architecture can be found in Figure 10, showing the interaction between gears and the ability to remove one stages ring gear and the others sun gear. The planets in each stage are coupled together and rotate as a complete system. Stepped planetary gearboxes are ideal for compact situations which require the possibility of a high speed ratio such as an FS vehicle [21].

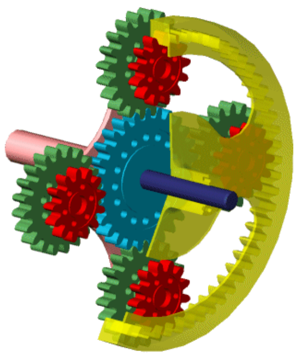

*Figure 10. Stepped Planetary Gear Example [22]*

Due to the common shaft, which supports both planets which will have different forces bending moment within the shaft will be present and must be checked for failure modes [19].

### 2.2.1 Applications

Understanding their alternative applications outside of an FSAE vehicle shows their functional operating conditions. Due to the high torque capacity and compact size planetary gearboxes are used widely throughout industry in varying capacities.

One application is the use within a helicopter. A planetary gearbox is used to transmit the power from the power unit up to the main rotor. A planetary gearbox is used due to the ability to transmit the major loads from a helicopter rotor. A helicopter such as the Bell UH-1 Iroquois includes two stages of a 3.087:1 gearbox for a final ratio of 9.53:1 transmitting up to 1,000 kw at 324 RPM or a torque of ~30 kNm [23]. A typical gearbox will use two to three planets but by using more than this it allows for greater distribution throughout the system by increasing the contact surface area [24], [25]. The helicopter in this example can achieve such high loads by increasing the amount up to six planets for each stage. A helicopter is sensitive to weight and packaging ability, if a compound gear box with parallel shafts were to be included the weight and size would increase significantly becoming difficult or near impossible to achieve the required design.

Another application is a tunnel boring machine these instances include even more torque at 3 MNm. They are also subjected to other loads like strong vibrations, impacts, high temperatures and pronounced external pressure lending the application to these conditions [26].

These applications show the idea that planetary gearboxes can be used in high load, high reliability, compact applications such as an FSAE car. The wheels on a race car are also subject to many external forces like those experiences by the heavy machine just at a much different scale. While each design with be specifically engineered to handle the forces present the ability to be able to achieve the performance is recognised.

### 2.2.2 SAE Specific

The use of planetary gearboxes throughout FSAE is well established with significant literature, featuring a range of designs and design methods reported within literature. Each design includes a trade-off between depth, iteration and optimisation.

Maruoka et al. developed a planetary drive system [27]. Utilising AGMA gear stress equations as well as a developed script tool used to select an appropriate number of teeth for each gear to design a compound planetary gearbox. Gear teeth were chosen on a geometrically fitting requirement and then check to meet stress requirements. Gear tooth selection was constrained to off the shelf componentry, with limited exploration of optimisation of teeth count with exception of the ring gear, manufactured to mesh correctly with the purchased gears. While purchasing gears enables quicker development and procurement it restricts the extent of which optimisation of the gear geometry can occur.

The use of 5 axis CNC machining allows for increased complexity for design to increase packaging and mass potential. Gears were mounted using press fit interference on shafts, requiring careful alignment during assembly, which may complicate and compromise the assembly and disassembly if required.

No sealing solution was implemented to retain lubricant within the gearbox. While designed and manufactured the prototype was untested and is based on the theoretical calculations, indicating factor of safeties below one, showing a potential limitation. The conclusions are limited to theoretical analysis only, with no validation of the performance.

Similarly, Patel et al. details the process of a single stage planetary to use an Emrax 208 motor [28]. Decision of the gear ratio is limited to achieving a target acceleration time and maximum vehicle speed. The gear ratio is not fully optimised for all track conditions and only is representative of a single event.

The design process is independent of an FSAE vehicle including no specific mounting or integration. In addition, primary focus on bending stress is considered with the use of the Lewis bending stress equation. While the contact stresses are not explicitly addressed.

Validation of the design was limited to simulation-based analysis, with no experimental testing or physical prototype. As a result, the predicted performance remains uncertain.

A planetary gearbox designed and manufactured within the School of Engineering at the University of Warwick iterates through the entire process from conceptualisation through development and design [29]. The use of a Nova 15 motor and a single stage planetary. Gear ratio is determined purely by a target top speed resulting in suboptimal torques delivery throughout a lap. The use of a MATLAB script generates suitable gear teeth to be checked for strength, creating an iterative process to find the optimal candidate.

The process utilises greater force analysis using conditions such as cornering, braking, accelerating and sudden bumps. Representing a more realistic operating envelope and improves the relevance of evaluation compared to a purely acceleration.

Strength verification was completed using analytical methods in addition to MASTA, a transmission analytical software. While the manufacture and assembly process is detailed the prototype is not manufactured and hence no testing applicable.

Makkonen shows the design of a planetary gearbox for the Tampere Formula Student team for a hybrid version of an FSAE vehicle [30]. A gear ratio is chosen with a combination of lap time simulations and excel spread calculations but lacks specific details, as well as considering the accumulator and the capability of the electrical integration. Due to a high ratio required, 23.3:1 a two-stage planetary is used.

The loading scenarios are broken down into braking, accelerating and cornering to give a better understanding of the forces subjected to the gearbox.

The use of KissSoft, another transmission modelling software is covered, driving the selection process for each tooth count in each stage but lacks depth and simply presents the final solutions without proper depth to boundary conditions.

Finite element analysis was performed on components validating the stresses within each component but lacks the detail of manufacturability. Despite the in-depth analysis manufacture was not completed resulting in a theoretical design lacking experimental data, assembly or durability data.

Another planetary gearbox design is presented by Beernaert [31]. Targeting a set ratio of 12 through a stepped planetary configuration. Multiple gear topology is considered and is selected with respect to the cost, performance and maintainability. Gear dimensions are assessed using a MATLAB script which includes both the bending and contact stresses, with results being verified within KissSoft.

The design process includes all aspects of the design, such as the lubrication methods, bearing selection and overall packaging. Manufacturability, final mass and assembly considerations are considered throughout the design process and create a comprehensive design. However, validation of the system remains as an unexplored and limits the paper to analytical methods.

Alexsson et al. develops a planetary gearbox with particular focus on the mass optimisation [32]. With the use of previous electric vehicle planetary gearbox a more guided representation of the gear ratio is used. Achieving a ratio of 11.5:1 in a single planetary stage. Loading of the system is considered for the gears and FEA is performed on the structural components and allow for optimisation of material and mass. The resulting design achieves a mass reduction to their previous planetary gearbox but is limited using a single stage. The mass optimised newer design achieved a mass of 3400 g at a 2.4% reduction compared to the original. The study presents the design, analysis, and comparison of the gearbox, but no validation through manufacture or beyond is reported.

White et al. presents a methodology for configuring a transmission system [17]. The use of two transmission stages is implemented. With the first stage being an offset spur gear followed by a planetary gearbox. This required the motor to be placed off axis with respect to the wheel.

The transmission was designed using Lewis bending equation to achieve an estimate for certain gear configurations to then transition to software for finer sizing. Bearings and gear life is estimated and a full-scale prototype is manufactured from nylon to verify assembly and clearances, this was only shown for the gear system, and any housing or casing system is not fully implemented.

Within the literature reviewed multiple limitations present themselves. Transparency of gear selection within a planetary gearbox design. In particular the iterative selection of parameters such as module, pressure angle, profile shift, and teeth numbers. Often not fully documented, with limited discussion on the final configuration.

In addition, gear ratio selection is often treated as a simple design choice, relying on a target acceleration or similar. With an EV a single fixed ratio is used and critical for optimal torque delivery across a lap. While some literature show a deeper analysis they are gated behind lap time simulators developed internally.

A gap is also present in the physical testing, while some of the designed gearboxes make it through the stage of manufacturing, they are not validated. This project aims to fill in these knowledge gaps to create a cohesive conceptual to complete design, through to manufacture and a bench top testing model. Building upon existing planetary gearbox design approaches to extend the current methodology.

By designing and manufacturing a single prototype planetary gearbox capable of the loading conditions expected within the WESMO vehicles, and testing under representative conditions to validate the calculations and estimates made throughout the process.

## 2.3 Gear Theory

Gear theory is a fundamental aspect of gearbox design and understanding, standing as a focus of this thesis. To optimise the gear geometry, teeth, module and other parameters understanding the influence of each parameter is critical. Understanding the limitations of how a gear is defined, manufactured and predicted to operate under different loading conditions lays a foundation to build upon.

Gear theory is an important characteristic of a gearbox design. It is important to understand how gears will respond to forces applied and how altering parameters affect the performance. A literature and technology review are performed in the following section to understand the concepts.

### 2.3.1 Gear Geometry

A transmission gear utilises an involute tooth profile, allowing for many different parameters to be changed to provide the mechanical properties desired. The selection of geometric parameters such as the pressure angle, helix angle and undercut has a significant effect on the load distribution and therefore stresses developed within the gear tooth. Understanding the effect each parameter has on these properties allow for careful selection to ensure a balance between strength, manufacturability and efficiency.

#### 2.3.1.1 Pressure angle

Pressure angle is a fundamental geometric parameter of a gear, that is linked to how the teeth transmit load. The pitch point is the point on the gear teeth where contact occurs and therefore the transmission of the load. As the gear rotates the pitch point moves from the base of the driving gear to the tip. Connecting these points form the line of action and can be used to measure the pressure angle between the pitch circle as shown in Figure 11 and Figure 12. For two gears to mesh correctly they must both have the same pressure angle

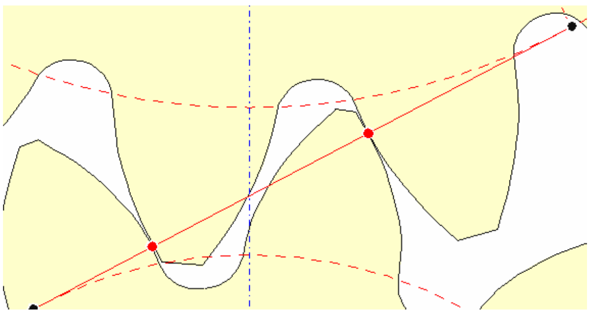

*Figure 11. Gear Line of Action [33]*

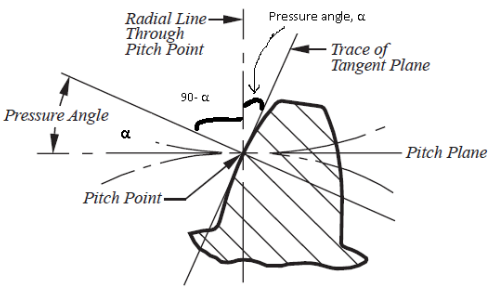


*Figure 12. Gear Pressure Angle [34]*

The pressure angle controls how the load is resolved into its radial and tangential component forces. The tangential force is the component transmitting torque while the radial acts perpendicular and acts to separate the gears. Therefore, pressure angle must be chosen to optimise both conditions.

A pressure angle of 20° is most commonly adopted within industrial gears, presenting an optimal balance between the two forces [35], [36]. A higher pressure angle allows for higher tooth strength while also increasing the friction and noise compared to a lower pressure angle [34]. The increases strength is due to the thicker tooth root providing resistance to bending. With a higher pressure angle the radial load will also increase. Optimising the pressure angle to be as low as possible to promote efficiency, reduced noise and smooth running is an important ideology while ensuring bearings and shafts can still hand the radial loads present.

Pressure angle also influences the contact ratio. The length of the line of action or known as the length of the path of contact, the lower the value of the contact ratio means greater load on one tooth creating a concentration of the load on one tooth subjecting to greater deflection and noise [37]. Increasing the pressure angle will decrease the contact ratio and must also be considered when selecting the pressure angle. This is opposite to the previous effect of pressure angle and therefore must be critically analysed and optimised for both conditions.

### 2.3.1.2 Helix angle

The helix angle is the inclination of the tooth along the length of the gear face, as shown in Figure 13 below. A gear with no helix angle will have teeth run parallel to the shaft and are known as straight cut gears.

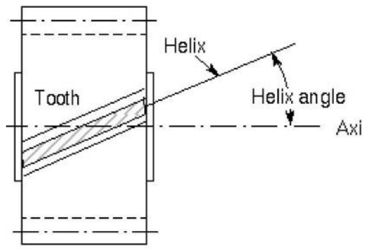


*Figure 13. Gear Helix Angle [38]*

A gear which includes a helix angle will allow the tooth to engage gradually along the face width of the gear compared to the sudden engagement a straight cut gear, the gradual engagement allows helical gears to run at lower noise and vibration levels [38]. The inclination of the tooth geometry introduces an axial force component in addition to the radial and tangential as mentioned previously. The axial load increases with the helix angle naturally due to its geometry. The introduction of the helix reduces the efficiency of the gear compared to the straight cut by converting a portion of the load into axial force, attempting to move the gear along the length of the shaft [39]. This requires additional support to resist these forces depending on the helix angle and load transmitted. A well-designed gearbox will likely have two opposite helix gears or a Herringbone gear to create equal and opposite axial load to cancel each out.

The helix of a gear must be selected when required and is a compromise between noise reduction and gradual engagement of the teeth improving load transmission capacity. The requirement for helix angle must be considered when selecting the final design of the gear system.

#### 2.3.1.3 Undercut and Profile Shift

When introducing a gear with smaller number of teeth for specific pressure angles undercut can be an artifact presented within gears. Undercut occurs due to the position of the cutter during manufacture and can remove a significant amount of material away from the root of the tooth.

To prevent undercut a terminology called profile shifting is added [40]. By changing the position of the cutter prevents the root of the tooth from being cut away, profile shift can be applied either positive or negative. A positive shift creates a thicker tooth root and hence a greater resistance to bending stresses.

By changing the profile the working pressure angle has a small shift due to the change of the pitch planes, profile shifting can also influence the centre distance by a small amount [41]. The effect of a profile shift on the tooth geometry can be seen in Figure 14. The effect of profile shifting is greater than just geometry, bearing life can be affected either positively or negatively based on the selection of the profile shift amount [42].

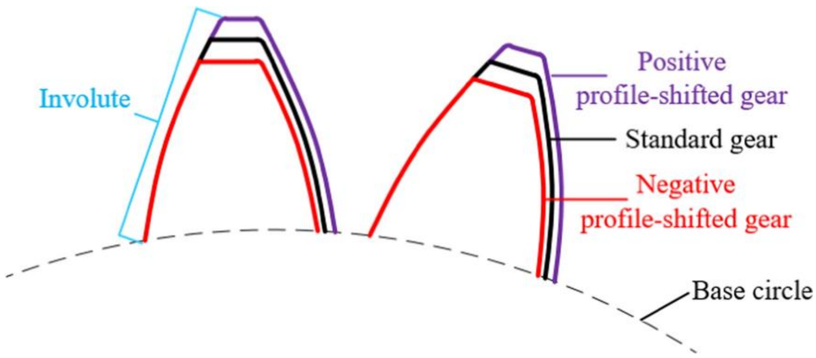


*Figure 14. Profile Shifted Gears [42]*

### 2.3.2 Gear Manufacture

Manufacturability is a critical design consideration to allow for efficient and cost-effective manufacture, while still being able to provide the required accurate geometry. Both internal and external gears are to be manufactured.

Manufacturing methods can broadly be categorised as subtractive methods and additive methods. Subtractive methods are the industry normal and have significant background while additive methods are new and emerging. Therefore, subtractive methods are more attractive for the given application and are to be considered. Each method is a combination of the production volume, materials available and achievable tolerances.

#### 2.3.2.1 Methods

##### 2.3.2.1.1 Hobbing

Gear hobbing is the most common method used to create an involute profile for an external gear, widely used in many industries due to the high repeatability and efficiency. The hobbing process utilises a rotating cutter against a gear blank to create the required profile.

In order to hob a gear there must be sufficient runout for the cutter, as the cutter rotates and is feed into the blank material it must be feed in enough to allow for the full depth of cut to form the full tooth [35].

Hobbing restricts the gear geometry due to the cutter, the gear must have the same geometry as the cutter. Each cutting tool will be designed to cut gears of specific teeth ranges, pressure angles and module. While majority of the time this is acceptable for highly specific applications, such as nonstandard modules custom tooling may be required to achieve the geometry required. The cost of nonstandard modules raises

##### 2.3.2.1.2 Shaping

Gear shaping has a similar process to hobbing, however instead of using a spinning cutter a reciprocating movement is used to create the profile, this allows for the runout to be much smaller and can form full teeth near to a shoulder [35]. Shaping can also be used to create internal gears, shaping a gear has an increased cycle time and cost due to half the time the cutter not removing any material.

Like the hobbing process the cutter must meet the final geometry expected for the teeth and therefore limits the ability to create nonstandard profiles.

##### 2.3.2.1.3 Broaching

Broaching is a common solution for creating parts with internal features, such as splines or teeth. By pulling a tool with the same geometry as the feature the tooling can progressively remove material. Broaching is limited by required a blind hole. Broaches of large diameters become costly and uncommon [35].

##### EDM

Wire Electrical Discharge Machining or wire EDM is a process that can recreate complex and high precision profiles in any conductive material. Material is removed using an electrical discharge between the work piece and the wire, removing the cutting forces and any induced stresses due to these. Cycle times for EDM cutters can be upwards of hours and therefore are not widely used as a standard manufacturing method. EDM is a common solution for teams utilising non-ISO standard gears with specific profile shifts or nonstandard modules

All hobbing, shaping and broaching tooling is specifically designed for the gear which is to be cut, making unique gears with specific profile shift, pressure angles, and modules become difficult or costly to obtain. EDM wire cutting however can create unique gears at the same rate as a standard gear on the same machine. With the prototype design likely to have specific bespoke gears wire EDM is a target manufacturing method.

#### 2.3.2.2 Material and Heat Treatment

Both the material selection and heat treatment are critical for resisting both the contact stresses and the bending stress within a gear. A ductile material is able to absorb the impact forces of each tooth during use. However, a ductile material has a small wear resistance [43]. Hardening the outer surface provides the wear resistance for each tooth while still allowing for a high toughness core to absorb any impact loads generated during operation.

Case hardening process are therefore widely used to obtain the strong, hard teeth while allowing for a tough core for a gear. carburizing, gas carburizing, nitriding, cyaniding, induction hardening, and flame hardening are available case hardening processes [36]. Each method provides different results and requires a different process. Selection of the right method is dependent on the requirement of the system, the environmental conditions, the allowable distortion, required case depth and the material.

The choice of material must be suited to each process or vice versa, therefore the heat treatment method and material choice and directly linked.

### 2.3.3 Stresses

The operation of gears is a complex study, undergoing cyclic loading conditions through which torque is transmitted. The use of transmissions is to transfer torques and some applications can result in high torques and therefore loads. Two major portions of the stresses acting on gears due to power transmission are the bending stress developed at the root of the tooth, for the thesis this is used interchangeably with root stress. The other form of stress is the contact pressure stress from the two interfacing teeth contacting, this is also known as contact stress or flank stress.

To evaluate the stresses, present in the complex system of a gear, internally recognised formula and methodologies are used. ISO 6336 and AGMA 2001 are major industry standard solutions and widely adopted as a true source of information. These formula utilise experimentally driven factors for different applications and expand on the fundamental mechanical formula.

In both standard the gear stresses are a conservative estimate and do not represent an exact physical stress experienced often over estimating the stress [35], [36].

### 2.3.3.1 Root

The root stress or bending stress is derived from the Lewis bending theory, modelling the gear tooth as a cantilever beam subjected a point load tangentially at the pitch circle. For the purposes of the report AGMA is the chosen method and thus the bending stress is expressed as the following for AGMA in Equation (1) [36]. While AGMA is chosen the ISO standard is similar and results only have a small deviation between the two [35], [36].

$$\sigma_b = W_t K_o K_v K_s \frac{1}{bm_t} \frac{K_H K_b}{Y_j} \tag{1}$$

The formula considered, from right to left the transmitted load ($W_t$), overload factor ($K_o$) dynamic factor ($K_v$), size factor ($K_s$), face width (b), module ($m_t$), Load distribution factor ($K_H$), rim thickness factor ($K_b$) and the geometry factor ($Y_j$) [36]. These all have their own specific definition and can be acquired from their own formula, look up tables and, gear parameters. All the applied factors aim to bridge the gap between the theoretical Lewis bending and real-world application. The selection of appropriate and applicable factors is critical in determining the correct stresses.

### 2.3.3.2 Contact

The contact stress occurs at the interface between teeth, the localised compressive force induces a stress across the face of the tooth. Derived from the Hertzian contact stress theory the formula used under AGMA is shown in Equation (2) [36].

$$\sigma_c = Z_E \sqrt{W_t K_o K_v K_s \frac{K_H}{d_{\omega 1} b} \frac{Z_R}{Z_1}} \tag{2}$$

The factors share similarities between the bending stress, where each factor remains the same. Introduced is the elastic coefficient ($Z_E$), pitch diameter of the pinion ($d_{\omega 1}$), surface conditions factor ($Z_R$) and geometry factor ($Z_1$) [36]. These factors are also from their own formula, tables or dependent on the gear parameters and geometry.

Understanding which parameters effect the gear stresses experienced can be used to fine tune gear design and limit the amount of exploration required when find the optimal solution.

### 2.3.4 Lubrication

While lubrication is not directly linked to the gear geometry or load transfer it remains a critical portion of the gear system. Controlling the friction within the system and allowing for the dispersion of heat generated [44]. Two primary methods are applicable for the application, a greased based system and an oil bath. Both have their benefits and downsides and dependent on the system for the best solution. For any lubrication method it must be periodically checked and contains no foreign matter, this can be a sign of wear within the gears or a opening to the outside letting contamination in. The choice between grease and oil can be dictated by the working speeds within the gearbox. At low speeds a grease application may be more suited and higher speeds trend towards an oil bath solution, while these are not requirements they represent general conditions [44].

For the application the likely solution is an oil bath, ensuring the correct viscosity and quantity depends on the design of the internal architecture. Cavitation can cause increased wear within a system, as well as a high viscosity can lead to increased drag of the gears through the fluid and lead to inefficiencies and decreases in service life [44], [45]. The choice of the correct oil is based on operating temperatures, speeds and required a proper analysis.

## 2.4 Gearbox Loading

Testing of the gearbox represents a critical stage in the process. As only a single prototype gearbox will be manufactured, full integration and validation of a vehicle system is not feasible. Creating a controlled testing environment is required to evaluate the gearbox performance under a representative load.

To load the gearbox and hence the motor the mechanical power generated must be absorbed or dissipated through an external system. The following section is aimed at understanding the methods available and their operating conditions. These systems are known as dynamometers or commonly referred to as dynos. There are two main categories of dynamometers, acceleration and absorption dynamometers. The acceleration dynamometers are able to measure the force output as the rotational speed changes, providing a torque speed curve [46]. The absorption dynamometer however can provide a constant resisting torque, either from mechanical friction, fluid friction or electromagnetic induction [46]. Supplying a constant torque allows a constant load on the gearbox for a given period of time and can be used for measuring durability and efficiency [47]. Each method of creating a load has advantages and disadvantages.

Such as mechanical loading, where the output of the gearbox is loaded using friction dissipating energy as heat. This method is simple and cost effective for low power or torque situations. As power increases the amount of friction increases and can cause failure within the friction device or excessive heat.

A fluid friction or known as a water brake creates friction through an impeller rotating within a stationary housing [46]. A water brake can supply high power resistance within a small package due to the higher heat capacity of water compared to air. Either a cooling system to cool the fluid for a closed loop system is required or a continuous supply of fluid is needed.

Eddy current dynamometers provide resistance through electromagnetic induction, providing fast and precise load control [47]. Making them an ideal use case for testing environments. While they are able to operate at a wide range of conditions, low speed reduces the torque capacity and limits the ability to absorb the power. Eddy current dynamometers, similar to water brakes require sufficient cooling systems to manage heat either through a closed loop system or constant supply.

Another commonly used approach is the electrical dynamometer, coupling the output of the gearbox to an input of an electric motor and running it as a generator. While the energy may be then converted to a useful form it is often converted to waste heat. Electrical dynamometers require complex control systems and must be power matched to ensure correct dissipation of energy [47].

Each loading condition presents trade-offs in terms of complexity, accuracy and thermal management. The selection of an appropriate system is dependent on the testing conditions which are to be determined.

## 2.5 Summary

The performance of modern electric vehicles, particularly those within FSAE and motorsport, is dependent on effective design and integration of many subsystems. One of these subsystems is the powertrain, transmission, or drivetrain playing a critical role in delivering the power from the motor to the wheels. FSAE adds an additional constraint through time, cost and knowledge.

Electric powertrains offer significantly greater flexibility in configuration and overall layout over the traditional internal combustion engine. Due to high power density and size of electric motors. Enabling a wide range of packaging solutions, each with their own design decisions, optimisations, trade-offs and complexity. These common configurations are a single inboard motor, dual inboard motor, quad inboard motor, rear wheel in-hub and the all-wheel drive in-hub systems.

Each configuration shows a difference in packaging ability, such as an in-hub solution locating the motors outside of the primary structure and allowing for freedom of component placement within the chassis. Each configuration has a different serviceability, integration and complexity.

A review of literature around planetary gearboxes, and those specifically integrated into FSAE vehicles shows limitations with teams relying heavily on analytical or simulation-based approaches, with limited gear optimisation. While these approaches are valid and are able to create a functional product, they are do not have any design validation through the use of experimental testing.

Fundamental gear theory is covered to understand the effects of pressure angle, profile shift or helix angle. Selecting appropriate parameters for the loading expected or manufacturability. Similarly, these parameters can also be altered by the manufacturing method. A process such as shaping may limit the ability to create a gear of nonstandard module while EDM will be able to create a bespoke gear design if required.

Evaluation of the gear stresses through AGMA provides a reliable baseline for expected gear stresses to determine the material and heat treatment options. Achieving a tough core and hard teeth on a gear allows for the best resistance to impact and wear.

This project aims to address these gaps and build upon what others have completed thus far. By designing, manufacturing and testing a single prototype rear wheel in-hub planetary gearbox. Providing a validated base line for future use, and a comprehensive approach for future students undertaking FSAE.

# 3 Design Requirements

The design of the gearbox must first have the boundary conditions set, understanding the loading conditions like the torque and speeds required under load is critical to a well thought out system and ensuring the prototype does not fail.

The powertrain is constrained by the tyres contact to the road. Understanding how the tyres operate is important to work within the traction envelope they create. Ensuring the powertrain is able to operate and deliver the maximum amount of torque to the wheels without exceeding traction and causing slip.

The selected motor defines the available torque and speed, which will constrain the gearbox and gear ratio required to achieve a desired performance. The gear ratio directly affects the torque experienced by the wheel, which must remain within the traction envelope. This traction envelope will have a limit which is based on the torque able to be delivered to the wheel and gear ratio, influenced by the motor. These three aspects create an iterative loop requiring gear ratio and motor selection to be refined in parallel to ensure the best performance.

Defining a gear ratio allows for nominal operating conditions to be estimated using track data from previous vehicles. This includes the nominal torque at the wheel and motor and the corresponding rotational speed. These values create the basis for analysis of the gearbox and testing validation.

In addition to performance conditions are geometric and safety considerations implied by FSAE-A.

## 3.1 Tyre Data

Arguably the most important part of any race car is the tyres, being the only contact point on the road and suppling one hundred percent of the mechanical grip. Understanding the tyres and how they will respond to the road while under so many factors is a complex area. For the scope of this thesis which looks at the driveline a small portion of tyre data will be analysed identifying a traction coefficient to create a functional envelop. For this section wet tyres have been excluded from analysis for reasons of trying to find peak torque the wheels can handle before slipping which will never be in wet conditions.

Finding the maximum traction coefficient the tyre can supply is an important criterion when selecting the motor. If the motor can generate greater torque than the tyres are able to handle this causes the tyre to break traction, slipping and resulting in no driving force. This analysis considers a simplified best-case scenario. Tyre performance and response is highly dynamic and influences by many more factors that are beyond the scope of this project. The purpose of the approach is to drive an estimate and ensure the motor operates within the tyres traction envelope. Detailed modelling and simulations and considering lateral acceleration could be implemented in future iterations but are not required for this stage for preliminary motor selection.

The FSAE Tyre Test Consortium (TTC) is an invaluable resource which uses a tyre testing machine by Calspan to look at tyre performance under different conditions and different tyres. The tyres which will be looked at the Hoosier 16x7.5-10 using an LC0. These are the tyres that the WESMO team has run since the 2023 campaign and have shown theoretical promise [48]. To obtain longitudinal traction coefficients to predict the acceleration characteristics an arm is required to attach to the tyre to read the longitudinal force. This becomes an issue when trying to analyse any tyre of 16-inch diameter as the arm is too large to allow for clearance against the traction surface. Therefore, to gain an insight into how the tyre would respond by comparing tyre that includes longitudinal data and creating an approximate curve on the longitudinal traction coefficient. Excel was used as the basis for analysis to present and visualise as well as easily editable for future powertrain engineers that may require the data. Each data file is inclusive of many short ‘runs’ these runs will run along with the run schedule where one variable is changed at a time.

For each run the slip ratio sweeps across a range of values, indicating if the tyre is accelerating or decelerating relative to the road. Slip ratio has multiple definitions based on the user, under the context of the TTC it is presented in Equation (3). Using variables such as the rotational speed of the wheel (N), Effective rolling radius (RL), linear velocity of the road (V) and the slip angle (SA).

$$SR = \frac{N * RL}{265.26 * V * Cos(SA)} - 1 \tag{3}$$

Each variable is simple and seen in many fields of engineering, except for the slip ratio and slip angle. Slip ratio is a ratio of the difference between the rolling surface of the tyre and the road. For a vehicle to accelerate is must spin its tyre faster than the road below it. Slip angle is the angle the tyre is turned relative to the direction of the road which may be induced from toe or steering angle.

Due to the analysis focusing on the straight line acceleration both steering angle and toe adjustment are analysed while at zero degrees, as this is the optimal condition for the tyre to be. Due to these factors the slip angle is therefore zero, leading to the cosine of the slip angle to be equal to one. While accelerating the tyres linear velocity will be greater so making N*RL > V and therefore if the slip ratio is a positive the wheel is accelerating relative to the ground and vice versa.

$$SR = \frac{> V}{V} - 1 \tag{4}$$

Figure 15 below shows a typical tyre test run for an entire longitudinal data set for a single tyre. Each "V" section is a small portion of the test each time changing a variable. When analysing the data each variable change is separated by a time change, leading to a sudden change in time step within the data file. The data is split into three major portions, each portion dictates one of the variable for this case above it is different tyre pressures. The test sweeps through a range of slip ratios as seen in the data, transitioning between accelerating and decelerating relative to the road.

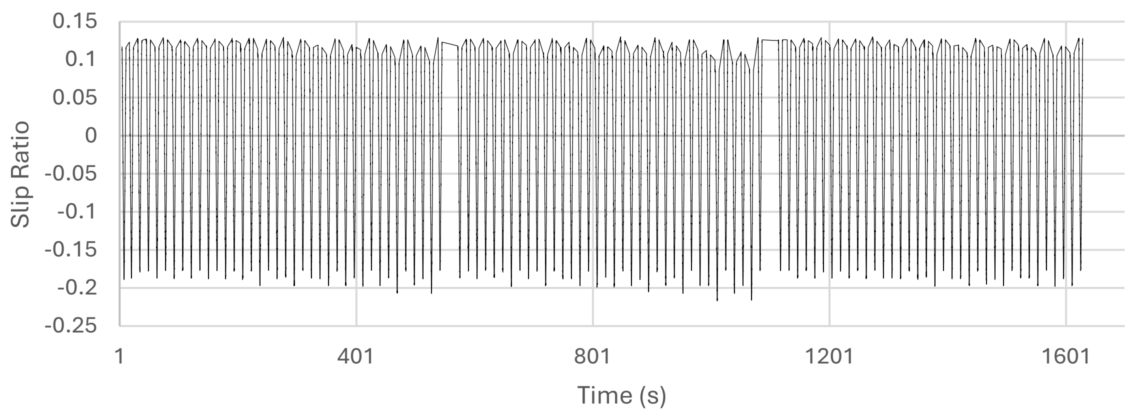


*Figure 15. TTC Raw Data*

Figure 16 below shows the first of the three major sections indicating each run analysed will be run at the same pressure. By plotting the other variables on against the same time values can show each condition the run is performed under. The exact value indicated on graphs are not critical but rather and important for a trend and able to compare each run conditions against each other with like conditions.

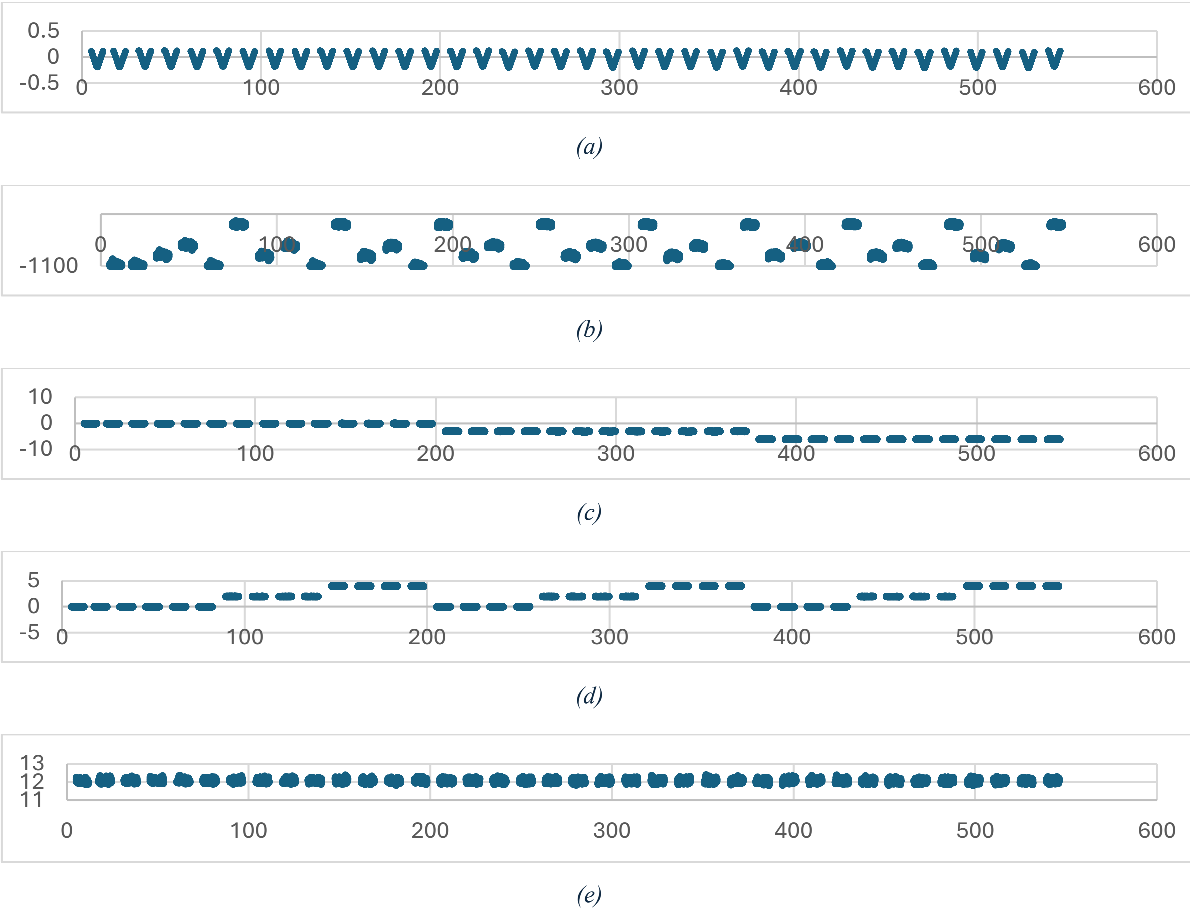


*Figure 16. TTC Data Split (a) Split Ratio (b) Normal Load (c) Slip Angle (d) Inclination Angle (e) Tyre Pressure*

To analyse the tyre only a portion of the data generated is important. For analysis points where the slip angle is zero is critical as mentioned previously. The inclination angle, commonly known and referred to as camber was chosen as zero degrees as this will provide the highest contact path and theoretical grip under ideal conditions. And a pressure of 12 PSI which has been run on the WESMO car in previous years.

Finding the maximum traction coefficient for each normal load can be used to find the theoretical maximum grip available. For each 'V' section the longitudinal traction coefficient can be plotted against slip ratio at different normal loads to find the curve.

As previously mentioned, the TTC only contains one tyre of the same compound to be tested under longitudinal conditions is the Hoosier 18x6.0-10 LC0. This causes issues as multiple variables are altered from the tyre in use. By making multiple comparisons a relationship can be used to create an approximated model of how the tyre being used will operate. An approximation of the traction coefficient will be reasonable at the level of the analysis for the project, future teams may choose to develop the traction coefficient to greater detail if there is an attainable benefit from this.

Initial consideration is to gather relevant tyres, as the 18x6.0-10 LC0 has a different width and diameter finding a factor or relationship between these two variables by analysing alternative tyres with all other properties similar. Understanding how traction responds to the change in slip ratio is important, Figure 17 shows initial traction rises quickly and linear up to a point where it starts to taper off and reach a maximum.

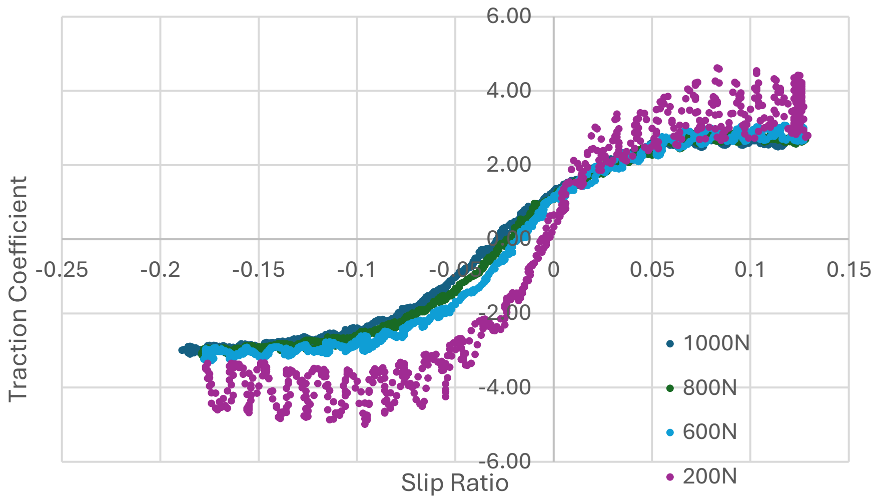


*Figure 17. 18x7.5-10 R25B Slip Ratio, Traction Coefficient at Different Normal Loads*

The traction coefficient becomes unpredictable at lower normal loads as shown within the 200 N trace, for subsequent analyse these have been omitted, likewise the normal load on the tyre is unlikely to be a small load. Additionally, the graphs show a high variability within the data, therefore a rolling average was taken to better represent the data. Each tyres raw data and averaged data is found within Appendix A.

An initial comparison between the compounds was taken, based upon the Hoosier tyre compound softness chart, shown in Figure 18. Both the LC0 and the R25B have similar softness and will likely have similar performance when analysed broadly. For the analysis if the tyres respond in a similar way they can be treated as equivalent.

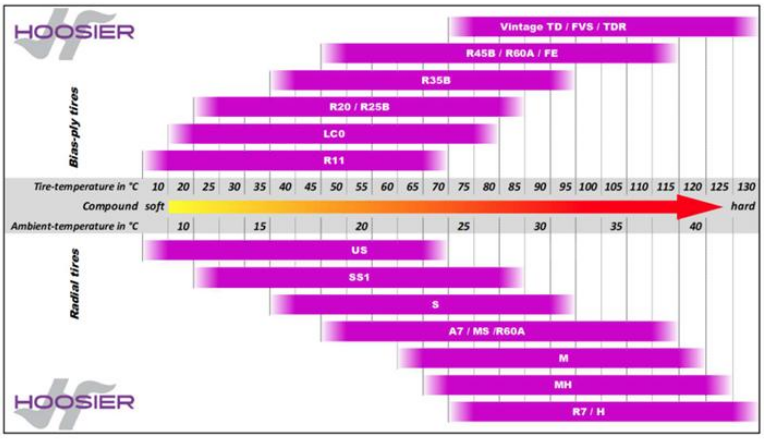


*Figure 18. Hoosier Tyre Compounds [49]*

Figure 19 shows that for each of the normal load the tyre compounds respond in similar ways at the upper limit of traction. This can be used to say both compounds are equivalent for the analysis. By making this assumption it reduces the amount of error that may be compounded if a factor were to be used.

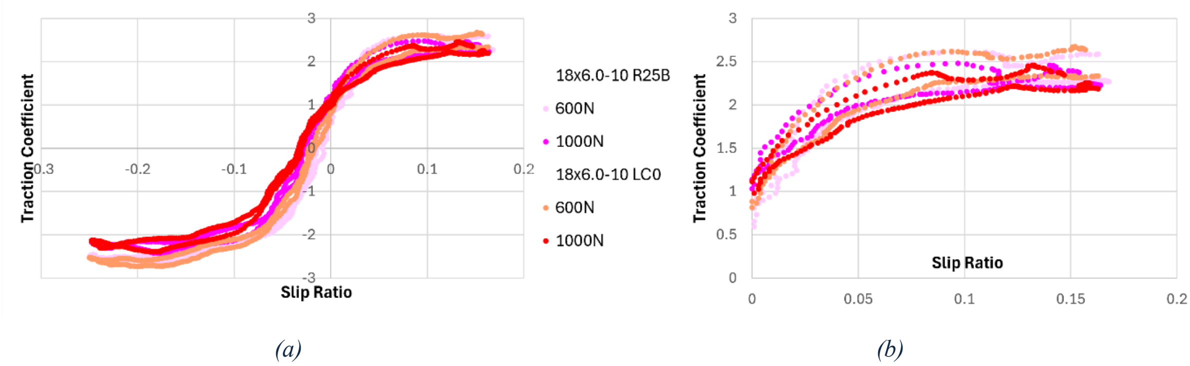


*Figure 19. Slip Ratio, Traction Coefficient. Effect of Compound (a) Whole Graph (b) Acceleration Region*

The 20x7.5-13 R25B and the 18x7.5-10 R25B are two tyres which have different side wall thicknesses while having all other properties equal. The 20-inch tyre has a wall thickness of 3.5 inches and likewise the 18-inch tyre has a wall thickness of four inch. These tyres allow for relationship between them linking the wall thickness and the effect on longitudinal traction coefficients

Overlaying the slip ratio, longitudinal traction coefficient graphs for the 18-inch tyre and 20-inch tyre to find the effect of the side wall, this graph is pictured in Figure 20. Each tyre curve shows slightly different behaviour across the normal loads. The higher side wall tyre shows a lower limit of traction. Small deviations are seen in the higher limit. while the comparison is based on a half-inch difference, compared to the one-inch difference of the two LC0 compound tyres and the relationship is unknown to be linear the variation is minor and for the approximation is considered sufficient to consider tyre wall thickness to have little to no effect for the preliminary analysis.

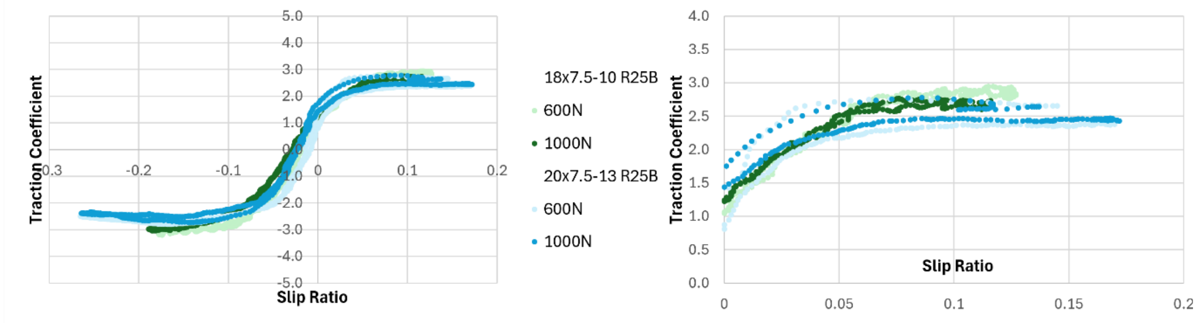


*(a)* *(b)*

*Figure 20. Slip Ratio, Longitudinal Traction Coefficient. Effect of Wall Thickness*

With the relationship between tyre wall thickness determined the importance of the width must also be considered. Using the same tyre from the previous analysis, the 18x7.5-10 R25B can be compared against the 18x6.0-10 R25B, as shown in Figure 21. This shows a measurable difference between each tyre.

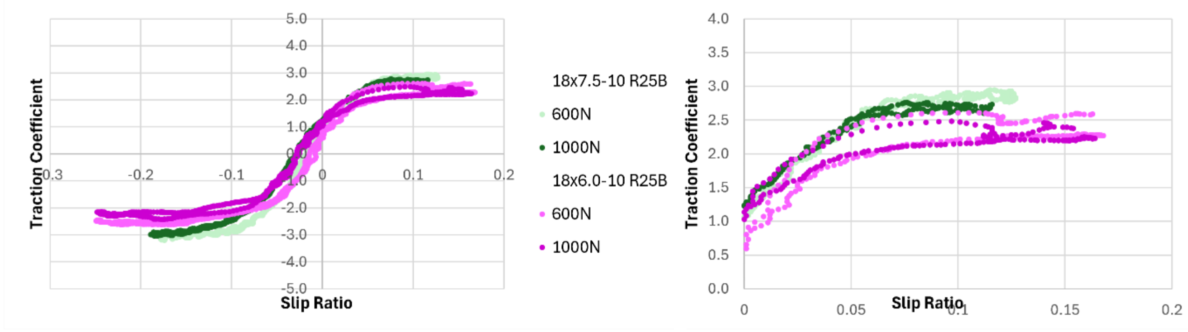


*(a)* *(b)*

*Figure 21. Slip Ratio, Longitudinal Traction Coefficient. Effect of Tread Width*

From the comparisons an estimation can be made to predict the traction coefficient expected within the 16x7.5-10 LC0 tyres. To reduce error through factors for tread width, the conclusion is the 16x7.5-10 LC0 can be represented by the 18x7.5-10 R25B at this level. As due to the comparisons the compound and wall thickness have minor effects. Therefore, as these are the only differences between the two tyres a direct equivalence can be made. While these parameters are likely to have a higher effect during track conditions the tyre data analysis is to serve as an estimation and guidance on other selection criteria and can be optimised to a greater extent remains out of scope for the project.

Once a traction coefficient is found it can be used to determine the maximum torque the wheel can handle before slipping. For the tyre to not slip it must be within the limits of the traction coefficient as defined by the following equation. When at the tyre is operating at the traction limit these two values will be equal. Equation (5) can be applied to free body diagram in Figure 22.

$$F_{x,r} \leq F_{z,r}\,\mu \tag{5}$$

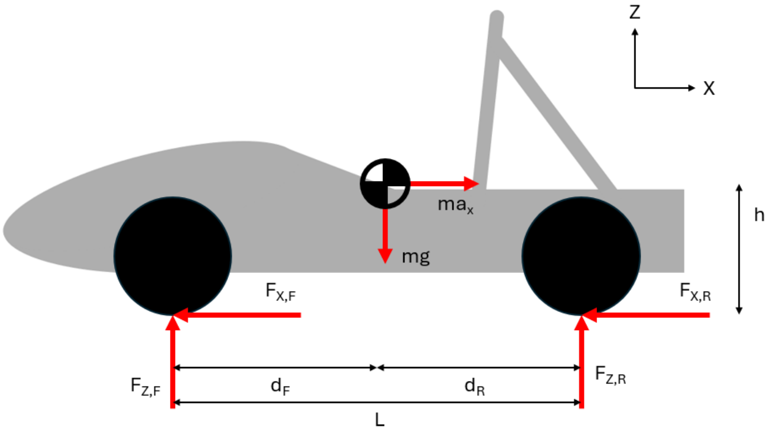


*Figure 22. Load Transfer FBD*

By analysing this free body diagram and taking the moments around the front tyre the equation can be formed. Assuming it is in equilibrium at the moment of acceleration as defined in Equation (6). It is important to note that the forces acting on each tyre in the diagram are the combination of the tyres of each pair of axles.

$$\sum M_F = 0 \tag{6}$$

$$-mg(d_f) - ma_x(h) + F_{z,r}(L) \tag{7}$$

Rearranging Equation (7) for $F_{z,r}$ gives the following.

$$F_{z,r} = \frac{mg(d_f) - ma_x(h)}{L} \tag{8}$$

Analysing the free body diagram for the forces in the x-direction will be able to find the acceleration with Newtons second law of motion. As only the rear wheels are supplying a drive force $F_{x,f}$ will be equal to zero.

$$\sum F_x = ma_x \tag{9}$$

$$ma_x = F_{x,r} \tag{10}$$

Substituting Equation (5) into Equation (10) gives force of the vehicle in relation to the vertical load rather than the longitudinal. This allows for calculation based on load transfer as the car accelerates it rotates and pushes the rear tyres into the track.

$$ma_x = \mu F_{Z,r} \tag{11}$$

Finally substituting Equation (8) into Equation (11) allows one to find a maximum acceleration given a traction coefficient and vehicle characteristics. Once rearranged the final acceleration is presented in Equation (13).

$$ma_x = \mu \frac{mg(d_f) - ma_x(h)}{L} \tag{12}$$

$$a_x = \mu \frac{g(d_f) - a_x(h)}{L} \tag{13}$$

Rearranging to only have a single $a_x$ variable gives the final equation for the maximum acceleration based on the tyre longitudinal traction coefficient and is given in Equation (14).

$$a_x = \frac{\mu g d_f}{L - \mu h} \tag{14}$$

The position of the Centre of Gravity is taken from the 2024 car which was measured using a tilt test. Using these values give a good estimate of an EV car manufactured by the WESMO team. The formula is used to calculate maximum acceleration based on the traction coefficient of the tyre as well as the vehicle. Due to the traction coefficient not being a single variable and depending on the normal load it becomes an iterative calculation, The higher the acceleration the higher load transfer to the rear and pushes the tyres into the track more, increasing the vertical load. To bridge the gap between the W-FS18 and the next generation WESMO vehicle the mass of the most recent completed EV at the time will be used, this adds error as the W-FS18 was much lighter at only 187.1kg compared to the W-FS24 of 280kg, both weights without a driver [50], [51]. meaning its on track performance and hence the data will be different it is the only data available and will still provide an estimate.

While this is a valid static analysis of the tyres it assumes they are behaving in the same way on track in all situations. Tyres are a much more complex system and could be analysed to much greater detail. Considering suspension setups, ambient conditions and using multibody simulations. The analysis completed remains a good benchmark for the prototype gearbox and what is required from it, implementing it and gathering more data and information on the performance would be the goal for long term.

By understanding the maximum acceleration allows for better understanding on what gear ratio and motor to choose. Ensuring the tyres are able to handle the load pushed through them and allowing for proper design of all driveline components as well as suspension components. Once the gear ratio and motor specifics is decided the iterative calculation can be computed seen in chapter 3.3, Gear Ratio.

## 3.2 Motor Selection

Motor selection is a crucial decision as it determines the required gear ratio and will dictate many design decisions of the vehicle, such as accumulator voltage and capacity, driveline configuration and capacity due to acceleration. Some manufacturers offer motors designed for specific use within FSAE. These are typically the best solution due to being fit for purpose. AMK Motion offer their DD5 synchronous motor which have seen very common use within in-hub motor FSAE cars but is not the only option.

Table 2 shows potential motors and their mechanical properties. Some of the specifics motor parameters are not available without data sheets from manufacturer, some of which require purchase and were thus excluded from the table. While each motor has important electrical properties such as operating voltages these have been left out as the future accumulator can be designed around this. Likewise, there are other important mechanical details like the output shaft or physical dimensions. These parameters are important but less critical to the selection process, as they can be designed around. Many other electric motors were considered and were short listed to applicable options based on size, power, speed and weight. Included is the Emrax 228 as a reference point for the previous WESMO EVs. As well as the Emrax 118 as it is common to see when an inboard RWD system is used.

*Table 2. Motor Parameters [4], [52], [53], [54], [55]*

| Motor | Power (kW) Rated/Peak | Torque (Nm) Rated/Peak | Speed (RPM) Rated/Maximum | Weight[1] (kg) | Configuration |
|---|---|---|---|---|---|
| AMK DD5 | 12.3/21 | 9.8/21 | 12,000/20,000 | 3.55 | In-hub |
| Fischer Motor | 15.4/35.4 | 11.1/29.1 | 13,250/20,000 | 2.8 | In-hub |
| NueMotor 4430 | 10/20 | /19.136 | /9990 | 4.132 | In-hub |
| Emrax 228 (MV) | 64/124 | 112/220 | /6,500 | 13.5 | Single Inboard |
| Emrax 118 | 34/60 | 52/100 | /8,000 | 7.9 | Dual Inboard |

Fischer Motors show performance promise from the initial investigation but contains caveats such as requiring additional machined components, which is unfeasible with the given scope.

Although the AMK DD5 synchronous motors have a high investment cost they have many benefits. Due to the popularity of their use within FSAE vehicles there is large amounts of knowledge surrounding their ability to perform, likely due to the motors being specifically designed for FSAE with low production volume. AMK offers an extensive catalogue of data and technical drawings available without purchase of the motor which greatly streamlines the process. Furthermore, teams such as FSAE47 and University of Canterbury Motorsport include AMK motors which are local to New Zealand and have offered to help WESMO in the past with any details [56].

Based on the assessment the AMK DD5 motor is selected as the reference motor for the gearbox design. Providing a high-power output with optimal data and motor characteristics available.

## 3.3 Gear Ratio

With the decision for using the AMK DD5 Synchronous motor decided an important step is the choice of the gear ratio. Since this will be the basic building block of the gearbox design and determine many fundamental aspects of the design and cannot be altered easily. By selecting a

[1] Motor only weight

gear ratio that can maintain optimal torque to the wheel and provide the required tractive force for competitive lap times.

While software such as Optimum Lap exists and can be used to simulate the lap time of a vehicle around a track, optimising gear ratio. This approach was not used in this study, instead analysing track data and motor operating speeds to find ratios at specific points and averaging results. This approach was chosen for simplicity and data readily available, as well as to allow for more time to be spend on the design and manufacture. Allowing for a gearbox that operates under the average condition. Simulation would provide a more accurate performance estimates accounting for accelerating, braking, aerodynamics and elevation changes, the approach taken is a simple holistic approach that will be sufficient for an initial design. This method can be expanded on by future members to achieve heightened performance.

By using the provided DD5 motor characteristics in conjunction with MoTeC data from previous WESMO cars can be used. The W-FS18 was used for data due to the significant amount of testing time they were able to achieve meaning they were able to understand their car and push it harder achieving more performance. While the W-FS18 did not run the same tyre that has been analysed it will still give a good basis. In addition, while the W-FS18 had a large amount of testing it was still driven by engineering students who were limited by their own skill rather than the tyre.

Figure 23 shows the linear velocity over a lap of the Winton autocross track, circled in red shows the portion of the lap when the car is coming back into the 'pit area' and therefore not pushing, this area can be seen in Figure 24. The data presented is collected from the average of the wheel speed sensors. Wheel speed sensor data was chosen over the GPS data to find the speed of the rear wheels, and thus the required speed of the motor. The wheel speed sensors additionally have a higher sampling rate giving more data.

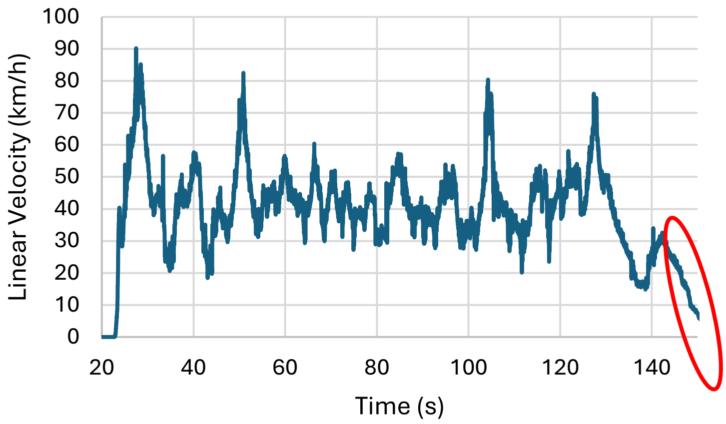


*Figure 23. Winton Autocross Lap Velocity*

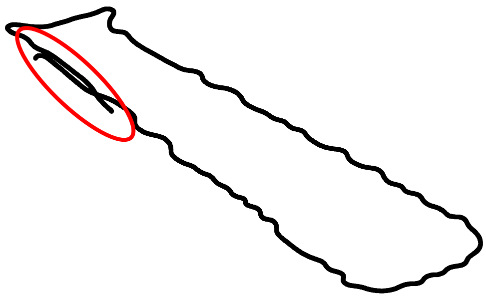

*Figure 24. Winton Autocross Track Layout*

Figure 25 Shows the pruned track speed, it also removed the initial acceleration as it will cause the gear ratio to trend towards infinity in future calculations. The specific lap analysed shows a maximum velocity record 85 km/h and an average speed of ~45 km/h.

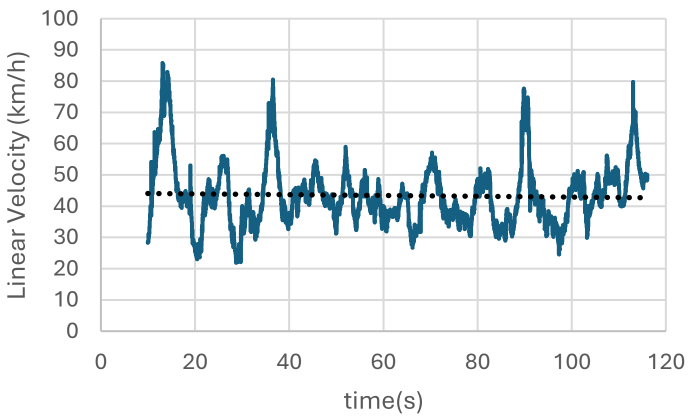


*Figure 25. Winton Autocross Lap Velocity Section*

To find an ideal gear ratio at each point a nominal motor operating point is required. AMK supplies a nominal operating point for the motor at 12,000 RPM, however this is much too high for the application, as once a ratio is calculated with this value a result of ~20 is achieved. With the volume limits and high torque this is deemed as unachievable. A lower motor operating speed was selected. Making an initial assumption of 8,000 RPM allows for an iterative process, choosing 8,000 RPM remains in the constant torque region as shown in the motor characteristics, dictated by the blue line within Figure 26. Allowing the motor to provide the same torque at a relatively higher and lower speed.

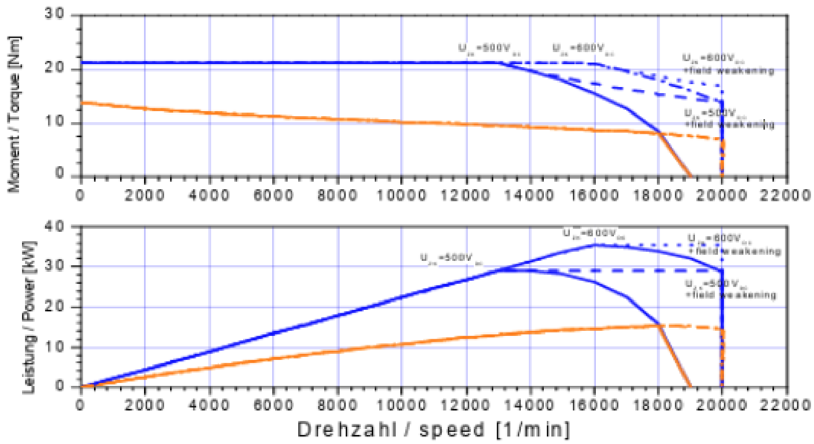


*Figure 26. AMK DD5 Motor Characteristics [52]*

Using Equations (15) and (16) an instantaneous gear ratio can be found for the motor to rotate at the now nominal 8,000 RPM and achieve the required linear velocity of the car. Shown in Figure 27, with an average trend line included.

$$\omega_{Wheel} = \frac{V}{r_{Wheel}} \tag{15}$$

$$GR = \frac{\omega_{Wheel}}{\omega_{\text{Motor}}} \tag{16}$$

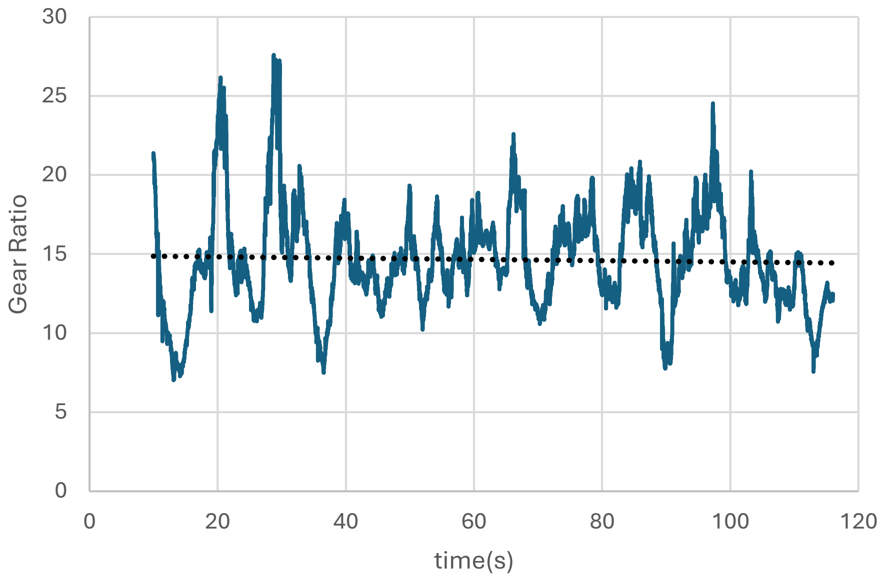


*Figure 27. Instantaneous Gear Ratio Required*

An average across the lap is found and for this specific lap shows 14.65:1. In conjunction with data analysed in the future 3.4 chapter the nominal motor torque can be established. For a gear ratio of 14:1 the nominal motor torque expected is 8 Nm. By using the efficiency map based on total losses given by AMK, shown in Figure 28 with an additional blue point included at the maximum efficiency. The specific operating point can be pinpointed and shows an efficiency of ~90.7% compared to the peak of 90.96%. The operating point considered is a reasonable estimate and can therefore proceed with the assumed motor speed value. While the gearbox will inherently have an efficiency less than 100, causing losses in the torque but this is ignored for this portion of the analysis.

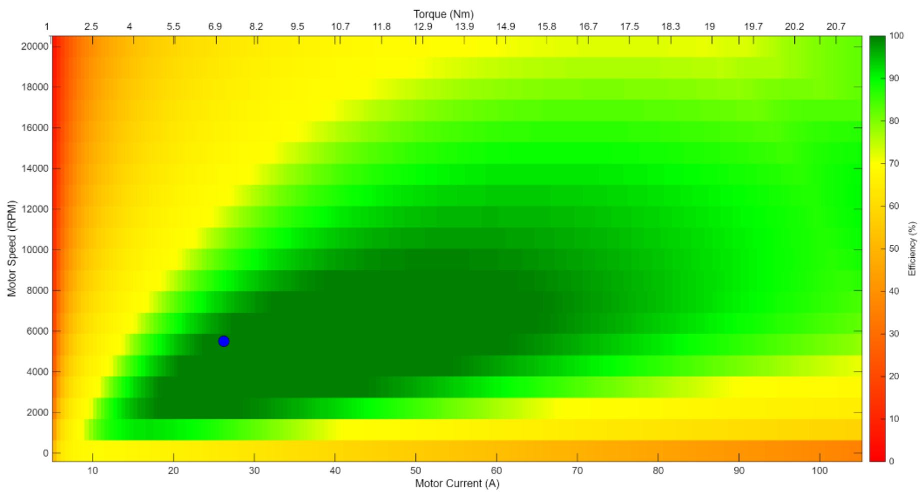


*Figure 28. AMK Efficiency Map*

With the motor operating speed known an analysis of all the data available can be completed in the same way. Each graph available in Appendix B. By doing the same analysis for multiple an average of the averages can be taken making for the most average gear ratio, shown in Table 3. Different operating cases were considered based on the data available, each Winton lap shows a single competition lap. Whereas Oakleigh GoKart track shows multiple laps of the same track compiled into a single data set. The acceleration is also a competition run but shows a different dynamic event compared to the previous. A skidpad portion should be included but this was unavailable within the data set.

*Table 3. Gear Ratio and Standard Deviation*

| Track/Lap | Gear Ratio Required (averaged) | Standard deviation |
|---|---|---|
| Winton (Autocross lap 1) | 14.65 | 3.32 |
| Winton (Autocross Lap 3) | 13.22 | 3.10 |
| Winton (Autocross Lap 4) | 12.78 | 3.08 |
| Oakleigh GoKart track | 13.63 | 15.39 |
| Acceleration | 8.98 | 2.91 |

From the analysed data the autocross laps around Winton show consistent results with similar standard deviation, showing that a singled fixed ratio can be used throughout a lap. In contrast the Oakleigh GoKart track shows a similar ratio, but with much higher standard deviation. This is likely due to the raw data, as the testing day shows multiple laps after each other with no written indication of the cars run plan. While the data could be filtered further to eliminate the variability and focus on faster portions the required time for this was deemed to intensive to be worth it, considering the averaged results align with other data. The acceleration run also shows another discrepancy with a much lower ratio again likely due to the run being much shorter than all others. A higher importance is placed on the Winton laps as they should be more representative of an expected EV performance. Overall, the average ratio expected for an autocross lap is 13.57:1. Providing an initial basis for gear ratio selection. Further supported by the Auckland FSAE team running 13.3:1 on their 2025 car and have been for multiple years [57]. To further analyse the impact of gear ratio on acceleration the 2023 WESMO team developed a tool using MATLAB Simulink model to estimate the acceleration time of a car using the Emrax motor. While the accuracy of this model is yet to be validated it remains as an estimate. By taking this tool and altering motor parameters to that of the AMK DD5 motor, an estimate of the acceleration time using two in-hub AMK motors can be found. By varying the gear ratio, a graph shown in Figure 29 can be created. It also shows the top speed the vehicle theoretically reached when limited by the motor spinning at 20,000 RPM.

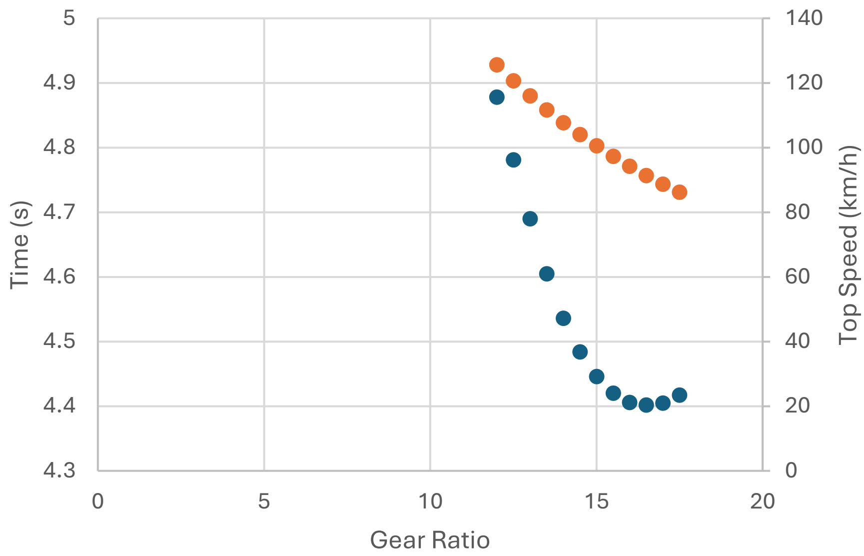


*Figure 29. Acceleration time and Top Speed with Gear Ratio*

From the estimates the optimal gear ratio for acceleration lies close to 16.5, at 4.402 seconds. This is a competitive time within the Australasia competition. With previous years showing similar results. Table 4 shows a handful of teams and the times they achieved each year, this means the gear ratio can be reduced and remain competitive in acceleration while becoming more competitive in other dynamic events. It is worth nothing that Auckland and Monash run AWD and Auckland is known for their acceleration times and hold the Australian record

*Table 4. 2022 FSAE-A Acceleration Times [2]*

| Team | Best Time (s) |
|---|---|
| The University of Auckland *F:SAE:47* | 3.81 |
| Swinburne University of Technology *Team Swinburne* | 4.39 |
| University of Canterbury *University of Canterbury Motorsport* | 4.59 |
| Monash University *Monash Motorsport* | 4.74 |
| The University of Newcastle *NU Racing* | 5.41 |

Both theoretical analysis in acceleration and autocross show a similar gear ratio requirement. While acceleration demands slightly higher than autocross. Ultimately autocross was deemed more important because of the different dynamic events and the points allocated to each. Based on all the data analysis the gear ratio of 14:1 was chosen, this still allows a balance between the required 13.57:1 for autocross and 16.5:1 for acceleration tailored more to autocross. This allows for a top speed of 107.7 km/h. predicted acceleration time of 4.536 s. compared to the 2024 EV car which did not have a predicted acceleration time but a top speed of 100 km/h [58]. Furthermore, after design of the gear profile a gear ratio of 14:1 is on the upper limit of what is achievable within the confines of the gearbox size. Having a higher ratio requires a bigger difference between teeth, and when in the same size housing the module must be reduced reducing the strength.

Based on the analysis the motor nominal operating speed is said to be 8,000 RPM and can be used in addition to the maximum speed at 20,000 RPM to define the gearbox operating conditions for future chapters.

With a gear ratio defined the maximum acceleration from the previous derived equation can be calculated, Equation (14). As mentioned, the vehicle parameters used are to be determined from the 2024 car were possible, and the traction coefficient. Using these values a maximum acceleration of 2.7 g is possible. This is an upper bound and likely to be much less, due to the ideal conditions under the TTC test conditions. To reach this acceleration the motor would be required to output 62 Nm. Based on the motor peak torque a maximum acceleration of 1.3 g could be reached with the tyre requiring a traction coefficient of 1.2. This operates within the tyre traction envelope. This acceleration could be increased by optimisation of the weight as the 330 kg estimate is a heavy vehicle.

## 3.4 Torque Demands

Knowing what the motor can do it is important, understanding what the vehicle wants while driving a track is just as critical. computing this out will allow for an acceptable testing condition, as well as the expected running conditions.

Using the MoTeC data from the same track as previously analysed can be used to find the acceleration of the car at each point. The raw MoTeC data is required to be manipulated because of the design of the 2018 car. The W-FS18 has the MoTeC data logger on the side of the vehicle at an angle. Figure 30 show the side and top view of the logger, accompanied by Equation (17),. (18) and (19) [50]. These equations have been altered to correct for any errors in the original formula.

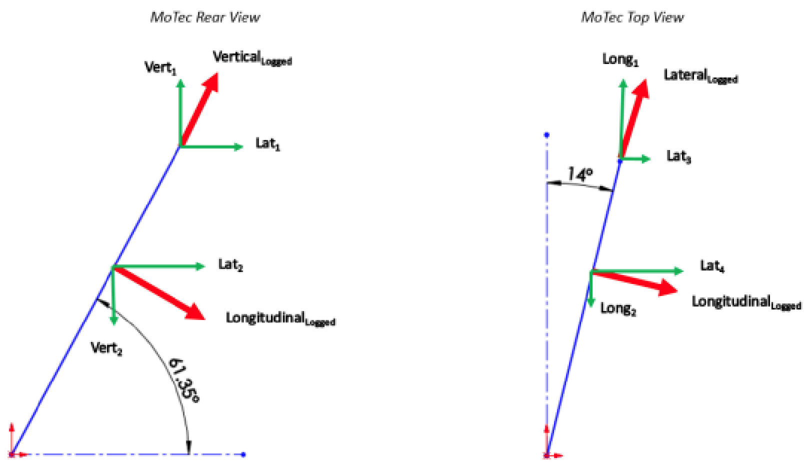


*Figure 30. W-FS18 MoTeC Layout [50]*

$$Acceleration_{Lateral} = Longitundinal_{Logged} * \sin 61.35 + Vertical_{logged} * \sin 14 + Lateral_{logged} * \sin 14 + Longitudinal_{Logged} * \sin 14 \quad (17)$$

$$Acceleration_{Longitudial} = Lateral_{logged} * \sin 14 - Longitudial_{logged} * \sin 14 \quad (18)$$

$$Acceleration_{Vertical} = Vertical_{logged} * \sin 61.35 - Longitudial_{logged} * \sin 61.35 \quad (19)$$

The use of the raw data can be analysed using basic laws of motion, shown in the equations below, Equations (20), (21) and (22). An assumed mass can be used which is the mass of the W-FS24, as done previously for the same reasons. As well as the effective rolling radius of the tyre 16-inch tyre.

$$F_{Car} = m_{Car}a_{Car} \quad (20)$$

$$\tau_{Car} = F_{Car}r_{wheel} \quad (21)$$

$$\tau_{Motor} = \frac{\tau_{Car}}{GR} \quad (22)$$

Analysing a competition acceleration run shows the torque demand from the car translated to the requirements for the moto assuming a 100% efficiency. Also over laid is the throttle position which when dips show lifting off allowing for a gear change. For one gear shift this causes the torque demand to peak which is of null concern for an EV which does not require any shifting as seen in Figure 31. Also seen in two peaks in the torque between 3.5 and 4.5 seconds, this could be due to any reason and based on the data is likely to be an environmental impact such as the track surface or similar.

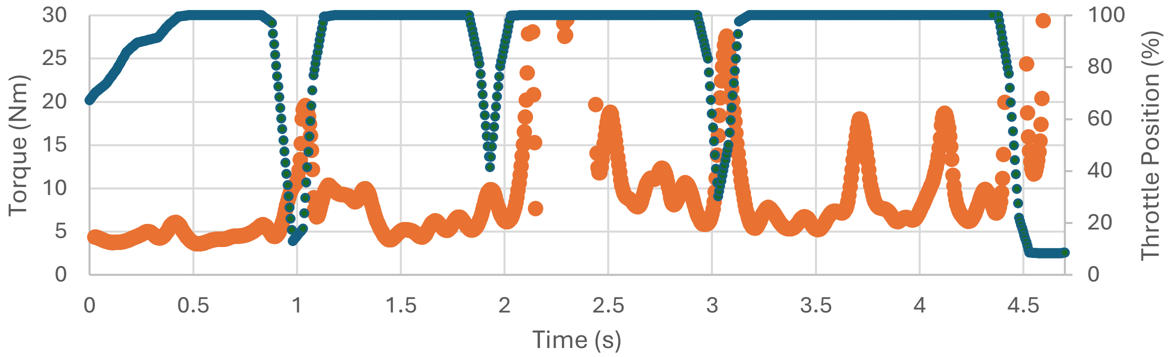


*Figure 31. Acceleration Torque Demands*

The acceleration run was used as the primary basis for determining the torque required as the throttle input is fully open during majority of the run other than initially and during gear shifts. This provides an estimate of the peak torque conditions expected.

While based on an ICE power unit, which is unable to deliver instant torque like an electric motor the acceleration event still offers the most consistent and practical basis for an estimate of the system without any EV data to be used.

The resultant torque demand is an taken as a 95$^{th}$ percentile and shows a value of 8 Nm. This is used as a nominal torque value for testing and any other nominal calculations.

Figure 32 shows the distribution of motor torques over an endurance lap for the Weingarten team in Germany, the graph is represented by the torque delivered by the motor for a given gear ratio of 12.69 [59]. The mode of the graph is shown to be zero Nm, with smaller peaks in the low range of 2-4 Nm. Adversely within the higher torques the mode lies at 8-9 Nm, falling within the range estimate. Although the gear ratio is slightly lower this is offset by the team car from the data source being lighter, balancing each other.

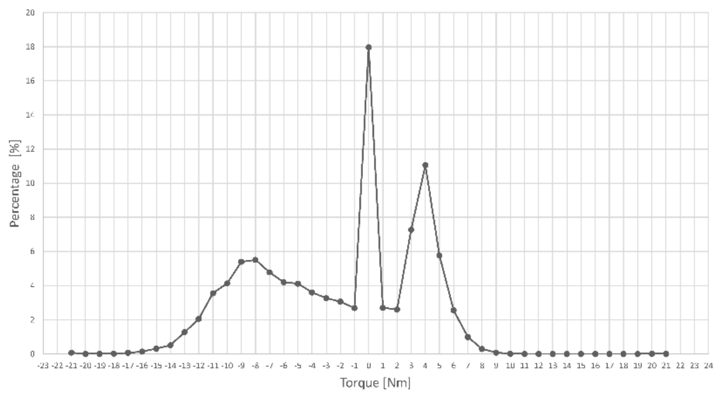


*Figure 32. Torque Presence of Motor Input Shaft Over an Endurance Lap [59]*

This backs up the original estimate and can be said to then be an acceptable estimate without further data collection or processing.

## 3.5 FSAE Requirements

The final design requirements that need to be established are the FSAE-A rules. These must be adhered to for the vehicle to compete in any dynamic events at competition. The powertrain has few specific rules, and when removing the chain, belt or other transmission types become fewer. There are no specific rules on outboard motors with more specifics on the connector or high voltage components which lie out of scope within the project of development [14].

For the gearbox to be useful to the WESMO team it must be fit for purpose and therefore fit within the wheel assembly, leave clearance for any critical components such as the suspension pickup points, brake calliper, brake disc and toe rods. These exact criteria are discussed as they become relevant in future chapters but remain important to be aware of.

# 4 Gearbox Design and Analysis

With the gearbox design parameter defined, including target gear ratio, torque and packaging requirements, the design process encapsulates conceptual design, and the process through to detailed design and implementation. This chapter describes the development of all required engineering decisions and why they were taken. Using mathematical analysis, software and established gearbox design methods. The design process focuses on creating a relatable platform which to be built on to improve in future years. Utilising many in house manufacturing processes and methods and allowing for service throughout its usable life. An exploded view of the final design is presented below in the Figure 33 as a reference to understand the final design during the process. Consisting of two internal carriers, two deep groove roller bearings, six needle roller bearings and a rotary seal. Use of a stepped planetary system using three planets orbiting to the sun gear where each planet rotates on their own shaft.

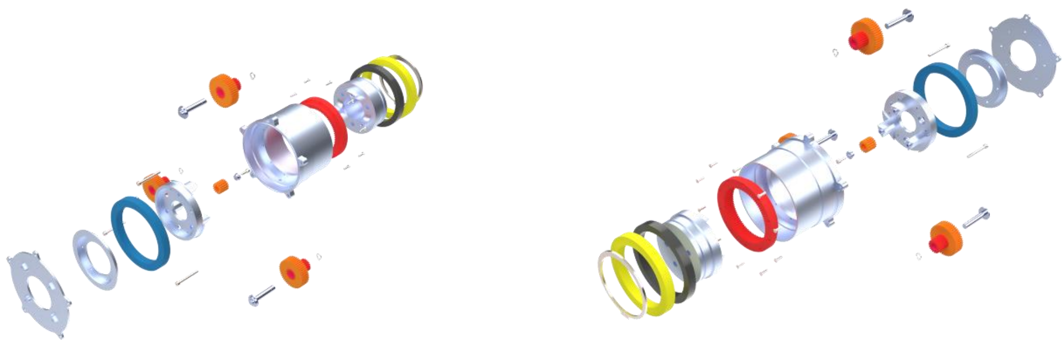

*(a)* *(b)*

*Figure 33. Gearbox Isometric View (a) Rear (b) Front*

A high-level flow diagram is shown below in Figure 34, providing an overview of the methodology used to develop and design, specifically around the gears. Utilising boundary conditions previously acquired. Aiding visually in the structure used and the iterative loop required. For the process an analytical programme called KissSoft and KissSys were used to act on the iterative loop and compute a greater number of configurations.

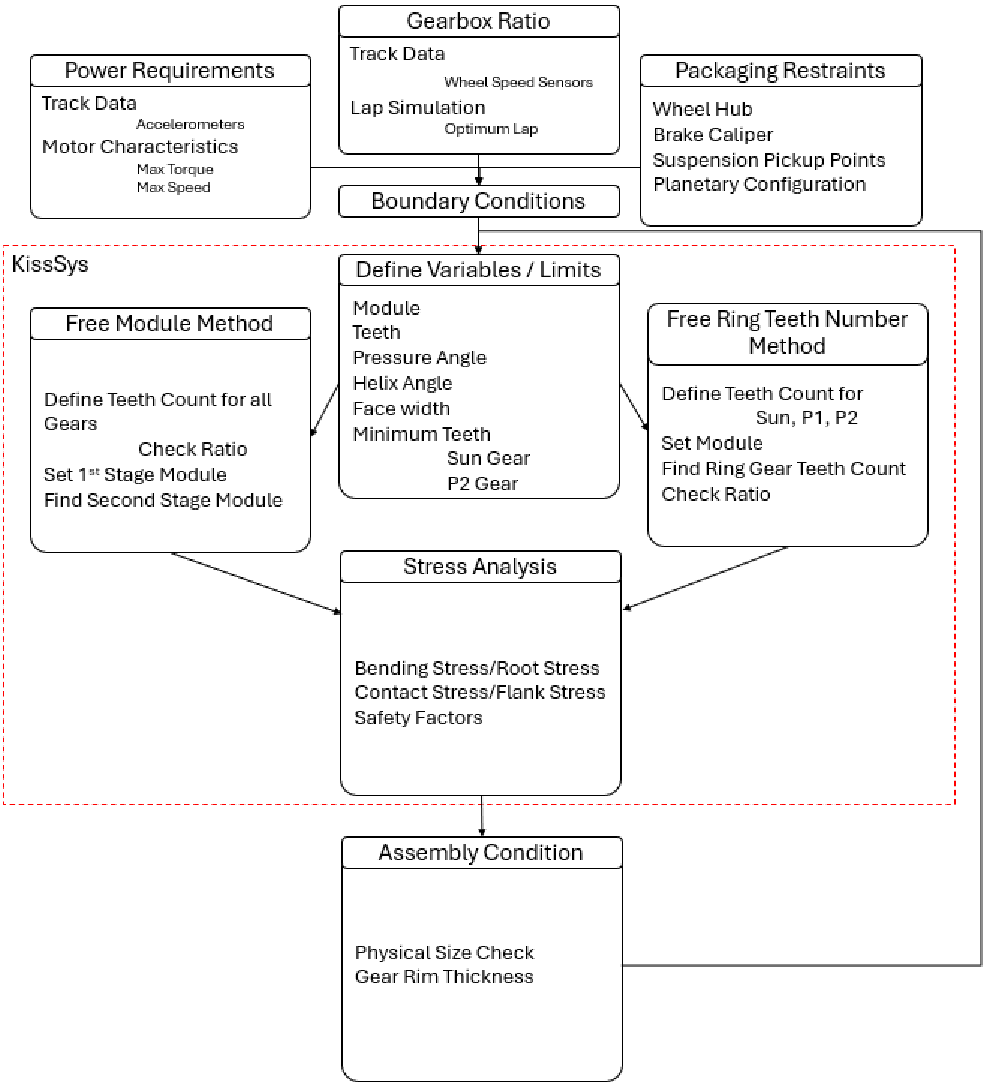


*Figure 34. Gear Design Methodology*

## 4.1 Applied Methodology

With the power requirements and gear ratio boundary conditions defined in previous sections the packaging restraints can begin to be analysed. These restraints limit the overall gear architecture and is major portion of defining the gears.

As mentioned in section 2, literature review a single stage planetary cannot reach a ratio of 14. Additionally having two single stage planetaries will increase the overall size significantly. A multistage planetary gearbox would require two sets of rings, planet and sun gears leading to greater unsprung mass and part count within the assembly. Depending on the setup having multiple stages might require two carriers rotating at different speeds, significantly increasing the complexity. Therefore, the decision to use a compound planetary configuration was an early decision. The planetary gearboxes gear ratio is dependent on the configuration. The power input shaft is fixed to being the sun gear by the AMK output shaft being central, therefore two options are available. Holding the carrier and planets fixed as the ring gear rotates and acts as the output or vice versa, where the ring gear is held stationary and the planets and carrier rotate to output power. The gear ratio for each configuration is given by Equations (23) and (24).

$$\frac{Z_{p1}}{Z_s} * \frac{Z_r}{Z_{p2}} = GearRatio_{FixedCarrier} \tag{23}$$

$$\frac{Z_{p1}}{Z_s} * \frac{Z_r}{Z_{p2}} + 1 = GearRatio_{FixedRing} \tag{24}$$

*Where,*

*$Z_s$, $Z_{p1}$, $Z_{p2}$, $Z_r$ indicate the number of teeth of the sun, planet meshing with the sun, planet meshing with the ring and ring respectively*

Based on the equations for calculating each ratio they both follow the same formula with one exception. When the ring gear is fixed the carrier is used as the output, the gear ratio of the configuration is increased by one compared to having a fixed carrier and utilising the ring as the output. The increase in ratio is due to the relative motion between the rotating carrier and the gears within the system.

Both configurations were trailed with the same gear ratio, on a laser cut MDF mock model. One utilising the fixed ring method as shown in Figure 35a with the alternative, the fixed carrier in Figure 35b. These mocks allowed for the initial investigation as to how each piece interacts with each other, showing the difference between. These prototypes were the first iteration and showed the importance of choosing the correct configuration and gear geometry.

*(a)* *(b)*

*Figure 35. Mock Laser Cut Model (a) Fixed Ring (b) Fixed Carrier*

While each option has its advantages and disadvantages. The decision was to utilise the fixed ring option, allowing for an extra plus one on the gear ratio means the gear ratio required by the teeth is only 13. By requiring a smaller ratio between teeth allows for the ability to use larger teeth within the same packaging increasing the safety factor or allowing for smaller packaging. Additionally having the ring gear as the fixed options means it can be directly integrated into the hub assembly. While having a fixed carrier option allows for the wheel to be mounted closer to the chassis as shown in Figure 36 and Figure 37. As the gearbox remains as a prototype the specifics of wheel integration is null factor and further testing and operation might reveal unforeseen specifics which might be better suited to other configurations.

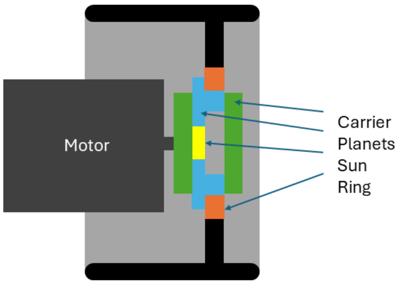


*Figure 36. Carrier Output Wheel Placement*

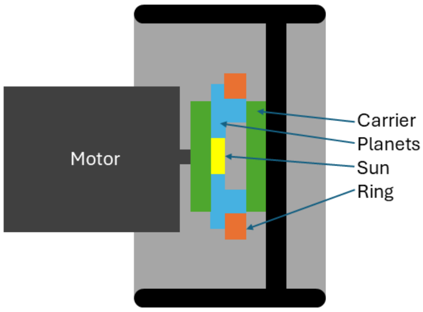


*Figure 37. Ring Gear Output Wheel Placement*

While the configuration of the gears influences how the wheel integrates with the wheel assembly the overall size of the gears and gearbox are limited by the sounding components. The maximum diameter of the gearbox is governed by three main constraints. The suspension pickup points, brake caliper mounting positions and the wheels rim inner diameter. The smallest of these was measured as the suspension pickup points, of which the 2024/2025 uprights were used as a benchmark. The envelope, which can be seen in Figure 38 shows the points where the suspension pickup points lie on the vertical axis. This makes the gearbox allowable size smaller again to allow for appropriate brackets and mounting to fit to these pickup points. While these could be designed and manufactured within the limits of the gears the decision to design within the boundary was made to allow for easier integration in future years, giving the suspension pickup points freedom to move along the total length of the gearbox greatly increases the longevity of the gearbox and eliminates the need to have to redesign. Introducing this restriction also enforces a compact design to keep the design mass low while not designing for mass.

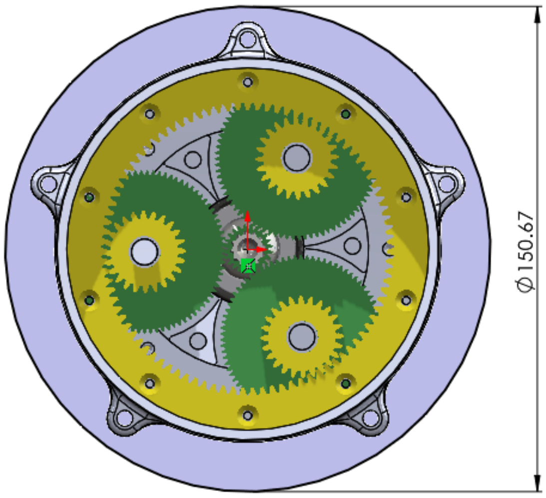


*Figure 38. Suspension Pickup Point Envelope*

Choosing the ratio distribution between stages is a key design decision in a compound planetary gearbox, as the allocation of the total reduction directly influences gear size, packaging constraints, and load distribution within the system. An overall reduction ratio of 13:1 is required by the gear teeth due to the ratio equation. This reduction must therefore be achieved through the combined effect of the two stages within the compound planetary gearset. Determining how this reduction should be divided between the stages is consequently an important step in defining the gearbox geometry and ensuring the design remains within the packaging constraints described previously.

Within the gears themselves are also boundary conditions which must be mentioned. The input sun gear must have enough material beneath the root of the teeth to the female spline that interfaces with the motor output shaft. With the motor spline designation W11x0,8x30°x12, giving a 10.5mm diameter hole the sun gear must have a dedendum diameter greater than this plus any additional extra required. This limits the combination of the module and teeth size for the iterative design portion.

In a stepped compound planetary gearbox configuration, the planets from both stages share a common shaft. As a result, the position of the first-stage planets fully defines the location of the second-stage planets or vice versa. This coupling significantly reduces the number of possible gear configurations, as the pitch diameters, based on the teeth count and module of the gears must satisfy the geometric constraints imposed by the shared planet shafts. For this reason, the design process was simplified by solving each stage independently. Once the first stage is defined, a large portion of the second stage geometry becomes fixed due to the shared planet locations, allowing the remaining parameters to be refined through further analysis.

When solving for the number of required teeth on each gear that gives the required ratio there are two main options. These both include leaving a free variable which will be solved for to allow for the rest of the system to align. Either one of modules or the number of teeth within any single gear. The approach of this thesis investigates as leaving the module of the second stage as a free variable but derives a formula for a free ring gear tooth count as well.

The common shaft radial position (a) can be calculated based off the sun and first stage planets module and teeth combination, shown in Equation (25). Similarly, the ring and second stage planet PCD can be calculated using their module, shown Equations (26) and (27). To ensure the meshing between the second stage gears the two gears must meet tangentially as shown in the Equation (28).

$$a = \frac{m_1\left(Z_s + Z_{p1}\right)}{2} \tag{25}$$

$$r_{p2} = \frac{m_2 Z_{p2}}{2} \tag{26}$$

$$r_r = \frac{m_2 Z_r}{2} \tag{27}$$

$$r_r = a + r_{p2} \tag{28}$$

By rearranging and substitution each equation the following formulas can be derived. These can be used to solve for the variable that has been left free, chosen by the designer which will be used later once some initial conditions have been established. Equation (29) is to be used when solving the for number of teeth on the ring gear for predetermined modules across stage one and two. While Equation (30) is for solving for stage two module with each gear tooth count determined

$$Z_r = \frac{m_1\left(Z_s + Z_{p1}\right)}{m_2} + Z_{p2} \tag{29}$$

$$m_2 = m_1\left(\frac{Z_s + Z_{p1}}{Z_r - Z_{p2}}\right) \tag{30}$$

This process uses Equation (30) due to the gears being manufactured with the wire EDM process and does not require a standard module as if it was to be hobbed or machined in any typical gear manufacturing methods without custom tooling. Module was chosen because it is it not required to be a whole number allowing the system to have a greater range of flexibility.

While the gear ratio and thus the integer number of teeth do not have to equate to exactly 14:1, leaving the module free was an easier approach and allows for an exact ratio of 14:1.

Initial conceptual designs were created, by creating a wide range of tooth combinations across each gear to achieve or close to the desired ratio. This process was used to create an idea of what a reasonable range of each criterion were. Module was also able to be changed to analyse the effect on the overall diameter of the gears.

Figure 39 shows an early prototype which has a ratio of approximately 14:1. From the prototype focus is put on the first stage and the size of the teeth, while calculations were done to show this meet requirements the resulting teeth were considered too small and impractical, where much bigger teeth were able to be used in place. The larger teeth would allow the gear tooth to have a higher bending stress resistance. The module presented in this design is 0.8 therefore this was opted to be too small, and the final design would have to have a higher module.

*Figure 39. Early Prototype*

Throughout the conceptual configurations it was discovered that although an equal distribution of ratio between the two stages would mathematically satisfy the required overall reduction, this approach is not ideal for the application. The first stage inherently tends to be larger due to the presence of the sun gear, which has a relatively small tooth count compared to the ring gear of the second stage. Assigning a smaller proportion of the total reduction to the first stage therefore helps reduce the size of the gears in this stage, allowing the planet shafts to be positioned closer to the gearbox centre and reducing the overall packaging size. This method of unequal distribution is ideal for reducing the total volume of the gearbox but required limits the strength of the higher ratio stage due to the larger difference between teeth count required.

For an equal split of the total reduction, each stage would require a ratio of approximately √13 ≈ 3.6. Instead, the first stage reduction was intentionally reduced to be that of approximately 70% of the second stage. This allows the first-stage gears to remain compact. While it demands more of the second stage these are less constrained by packaging and can therefore accommodate the increased ratio. The required ratios can be calculated using (31) and (32) resulting in a required ratio of the first stage, $R_1$ as 3:1 and forcing the second stage, $R_2$ to have a ratio of approximately 4.3:1.

$$R_1 = 0.7R_2 \tag{31}$$

$$GR = R_1 R_2 \tag{32}$$

By defining the single stage ratio allows for the use of the software KissSoft and KissSys, an industrial standard application that is used for transmission solutions. Able to size, analyse and optimise elements and machines. By creating a model of the planetary gearset a large amount of the process can be streamlined and allow for greater number of comparisons of configurations. The model, which is shown in Figure 40 consists of a stepped planetary system with an applied input force on the sun and an output load on the carrier, also included is a block representing the motor and shafts which can also be used to calculate bearings loads and any forces within the shafts. The feature tree is included as a reference of a planetary model and the features included. The model can be further developed to allow for greater control such as the shafts, the model developed for this process focuses on the gears.

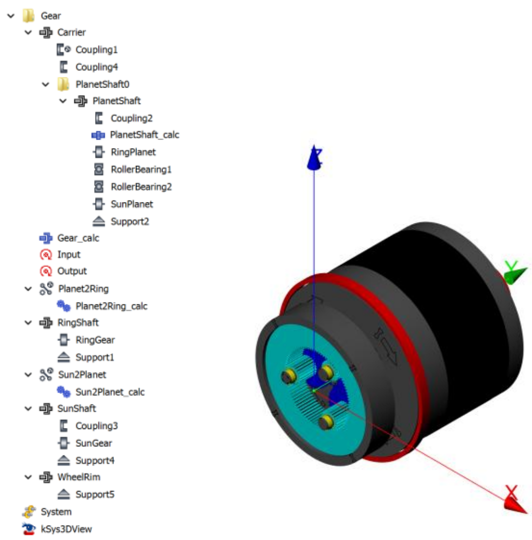


*Figure 40. KissSoft Model*

To validate and better understand the capabilities of the model a simple compound gearbox was created, providing a control case with simple loading conditions. Basic hand calculations were performed using the Lewis equation to find gear stresses based on the loading and geometry of the gears. These results were compared to the stresses reported within KissSoft. With the same additional factors applied as the software, which include the applications factor, dynamic factor and transverse load factor. The hand calculations resulted in the stresses aligning closely with those produced by the model. This process verified the accuracy of the software and provided knowledge of how stress values were calculated.

As mentioned, the software is a powerful tool which for this project is underutilised. The use of KissSoft was limited to the gear sizing, stress calculation and validation, rather than full optimisation of the system. As the goal is to create a foundation of a planetary gearbox emphasis is put on creating a baseline which can be optimised over time.

With some initial requirements set, KissSofts and KissSys were used to model the gear train as previously shown to find optimal solutions. This would be able to show the forces present on gears, bearings and shaft. Becoming an invaluable tool in the process. To begin the process a fine microgeometry sizing was used for the first stage. With open parameters such as module, pressure angle, ratio, centre distance and helix angle. By selecting minimum and maximum bounds as well as a step size the program can step through each iteration that would satisfy the power input conditions. The fine microgeometry sizing ability requires a target ratio with a given variation, with the equation derived previously the ratio target can be set to three. For the analysis the maximum power available from the motor was used, 20,000 RPM and 21 Nm. This power will be greater than the motor will ever be able to produce as at higher rotational speed limits the torque begins to decrease. By having created design estimates previously an educated guess at the boundary conditions could be done, which are shown in Table 5 below.

*Table 5. KissSys Input Parameters*

| | Minimum | Maximum | Step | Unit |
|---|---|---|---|---|
| Module | 0.7 | 1.1 | 0.05 | mm |
| Pressure angle | 18 | 22 | 1 | ° |
| Helix angle | 0 | 0 | 0 | ° |
| Centre distance | 30 | 35 | 0.5 | mm |

Based on these inputs, KissSys can generate gear configurations to meet the required ratio of three varying teeth count in both the sun and planet gear. While there are many factors calculated for each configuration the main point of interest is the stresses, and thus the safety factor of each the flank and the root. This analysis computes a large number of factors including but not limited to noise (dB), mass (kg) and efficiency (%). While these factors would be considered they are not the main selection criteria.

Presented in Figure 41 shows how each configuration compares and shows the trend of module, a higher module is typical of a higher root safety while the flank safety is much more varied with module. The analysis considers the material currently selected within the software, which has not been chosen yet therefore the exact flank and root safety values presented will not be representative of the final value but show the same trend and can be used as a guide but require further analysis to check their eligibility.

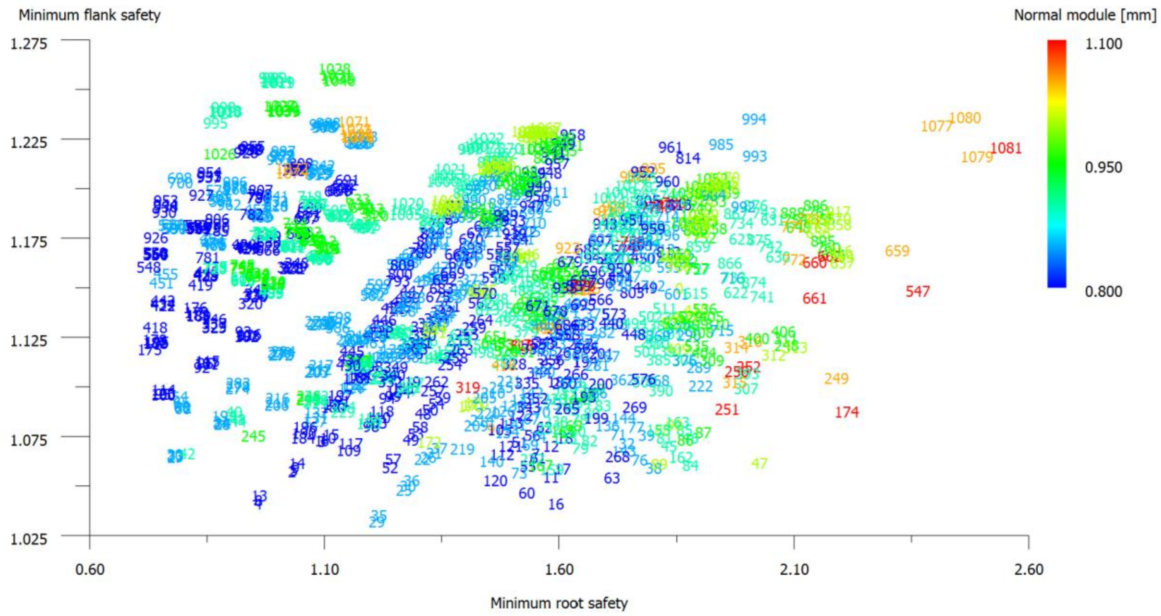


*Figure 41. Flank and Root Safety*

This graph shows the sheer number of possible configurations, as this is only representative of the first stage a large amount of manual checking was still required to check the second stage and ensure this still is within range. By introducing other variables, a better idea of the location on the graph to select can be inferred. Using the efficiency (%), mass (kg), dynamic factor and face load factor. Each factor pushes the ideal configuration into a section of the configurations. Naturally mass is to be minimised, efficiency maximised and the two factors also to be minimised as these are a multiplier on the stress and hence a lower value has less stress concentration.

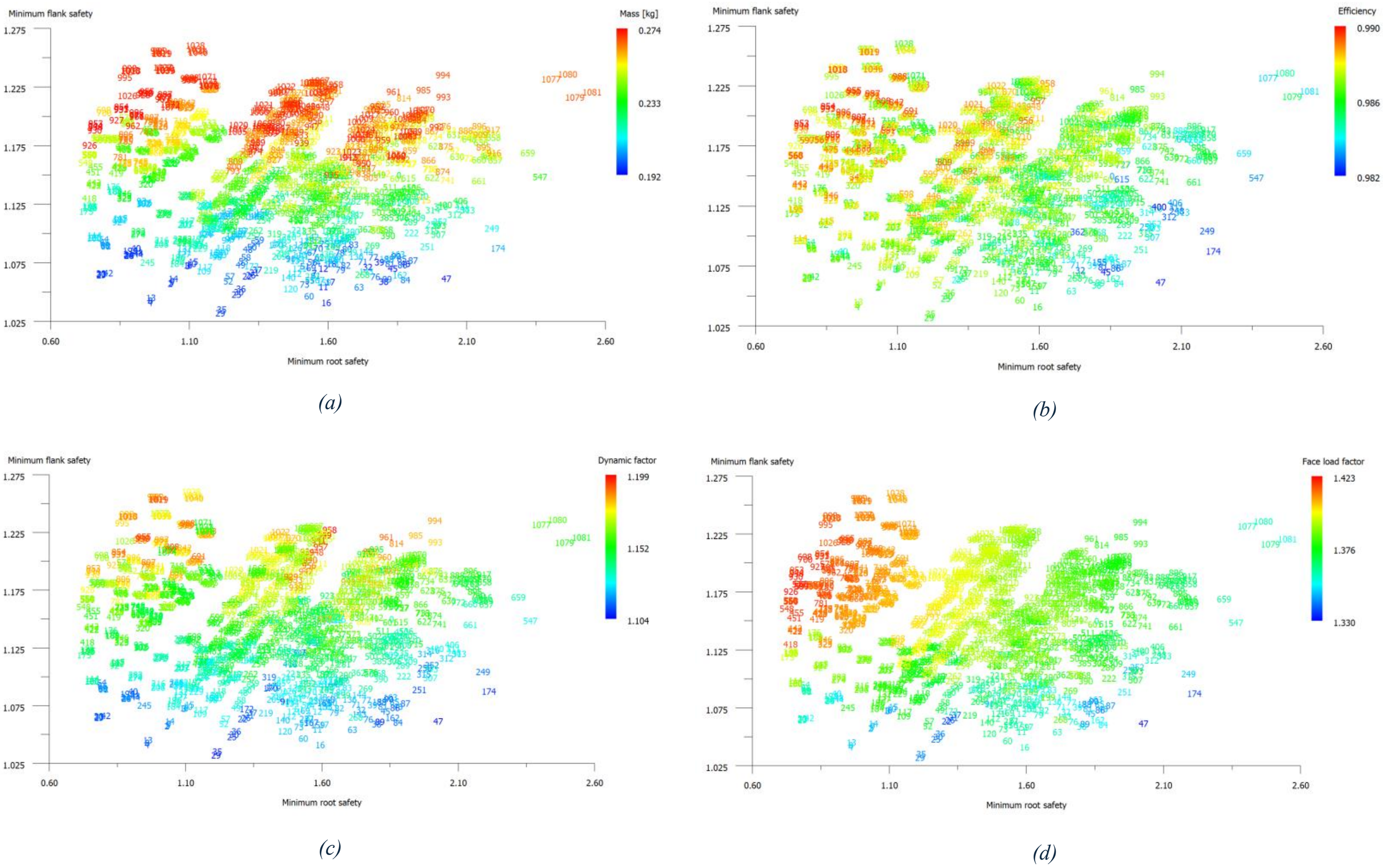


*Figure 42. Gear Safety Factors (a) Mass (b) Efficiency (c) Dynamic Factor (d) Face Load Factor*

A relationship seen is that of the factor of safety effect due to the centre distance, increases to the centre distance increase the flank safety as seen in the Figure 43 below. Likely due to a change in the meshing position and reducing the curvature between two meshing circles. While a larger centre distance provides greater flank safety it will inherently create a larger outer diameter and therefore a larger housing.

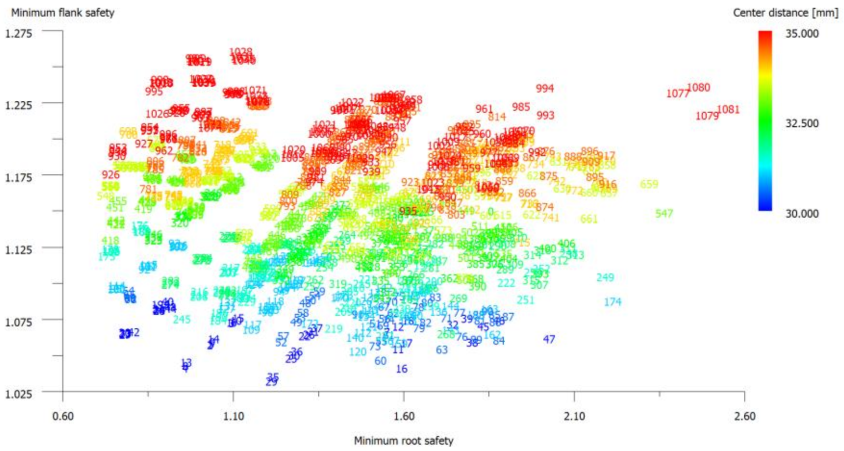


*Figure 43. Gear Safety Factors, Centre Distance*

From the analysis the ideal position on the graph is on the lower right-hand side without reducing the flank safety too much, a configuration can then be picked. For this application once picked the same process is done for the second stage, as the first stage defines the module and the teeth on the sun and the first stage planet. With greater restrictions the number of possible configurations drop significantly. With the given constraints a feasible configuration for the gearbox system can be selected and is presented below in Table 6. These values can be carried forward into greater analysis and design validation. While a given pressure angle is included this is left as a changeable variable based on the loading condition with proper boundary conditions. The gear teeth and module are the critical conditions and remain as difficult to change without effecting other conditions. With the teeth configured the final ratio can be calculated using the formula derived earlier, giving the configuration an exact ratio of 14:1 overall.

*Table 6. Selected Gear Teeth Configuration*

| | Teeth | Module (mm) |
|---|---|---|
| Sun Gear (S) | 16 | 1 |
| First Stage Planet (P1) | 48 | 1 |
| Second Stage Planet (P2) | 21 | 0.914 |
| Ring Gear (R) | 91 | 0.914 |

To ensure the proper operation of the gear selection the stress analysis is to be completed. Using the motor peak operating conditions, 20,000 RPM and 21 Nm. While both are factors that influence the stresses seen, the torque is the primary influencer driving both the stress generated at the root of the tooth and on the face through contact. The rotational speed is still an important secondary consideration as it effects the dynamic factor.

To calculate the applied safety factors the material must be selected. As mentioned in the literature review a gear with high core toughness and hard teeth is optimal. KissSoft has material presets included which show the materials allowable stress, fatigue limit as well as other mechanical properties. By choosing between the case hardening steel as well as nitriding steels a decision could be made to which material was able to provide a sufficient safety factor in the worst case. The material selected was the 18CrNiMo7-6, or 1.6587 Steel. A common steel used in high strength applications ideal for situations such as gears [60]. However, this material was not available by local suppliers, instead opting for EN39B a similar alloy capable of the same mechanical properties under the right treatment conditions.

The pressure angle can also be varied to slightly adjust the amount of force required for the gear tooth, by changing the value the amount of force split between the tangential force and radial can be altered slightly. An initial estimate of 20° was used due to being a standard, from there the second stage had to be increases slightly resulting in a 22° pressure angle.

KissSoft can effectively apply the required profile shift to prevent undercut and allow the tooth the greater bending stress applicable. Resulting in the final meshing geometry which is presented in Figure 44 as well as all gear geometric parameters presented in Table 7. This profile shift is also required to the change in centre distance, to provide greater flank strength. By increasing the centre distance to 32.5mm compared to standard 32mm adds an additional amount of flank strength and required an amount of profile shift. This is also a critical reason to using EDM wire cutting to accurately recreate the desired geometry.

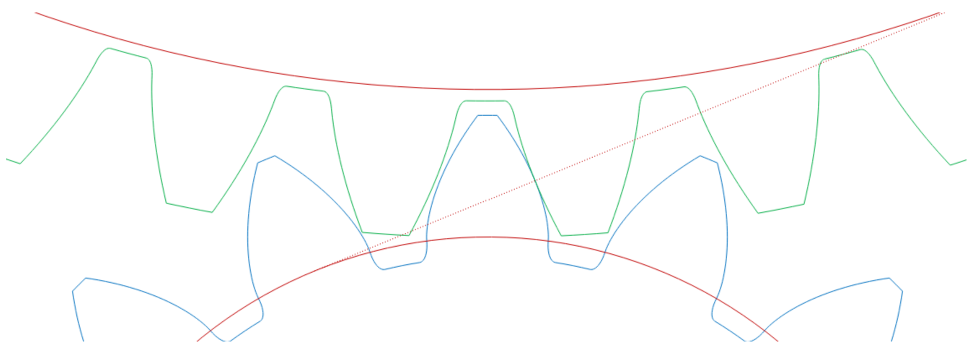

*(a)*

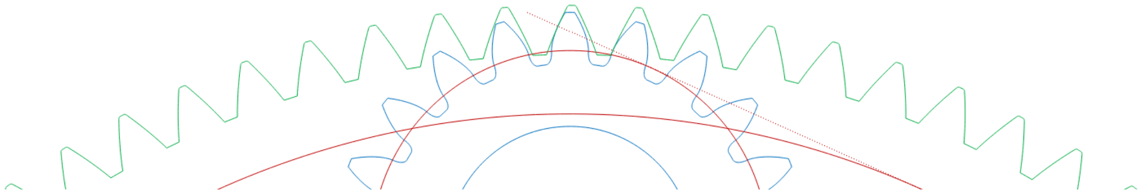

*(b)*

*Figure 44. Meshing Geometry (a) Stage One (b) Stage Two*

The last criterion for a gear is the face width. Having a direct effect on the stresses present. In both cases a larger face width reduces the stresses. While increasing the face width reduces the stress the bending moment on the shaft will increase due to the increase to distances, the mass will also increase. The face width was chosen for the current geometry to achieve a factor of safety of over one.

To ensure that each planet engaged along the face of the gear each face width was altered to allow for slight overlap. The final gear geometry is presented below in Table 7

*Table 7. Complete Gear Geometric Parameters*

| | Teeth | Module (mm) | Face Width | Pressure Angle | Profile Shift |
|---|---|---|---|---|---|
| Sun Gear (S) | 16 | 1 | 18 | 20 | 0.5280 |
| First Stage Planet (P1) | 48 | 1 | 15 | 20 | 0 |
| Second Stage Planet (P2) | 21 | 0.914 | 20 | 22 | 0 |
| Ring Gear (R) | 91 | 0.914 | 18 | 22 | 0.5840 |

After the final refinements, the final gear geometry was checked within KissSoft to determine the resulting safety factor for each gear. Both root and flank safety were considered and check under different load conditions. The final safety factors presented in Table 8. Each load condition follows either peak torque and speed, maximum speed where maximum torque occurs based on the data sheet, and nominal speed and torque as calculated previously. This furthermore backs up the fact that the torque is the main limiting factor for gear strength.

*Table 8. Gear Safety Factors*

| | 20,000 RPM 21 Nm | | 14,000 RPM 21 Nm | | 8,000 RPM 8 Nm | |
|---|---|---|---|---|---|---|
| | Root | Flank | Root | Flank | Root | Flank |
| Sun | 1.916 | 1.138 | 1.988 | 1.146 | 5.148 | 1.813 |
| First Stage Planet (P1) | 1.784 | 1.189 | 1.851 | 1.231 | 4.793 | 2.042 |
| Second Stage (P2) | 1.081 | 1.297 | 1.102 | 1.330 | 1.887 | 1.765 |
| Ring | 1.025 | 1.548 | 1.044 | 1.588 | 1.740 | 2.108 |

The minimum safety factors presented are very close to one but due to the highly unlikely nature of ever reaching these peak values they are deemed to be sufficient. Further testing would be ideal to ensure they are able to handle the loads and not prematurely fail.

With the gear selection the design of the housing and associated components can be completed detailed in the next section.

## 4.2 Detailed Design

With the primary design constrain of the gears decided work can begin on the overall architecture. Design of each component was primarily driven by geometric constraints and assumes the gears will be the weakest portion of the design. Hand calculations or Finite Element Analysis (FEA) performed on pieces which have thinner cross sections or made of weaker materials.

### 4.2.1 Gear Positioning

To maintain compactness the ring gear was thought to be placed on the motor side of the system. This would decrease the total length, a depiction of how each gear would interact is shown below in Figure 45, where each gear is simply represented with a black input, and green stationary ring gear. This would also allow for greater serviceability by being able to access the planets from the wheel side likely avoiding the need to remove the gearbox off the car completely. The configuration however was unobtainable due to the length of the motor splined shaft, which would not allow for significant face width of the second stage planets and ring gear. Construction of an adapter to effectively extend the motor shaft is achievable, although this was opted to be left out of the design to simplify the manufacturing stage. The shorter motor shaft also reduces the amount of stick out and will lead to a more stable rotation.

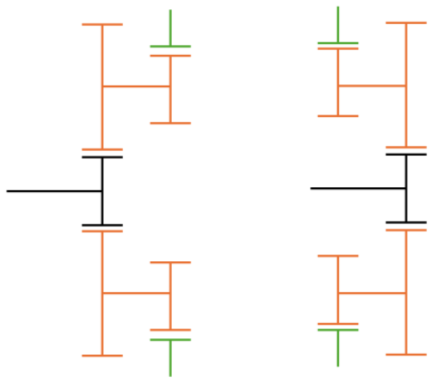

*Figure 45. Stepped Planetary Detailed Configurations (Left) Ring Gear Wheel Side (Right) Right Gear Motor Side*

### 4.2.2 Housing and Carriers

The housing and carriers are critical components, combined create the structural backbone of the gearbox system. Creating a skeleton for components to attach to and creating load paths, the design of each component is primarily driven by geometric constraints but must be checked to ensure failure does not occur.

Aluminium alloy 6061-T6 was chosen for the primary alloy for each component due to its high strength to weight ratio. Where weight is of major concern adhering to low weight materials are critical. Aluminium alloys are readily machinable and make a suitable candidate for the application.

The design scope of the carrier and housing were intentionally chosen to be gear box specific. Integration of external systems such as suspension pickup points, brake caliper mounting, and wheel attachment methods were left unexplored, and considered out of scope. This separation simplifies the design in portions and allows greater detail in the specifics of the gear systems and functional components.

To ensure the component does not fail during use an FEA analysis was completed on the motor side carrier. The selected component represents the critical case, featuring thinner cross sections and an increase in stress concentrators.

The model was constrained using a bearing support applied to the bearing mating surface, representing the bearing and allowing for rotational motion while constraining movement in axial and vertical direction. The maximum torque of 294 Nm was applied as distributed across each shaft location to represent the transmitted load through the gear system. The shaft locations are presented in the figure beginning at 12 o'clock and spaced 120° apart. The bolt holes present were fixed to fully constrain the model, as well as a roller support on the mating face between the two carriers as though bolted together. Each bolt hole is shown in the figure beginning at 6 o'clock and spaced 120° apart.

The resulting stress distribution shows large areas of low stress with high values around the stress concentrators as expected. These areas of high stress are still within the yield strength of aluminium 6061 T6 of 276 MPa [61]. The minimum safety factor is then therefore 2.6. These areas of stress concentration can be seen in Figure 46 and Figure 47

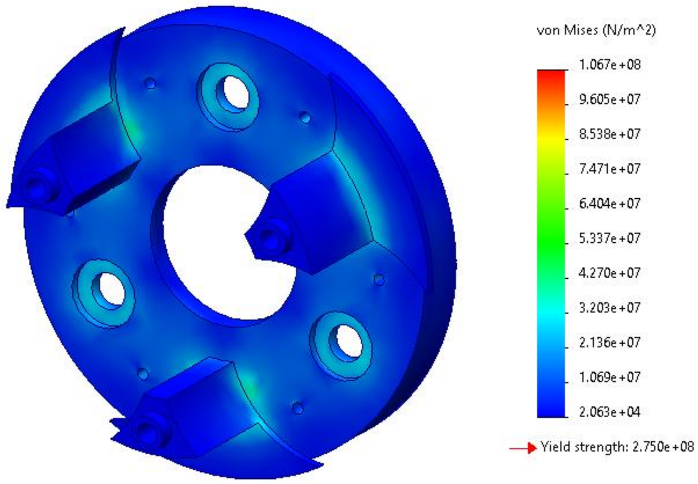


*Figure 46. Motor Carrier FEA*

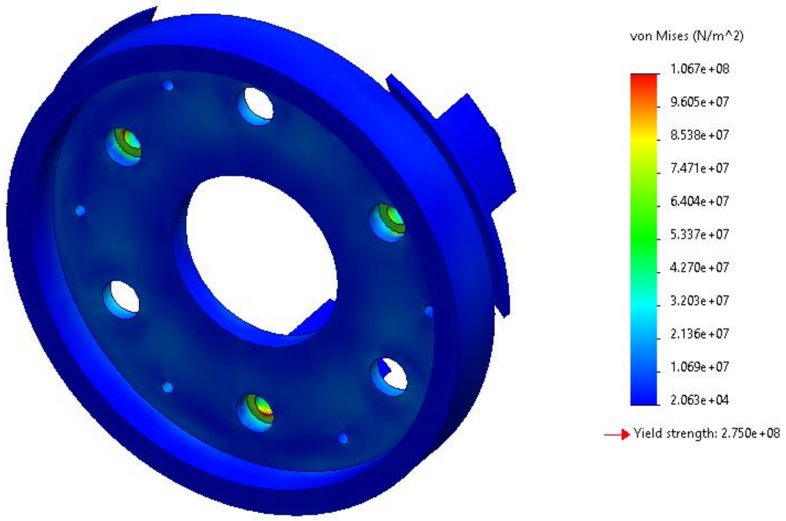


*Figure 47. Motor Carrier FEA Opposite Side*

Stress concentration within the model is likely to be inflated from actual, due to the sharp edges present within CAD. In practise manufacturing tooling includes a small radius as a part of the cutter geometry. While these may have small effects on the stress present but are negligible due to the safety factor present.

### 4.2.3 Shafts

The common shaft which allows for the planets to spin on a separate axis compared to other rotating components is a critical component. The torque generated by the motor is increased by the gear ratio, while also being ideally distributed among the planets. Both these values are equal to three and hence cancel each other out leading to the torque in the common shaft being equal to the motor output torque.

To facilitate torque transfer between the two planet gears they must be coupled together. There are multiple options that allow for this, making the two gear stages of one piece is a practical high strength method, however for the gears to then be wire cut would not be possible. Two separate pieces must then be considered.

Torque transmission between the two planets can be achieved through an splined interface. Using the external gear profile of the smaller second stage planet as male spline profile, mating with a corresponding internal matching profile on the larger first stage planet. Allowing the two gears to be pressed together to form a single rotating component. As torque is distributed between all teeth within the spline able to provide sufficient strength. An exploded view of the arrangement can be seen below in Figure 48.

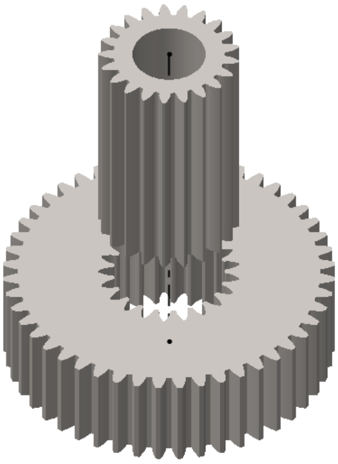

*Figure 48. Exploded Gear Spline Configuration*

The gear assembly can then be coupled onto the shaft using bearings which are further analysed in the bearing section. A shoulder can be added to one end of the shaft and a circlip groove added to the opposite end to prevent axial movement.

When the shaft is installed into the carrier they are floating, with allowable movement back and forth, allowing some movement will cause the gears to shift into their natural position and not cause unnecessary stresses due to misalignment.

Due to the gears mounted on the shaft the force will be transmitted through into the shaft. At the maximum motor torque the shaft will experience 21 Nm. Each gear will introduce a tangential and radial force on the shaft based on the fundamental torque formula.

Using the pitch circle radii of each gear, the tangential force ($F_t$) can be calculated. Additionally, the radial force ($F_r$) along with the resultant force ($F_R$) can be calculated using Equations (33) and (34). With the pressure angle ($\alpha$) of each gear set at 20° and 22° for planet one and planet two respectively the resulting forces can populate the table below, Table 9. Although each shaft has a different working pressure angle due to the profile shift this effect is negligible, using the adapted pressure angle results in a change to the resultant force of 916N to 931N a 2% difference.

$$F_r = F_t \tan \alpha \tag{33}$$

$$F_R = \frac{F_t}{\cos\alpha} \tag{34}$$

*Table 9. Shaft Forces via Planet Gears*

| | Ft (N) | Fr (N) | FR (N) |
|---|---|---|---|
| P1 | 861 | 313 | 916 |
| P2 | 2153 | 869 | 2323 |

A free body diagram can be constructed, assuming each gears resultant force acts as a point load, and each end acts as a roller support, as there is no fixture or fastener locking the shaft axially. Utilising the forces, as well as the length of the shaft and where the shaft is not supported by any material within the gearbox will be able to calculation the bending moment along the length of the shaft. The free body diagram is made and found in Figure 49 and can be used to find the reaction forces, shaft shear force diagram and shaft bending moment diagram and an estimate of the maximum deflection.

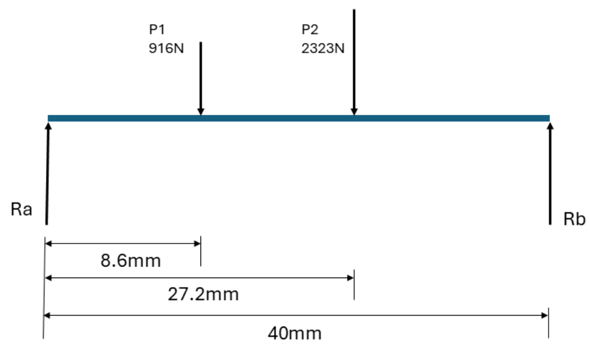


*Figure 49. Shaft FBD*

The shear force and bending moment diagram can be obtained from the applied loads, where detailed calculations are provided within Appendix C. Each graph is presented in Figure 50 showing the maximum shear expected is 1777 N and maximum bending is 22.7 Nm and where they occur.

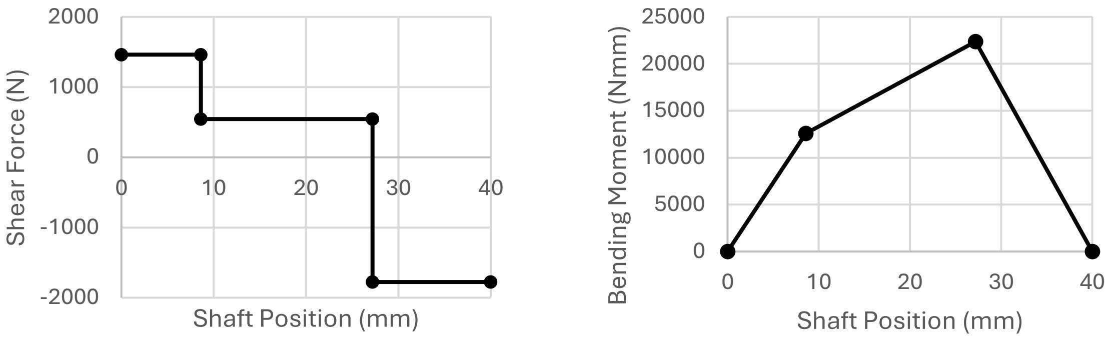


*(a)* *(b)*

*Figure 50. Shaft Force Diagrams (a) Shear Force (b) Bending Moment*

With maximum bending moment found can be adapted into the bending stress experienced by the shaft, using Equation (35). Based on the shaft diameter found within the bearing section of 8mm used the stress can be calculated and results in 445 MPA

$$\sigma_b = \frac{My}{I} \tag{35}$$

The shear stress induced by the torque is also be calculated based on the maximum input torque. Where J indicates the polar second moment of area, calculated based on the circular cross section with the appropriate diameter. The torsional stress can be calculated using Equation (36) resulting in a shear stress of 209 MPa

$$\sigma_\tau = \frac{Tr}{J} \tag{36}$$

As with the bending stress the polar second moment of area is dependent on area and will be different for each gear. The following calculations can be performed to gather a more realistic shear stress value.

The Von Mises stress is calculated to determine the combined effect of the bending and shear stress. For a circular cross section subjected to each of these conditions Equation (37) can be used [36]. Using the values for the shaft maximum bending stress ($\sigma_b = 445\ MPa$) and the shear stress ($\sigma_\tau = 209\ MPa$) results in a stress of 573.6 MPa.

$$\sigma_{vm} = \sqrt{\sigma_b^2 + 3\sigma_\tau^2} \tag{37}$$

The bending moment stress is the main contributor to the stress experienced by the shaft. Based on the stresses applied high tensile 4140 steel is a suitable candidate. The steel supplied is hardened and tempered with the minimum yield stress of 850 MPa [62]. Giving the shaft a safety factor of 1.5 under maximum, worst case operating conditions. While still being machinable and provide a smooth surface for the bearings to run on.

An estimate of the expected deflection is also calculated, although the unsupported span is very short at only 40mm, determining the deflection provides a useful check to confirm the shaft stiffness is sufficient and the gear alignment is not influenced. An estimation calculator is to be used instead of full integration from the Euler-Bernoulli beam theory for simplicity. By creating a model and using the correct stiffness and moment of inertia is able to estimate the maximum deflection of 0.08mm [63]. The estimated deflection is minor to any other tolerances and therefore the shaft deflection does not have an influence on the system. Making the shaft suitable for application.

Under operating conditions, the presence of the gears is likely to contribute to a decrease in stresses due to the increased radii, and therefore second moment of area. The gears will resist bending. This is a consideration which will increase the shafts safety of factor throughout operation.

### 4.2.4 Bearings and Seals

A major portion of the gearbox design is the bearings and seals and their integration. With the housing remaining stationary and the central carrier rotating there must be bearings at the interface between the two to support the radial and axial load. Many of the components detailed design are influenced heavily by the bearing selection. As commercially available bearings and seals are used, they must integrate within the design. To provide support on the carrier two bearings were implemented, one the motor side and one on the output side reducing any bending moments within the carrier.

Estimates of the required dynamic load rating were taken from previous design reports of the rear uprights, showing a required load rating of 20.9 kN across both bearings [64]. While this value could have been recalculated for the application, the validation of previous upright designs was deemed sufficient, as well as the bearings selected being significantly above the required value. This was due to the selection being primarily governed by the physical dimensions.

These design reports also note the type of bearing used, deep groove ball bearings. Although the bearings in the gearbox will be subjected to axial load, transmitted from lateral loading of the tyre through the gearbox into the suspension arms. The deep groove ball bearings are still able to take a portion of axial load and have been considered when finding the required dynamic loading. The loading condition is like previous upright designs used within WESMO which have had no issues with axial loading on the bearings.

Additionally, deep groove ball bearings allow a much simpler installation compared to alternatives such as angular contact bearings. While angular contact bearings can support much higher axial load comparatively, they require a set preload for optimal running.

This makes deep groove ball bearings a suitable selection to balance load capacity and simplicity.

The bearing supporting the motor side, subsequently named the motor bearing. Not to be confused with the bearings internal to the motor. This bearing was primarily constrained by the packaging requirements of the carrier and the planets. As the planets are located on the wheel side of the bearing, they must pass through the area where the bearing is positioned during assembly. This can be seen visually in the Figure 51 below where when assembled from the right hand side of the page. The orange gear tip envelope intersects with the blue bearing envelope, demonstrating that the bearing outer diameter must be greater to allow for assembly clearance.

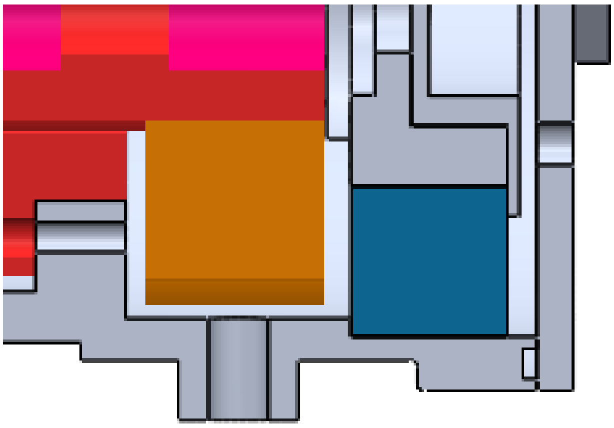

*Figure 51. Bearing and Gear Tip Envelopes*

This requires the bearing outer diameter (OD) to be larger than the addendum of the sun planet gears to allow for clearance during assembly. By The measured value based on the tip diameter of 49.93mm, obtained from KissSoft and measured using SolidWorks. The results show the minimum internal clearance diameter of 113.93mm and to ensure enough at least 115mm is selected as the minimum internal diameter of the housing.

The bearing must have an OD larger than this value of 115mm, while still allowing sufficient material for a locating shoulder. Standard metric bearings at these sizes are available in discrete measurements of 5mm. With the given criteria an OD of 115mm would not allow for clearance and a locating shoulder therefore, a larger OD is required and thus the next available size is 120mm and is the minimum viable option. As the OD is the only constricting dimension following dimensions had the goal of minimising the mass via the cross section and width. By reducing the cross section enables thinner sections of the steel bearing and allows for lighter aluminium to be used in place instead, which as mentioned previously is a large goal for the unsprung mass. From the options available the SKF 61819 Deep Groove Ball bearing was identified, having an OD of 120mm, 95mm ID and a width of 13mm as well as a dynamic load rating of 19.9 kN [65].

In addition to its mechanical properties the catalogue mentions the minimum radius on the edge and thus the minimum shoulder required. With a minimum edge radius of 1mm a 1.5mm shoulder allows for sufficient shoulder material and still allows for a 117mm internal clearance bore for the planets. Additionally, as the bearing is retained within the housing assembly and thus within the flooded gearbox it can remain as an open type, allowing for lower friction without the bearing seals and still ensuring sufficient lubrication. A seal was not required for the motor side as the motor comes equipped with a seal to prevent leaking of fluids.

A similar process was undertaken for the output, or wheel side bearing. Similar restrictions applied with the boundary condition now being the side of the ring gear. While this ring could have been designed to installed from the motor side and allow the output bearing greater freedom, this configuration option was not considered during the initial design phase and presents an area of improvement if required.

The output side also requires a sealing solution to prevent leaking lubricate. A rubber O-ring was considered but the use of a rotary seal was deemed more robust. By having both the bearing and the seal as the same OD results in a simpler design and therefore manufacture when machining the bore. A smaller ID on bearing allows for the output side of the carrier to be used as the shoulder instead of directly interacting with the seal as a shoulder. Alternatives were considered such as using circlips as shoulder but removed to ease with assembly. However, a single circlip remained to prevent axial movement of the bearing out towards the wheel.

Similarly with the motor side bearing the cross section and width were minimised to save on mass, leading to a selection of the SKF 61818 paired with a 115x12x95 seal. An SKF 61818 has a OD of 115mm, 90mm ID and a width of 13mm, paired with a dynamic load rating of 19.5kN [66]. Across both supporting bearings these ensure they meet the required dynamic load rating as established previously. Both bearings also exceed the limiting speed as shown in their catalogue expecting only low speeds of up to 1428 RPM when experiencing the maximum motor speed.

The final bearings of the system are those that allow the planets to spin, as the planets will rotate at a different rate and on a different axis to the carrier. Requiring to support the rotational loads and orbital loads. Two main configurations are available, the planets spinning on the shaft or the planets coupled with the shaft with the entire system spinning. These configurations are depicted in Figure 52 and Figure 53. The decision has significant implications on the packaging and bearing selection of the system.

An alternative was considered to use a plain bearing relying on a thin oil film, similar to a crank shaft found within an engine. This was avoided due to the complexity, compared to a simple ball or roller bearing.

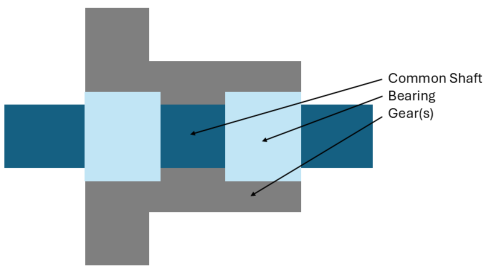


Figure 52. Planets Rotating on Shaft

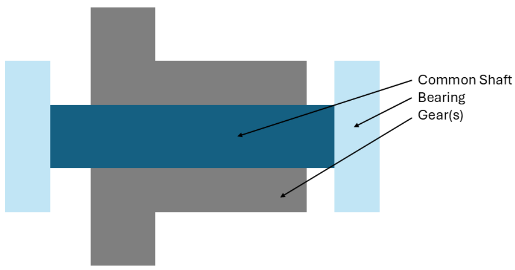


Figure 53. Planets Rotating with Shaft

Placing the bearings on the end of planet shafts as with the rotating shaft configuration enables the use of larger capacity bearings with the increases volume to work within. However volume within the gearbox is a premium to avoid unnecessary bulkiness. This design is feasible for the output carrier side with volume available in the carrier but heavily constrained on the motor side. Additionally the configuration requires the shaft and all associated mass to rotate increasing the rotational inertia, influencing the dynamic performance. Further more this design would require higher precision to ensure concentricity for smooth operation.

Adversely allowing the planets to freely rotate on the shaft simplifies design, manufacture and assembly. Reducing the number of required components such as the bearing retaining features and power transmission between the shaft and planet gears. Therefore the free rotating planets were selected for the final design. This comes with the additional benefit of minimising the rotating mass and reducing the rotational inertia.

With the bearings required to be integrated into the planet gears themselves a thin section bearing is required, needle roller bearings are ideal for the situation due to their reduced cross section profile. The selection of the needle roller bearings is constrained is imposes by the gear design of the planets, in which the smaller ring planet is pressed into the larger sun planet. This limits the available bearing envelope to the dedendum or root diameter of the ring planet gear, 16.8mm.

Alternatively, a larger bore could be machined in the sun planet and allow for a larger diameter bearing to be used on the sun planet side. This would strengthen the system but would limit the length of engagement between the two gear pieces. Limiting not only the torque transmission the but the axial retention strength. Given that the loading on the larger gear as shown previously is lesser this decision was deem not required. Utilising two of the same bearings on each end of the planet gear assembly allows for greater serviceability by including a smaller number of unique parts.

Unlike the larger wheel bearings discussed previously the use of the needle roller bearings have not be integrated into an upright or gearbox before requiring deeper force analysis. From the force analysis from the gear section. The bearing supporting the load from the smaller ring planet gear is the limiting criteria

Based on the force calculations throughout the shaft the bearings would be subjected to a maximum of 2.323 kN radially. Subjected to little to no axial load this is the dynamic load a bearing must support. It is assumed that each bearing supports the force closes to it, while this may not be accurate it gives a reasonable estimate.

To reduce the selection criteria some assumptions were made to the design of the shaft and bearing. Assuming a shaft range of 7-9mm and hub bore of 11-14mm allows for the available options to be reduced to a handful. Of those present the higher dynamic load rating options were both above 5 kN, the K 8x11x13 TN and the K 9x12x13 TN, their designation shows the dimensions listing IDxODxWidth.

As both bearing have similar dynamic ratings the decision to use the smaller of the two was chosen, this allows for the gear to have more material beneath the root and provide greater support for the gear teeth. This also decides the diameter of the shaft.

Based on the dynamic load rating of the bearing and the forces present a $L_{10}$ estimate can be calculated using Equation (38). This is the time 90% of bearings are able to achieve under the same loading. Within the equation the $L_{10}$ represents the cycles, $C_0$ dynamic load rating, ρ a constant either three for ball bearings or 10/3 for roller bearings, lastly P as the load experienced.

$$L_{10} = \left(\frac{C_0}{P}\right)^{\rho} \tag{38}$$

$$\left(\frac{5.01}{2.323}\right)^{\frac{10}{3}} = 12.96 * 10^6 \ cycles$$

Factoring in the rotational speed of the gears on the shaft which can be calculated using Equation (39) below [67]. A maximum motor speed each planet gear rotates at 4761.9 RPM and gives 45.36 hours of run time. This can be further approximated to distance of 5278 km much higher than the predicted requirements. This is inconsistent with the results presented by KissSys showing 61 hours, for the same bearing. This discrepancy is likely due to the load applied to the bearing due to the supports added into the model which take a small amount of reaction force. As well as KissSys reporting a different working pressure angle. While the results show a 17% difference the much higher life expectancy of the second bearing due to the lower forces can be estimated using KissSys for simplicity. The $L_{10}$ for the second needle bearing can be said to be 421 hours, significantly higher.

$$\omega_p = \omega_c(Z_{p1} + Z_s) - \omega_m Z_s * \frac{1}{Z_{p1}} \tag{39}$$

*Where*

$\omega_p, \omega_c, \omega_m$ *– rotational speed of planets, carrier and motor respectively*

$$\frac{12.96 * 10^6}{4761.9 * 60} = 45.36 \ hours$$

The $L_{10}$ of a bearing indicates 90% reliability it can be assumed the life will be longer, additionally the time constant is under maximum load, when subjected to the nominal loads calculated the $L_{10}$ becomes 3992 hours or 185,796 km.

The figure below shows a complete cross section, including the position of hardware. Where blue represents the 61819 deep groove ball bearing, yellow represents the 61818 deep groove ball bearing, black the rotary seal and pink the needle bearings, which are present within all three gear assemblies. Once bearings were selection a conversation with the bearing supplier was had confirming fit for application and any details which required attention of which none were seen.

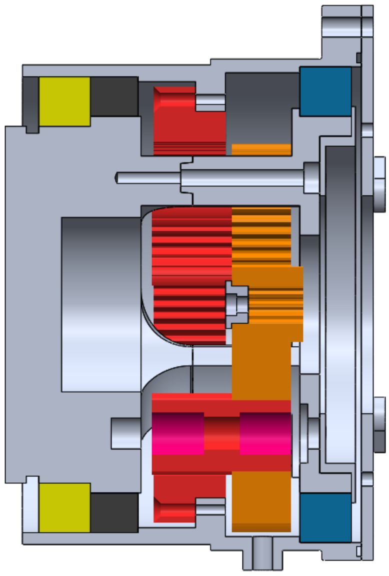

*Figure 54. Gearbox Cross Section*

Unlike the wheel side the motor side has a plate to separate the inside from the outside, as the motor includes a seal. Therefore, a way to prevent the leakage of oil between the interface of this plate and the gearbox housing must be included. Figure 55a illustrates the area where the motor plate and housing meet. While a gasket could easily be laser cut of gasket paper an alternative design solution was instead adopted. The decision was made to increase the wall thickness and incorporate a groove for an O-ring, due to the eventual repeated disassembly as well as to give a visual indicator for a sealing method to future students, minimising the risk of it being left out.

Due to large sealing diameter, suitable off the shelf O-rings are unavailable to source in the required size. The O-ring required would then have to be made fit for purpose made from a O-ring chord and adhesive. To minimise the additional material needed to be added a smaller 1.6mm diameter chord was chosen to be used. Figure 55b shows the eventual groove which is added to the housing.

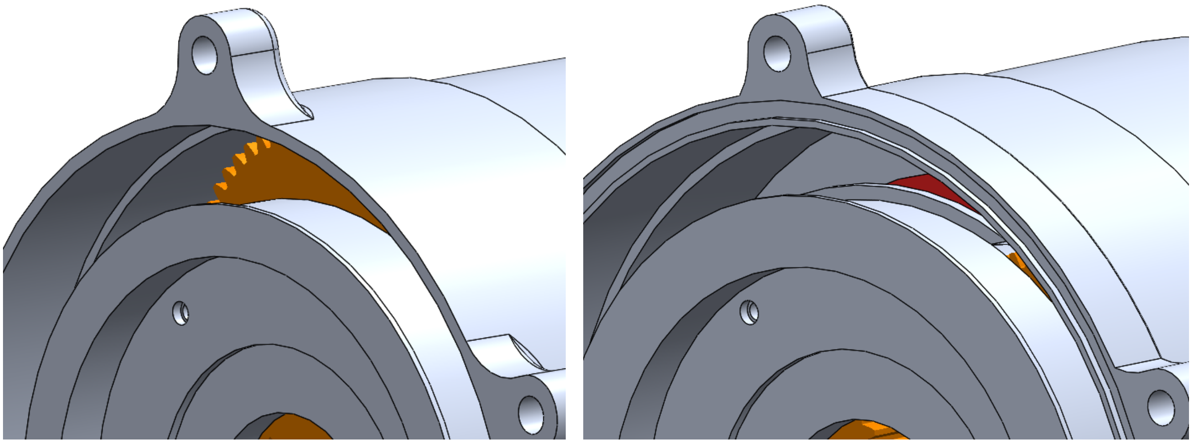

*(a)* *(b)*

*Figure 55. Motor Plate Sealing Face (a) No Groove (b) Grooved*

For an O-ring to operate and seal correctly the groove must be correctly dimensioned. Ensuring the correct amount of squeeze and volume fill, which are recommended as 8% to 35% and <85% respectively [68]. By adhering to these recommendations, it ensures the O-ring is not over compressed leading to early failure or not sealing.

Manufacturability is a large consideration also, the groove must be able to be machined with available tooling, ideally with a trepanning tool or similar. As machining tools on hand are minimum 2mm wide the groove must meet this condition, making it the primary boundary condition. While many configurations exist that are plausible the option used is a 1mm wall on either side of the groove leading to a 122mm ID and a chosen 127mm OD, leading to a 2.5mm groove width. After which the depth can be varied to achieve the required amount of squeeze and volume fill. Using an O-ring designer calculator, the selected groove depth of 1.2mm resulted in a squeeze of 25% and a volume fill of 66% falling within the recommended values [68]. Naturally the manufacturing will not be ideal and will fall short of exact due to not having the exact right tooling but remaining in the middle of the recommended values for squeeze allows for difference between the CAD model and real-world part.

This same sealing method was used for the cooling jacket interface which will be mentioned in a later section.

#### 4.2.4.1 Tolerances

With the bearings and seals selected the correct tolerance must be applied to ensure for smooth, effective running and achieve the load rating a life expected. The required fit is dependent on the types of load the bearing will experience, as well as the relative stationary components.

For this design where considering the deep groove ball bearings, which have the load rotating on the inner race or the carrier and the stationary outer race interfacing with the housing. In these situations a clearance fit is recommended on the housing and an interference on the shaft [69].

Based on SKF table 1, a k5 interference on the shaft is selected [70]. However, this value is typical for solid steel shafts, as each bearing is mounted of an aluminium shaft it was increases to be one step tighter, allowing for the different in materials thermal expansion properties. This results in a k6 fit on the shaft for each deep groove roller bearing. Similarly the housing tolerance was explored, table 4 indicates an H7 fit [70]. The same methodology applies and the resulting fit is selected to be one step tighter for aluminium at H6. The resultant fits therefore are selected to be H6/k6.

The resulting tolerance band for both deep groove roller bearing is H6/k6. Using an ISO 286 limits and fits table this translates to a dimension tolerance of 0 to 22 microns on the hub of clearance and 3 to 25 microns of interference on the shaft [71]. Both bearings lie within the same dimension band and therefore have the same measurements associated.

As the wheel side bearing and seal share the same housing bore it was opted to share the tolerance, while increasing the dimensional precision required for the seal it would be more effective than machining both surfaces to be the same.

Unlike the previous aluminium housing and shafts the needle roller bearings are operating between the steel shaft and steel gear, allowing for the tables provided by SKF to be directly applied. Table 2 gives three tolerance zones, the medium operating conditions were selected and used resulting in G6/h5 fit [72]. Translating to a dimensional measure results in 0 to 6 microns of clearance on the shaft and 6 to 17 microns clearance on the gear. While these are very tight tolerances the difficulty of the manufacture is detailed further in the manufacturing section.

With tolerances for individual bearings and press fit established it remains as not the only contributing factor. The concentricity between each bearing set and the circularity of a single seat is important. From the same tables as each bearings fit a radial runout tolerance can be established. For each major deep groove ball bearing the radial runout is specified as IT4/2 for the shaft and IT5/2 for the housing [70].

### 4.2.5 Shear Bolts

Due to the tight packaging of the bolts holding on the ring gear a large quantity of small diameter were employed. Under the maximum torque condition applied through the ratio the ring experiences 294 Nm, resulting in 5680 N distributed among the bolts. A similar calculation was performed for the carrier, in the worst case all shear stress is assumed to be transmitted through the three bolts holding each half of the carrier together. With proper preload the torque can be transmitted through the friction between the two pieces as well as the pins on each end of the legs in addition to the bolts. The carrier is subjected to the same torque as the ring gear of 294 Nm, resulting in 9187 N distributed on the three bolts. In each of these conditions the stresses are calculated as single shear.

The shear stress of a bolt can be approximated as a proportion of its yield strength giving $0.577\sigma_y$, the yield stress of a grade 12.9 bolt has a minimum of 1100MPa. With Tensile areas of M3 and M4 bolts given as 5.03mm$^2$ and 8.78mm$^2$ respectively the safety factors for each of the mounting solutions above can be computed [36]. Each of the ten ring gear mounting bolt experiences 113Mpa, leading to a safety factor of over five. While overengineered for strength it allows for proper installation of the ring gear and keeps it flat against the housing in all positions preventing binding among the planets. Each carrier bolt experiences a much greater 350Mpa, showing a safety factor of 1.8 in the worst case sufficient for normal operating. The lower safety factor gives the added benefit of in the unlikely scenario of extreme overload these can shear and protect the motor from serious damage.

### 4.2.6 Motor Cooling

During testing of the gearbox the AMK motor must be cooled within the specification supplied by AMK, to achieve this a cooling sleeve that fits over the motor was designed. Using O-rings to prevent water leakage from the front and back. The cooling channels in which water runs was not optimised as this lies out of scope of the project. The jacket utilises a simple square spiral channel to promote water flow from the inlet to the outlet. With water flowing over the motor outer casing. The design incorporates blind internal tubes and can be manufactured using additive methods. The prototype manufactured is from PLA printed using FDM, for small scale test and running this may be suitable it is recommended to use a material suited for higher temperatures to avoid warping and leaking. With AMK logos debossed on one side to satisfy sponsorship conditions and a WESMO bull on the other the side for style. The final design of the jacket can be observed below in Figure 56.

*Figure 56. AMK Water Cooling Jacket*

As mentioned, the jacket also incorporates an O-ring style seal similar to the motor plate, to prevent the coolant from leaking from either end. To prevent unwanted leakage in the case of failure a dual O-ring setup was used on the end which has the high voltage connections and one on the opposite end. The same O-ring groove calculator was used under different conditions, such as a static piston situation. Given the low operating pressures this approach was considered sufficient without any further development.

### 4.2.7 Final Design

Additional components were designed that require little description but are still critical to the overall operation of the system. A small piece to hold the sun gear on with a bolt to the motor shaft to prevent axial movement. A bearing retaining plate to capture the bearing on the motor side, this plate also covers the three carrier bolts preventing these from coming loose. A motor plate which the motor will connect to and seal the gearbox. Small tabs to connect the water cooling jacket to the motor, using counter sunk bolts so that it can lie on top of the motor plate. Hose barbs for plumbing in the motor jacket. These can all be seen in the final design present in Figure 57 excluding the tabs to hold the cooling jacket.

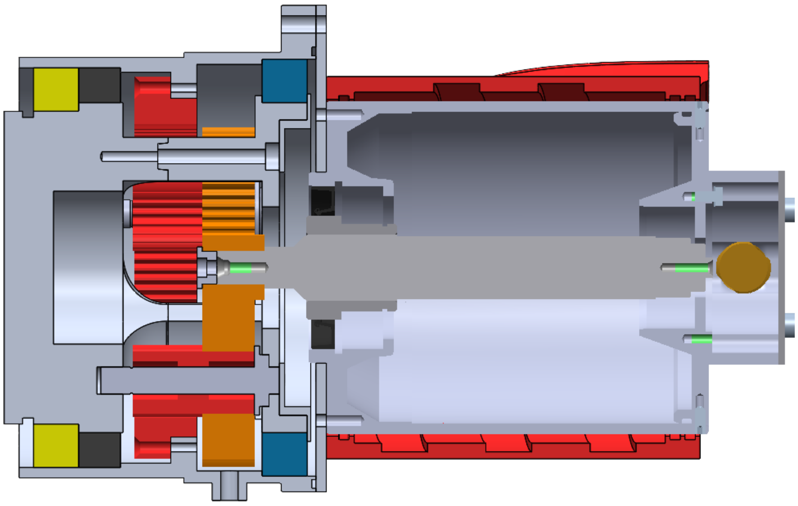

*Figure 57. Final Design Cross Section*

Fused Deposition Modeling 3D printing was used extensively throughout the design and manufacture process, ensuring that designs had enough clearance and was able to be assembled. Being able to design components and rapidly print them to ensure they assemble in the desired way is critical. As manufacturing each piece of aluminium on a manual lathe is a large time investment to find out modifications are required. An entire system was able to be printed from the gears to the housing, creating a complete working model before manufacturing began. Some of the pieces are shown in Figure 58 and can be compared to their final manufactured pieces as they are machined.

*Figure 58. FDM Printed Test Pieces*

With the final design complete, with only minor changes due to manufacture to occur a volume of the cavity can be taken to find the oil volume needed. Creating an additional part within SolidWorks and using it to find a volume using a cavity feature to predict the quantity of oil required. While the cavity will not be exact due to missing bolts within the model as well as representing seals and bearings as a solid cylinder rather than their actual cross section. The volume measured is therefore only an estimate but with a small enough margin to consider it accurate. The shape, as measured from CAD software has a volume of 318 ml.

Having the correct quantity of oil is important to ensure enough to cover and coat the gears to provide sufficient lubrication as well as have enough thermal mass to not overheat. But not too much to cause drag problems and causing low efficiencies within the gearbox. These estimations are required as a sight glass or other method to check the oil level is not implemented.

The minimum volume of oil required corresponds to the level tangent to the lowest ring gear tooth. Modification to the cavity geometry, this volume is determined to be 24 ml or 7.8% of the full cavity under the condition when no rotating planet gear is present to displace any oil.

To reach the common shaft centre line or half height of the rotating planets in their lowest position requires 37 ml (11%) or 86 ml (27%) when the rotating planets are at their highest position relative to the flat surface.

While these values are only estimated they give more detail compared to using a factor based on total volume. This factor would be off mainly due to the large mass saving area machined into the wheel side carrier, leading to a large void. More oil may need to be added do due to factor that it will still fill this void and become trapped due to the centrifugal forces that will be present. This could have been rectified by using a conical void rather than a cylinder to promote flow out of the space.

The analysis is however only a static analysis once the gears and carrier start spinning it will become a dynamic situation with oil being flung everywhere, during testing it will be observed through the clear backing plate. More analysis of the specifics of the flow could be completed with fluid dynamic simulations to obtain a better understanding but are unnecessary for this project and unlikely to make a large difference.

# 5 Manufacture

The manufacture of the gearbox and all associated components required a significant investment of time, planning and resources. With no access to CNC machines, all components were opted to be machined on manual machines. This constraint heavily shaped the manufacturing process and the design.

Manual machining methods were the main method for all shafts, housings, carriers and features such as shoulders and grooves. alternative manufacturing tools and processes were also used to complete the build. Including arbor presses for bearing installation, welding for miscellaneous fitting and general hand tools like taps, dies and emery paper to achieve a final fit and finish.

This approach allows the system to be manufactured in house, which while more time intensive allows for significantly more knowledge to be collected around the manufacturing processes and design for manufacture considerations. A large amount of intention was needing during setup of each critical component, ensuring concentricity, alignment and dimensional accuracy.

Throughout the process an engineering drawing was created for each part, their drawings can be found within Appendix D

## 5.1 Carriers

During manufacture concentricity of the parts were considered critical. Some of these parts were more important that other parts, of these were the two rotating carriers. These two parts needed to be as concentric to one other with their features to prevent unnecessary misalignment and therefore increases stresses. To circumvent this issue both pieces were machined as one piece with all critical alignment features between the two pieces being machined while they remained married together. The features that were required in this configuration are the bearings seats, carrier bolt holes and shaft holes. The combined piece can be seen in Figure 59.

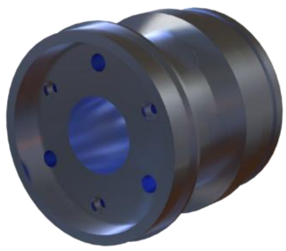

*(a)*

*(b)*

*Figure 59. Combined Carrier Render (a) Isometric (b) Side View*

## 5.2 Housing

The housing, commonly referred to as the upright geometry is a single piece construction. Due to the large difference between the internal bore and the largest outer diameter is turned from a solid billet of aluminium, as the supply for tube sections with significant enough wall thickness is not available.

As mentioned, the alignment between the two bearing faces is critical, an extra amount of care must be taken to align these faces. The use of a four jaw chuck is important to finely adjust and use of a dial indicator to check the concentricity and ensure the piece is within tolerance.

Incorporating a drain plug onto the housing is an important step, being able to drain the oil once testing or running is complete to collect a sample and analyse it can lead to early diagnostic of any issues. Two options were considered during the manufacturing process to achieve the same result. Machining the piece directly from the parent stock of the housing or creating an additional component to be pressed in.

Integrating the feature directly would allow for continuous material but make the turning of the outside more complex. This was deemed unnecessary due to the simple nature of the drain plug. Given this fact the decision for a pressed in piece was used and ultimately welded in to prevent a leak between the two components.

During the turning operation, the bearing seats were found to be slightly oversized, instead of remanufacturing of the entire system scrapping the piece, the use of bearing retaining compound was considered. Different compounds of Loctite were considered, and chosen based on their operating temperature, gap thickness, strength, materials, and compatibility with oil.

Ultimately the decision was Loctite 609, this compound required a gap of 150 microns, the piece was able to be machined to this specification.

This has the additional benefit of allowing for easier disassembly after testing. Able to heat the housing and softening the compound to easily release the bearing.

## 5.3 Gears

Figure 60 shows the initial conditions of the manufactured gears, the gears show uniformity between teeth and are able mesh well. The gears show a consistent surface finish along the length of the face width, each surface has some roughness due to the manufacturing process, this roughness is only minor and not considered a concern.

No major surface irregularities, imperfections, burrs or chips were noticed and were ready for assembly and testing. This indicates that wire EDM is a suitable choice for the gears at this stage.

*Figure 60. Wire EDM Cut Gears*

As per the design the planets were able to be pressed together, the use of a hydraulic press and a small quantity of assembly oil. As all teeth need to engage as one it was tried to add a lead in chamfer to the edge to be pressed in, this made no noticeable difference and is therefore only present on one gear. For an easier assembly the smaller planets were placed in the freezer to shrink beforehand, while not required this reducing the force required for the press fit. After each gear pair were pressed there was no notice of any axial movement.

## 5.4 Concentricity

The ring planet gears were measured for their concentricity between the bearing seats and the gear teeth, using a vee block and a dial indicator, shown in Figure 61 and Figure 62 below by rotating the gear showed less than 0.01mm of runout, which is within a reasonable tolerance. The same test was done once the bearing and shafts had been included. The results showed similar results up to ±0.05mm.

*Figure 61. Gear Concentricity Check*

*Figure 62. Gear Shaft Concentricity Check*

During assembly each shaft, pressed planet gear assembly, and carriers were stamped with a identifying number of one through three, while strictly not required this allowed for the same gears to fit onto the same shafts, and into the same position within the carrier. Ensuring alignment due to slight manufacturing differences, as well as an identifier for any issues during testing for future knowledge.

## 5.5 Mass

Due to the unsprung mass being important for the vehicle suspension response, a mass breakdown is included.

Once completed a dry weight of the assembly could be taken, each piece was measured with an accuracy of one gram. Final weights as well as the predicted CAD measurements are shown in Table 10 and Table 11, some discrepancies between the measured parts are included. such as the measured weight of the sun gear could not be weighed due to being welded to an input shaft as mentioned further, as well as circlips as a theoretical weight was difficult to find accurately. However, due to this the final estimated weight and the final weight show alignment. Both theoretical and practical common shaft assemblies show similarities. The wheel carrier shows the largest deviation.

*Table 10. Measured Weights*

| Component | Measured Weight (g) | Note |
|---|---|---|
| Rotary Seal | 70 | |
| Ring Gear | 407 | |
| O-ring | 0 | |
| Upright | 384 | |
| Bearing Retaining | 39 | |
| Motor Carrier | 412 | Bearing Included |
| Wheel Carrier | 934 | Bearing, Circlip Included |
| Common Shaft Assembly One | 263 | Shaft, P1 & P2 Gear, Circlip, Needle Bearings Included |
| Common Shaft Assembly Two | 261 | Same as Above |
| Common Shaft Assembly Three | 261 | Same as Above |
| **Total** | 3031 | Sun Gear, Motor Plate and Fasteners Excluded |

*Table 11. Theoretical Weights*

| Component | Theoretical Weight (g) | | Note |
|---|---|---|---|
| Rotary Seal | | 79.1 | SKF |
| Ring Gear | | 419.64 | |
| O-ring | | - | |
| Upright | | 371.65 | |
| Sun Gear | | 19.39 | |
| Bearing Retaining | | 32.14 | |
| **Motor Carrier Assembly** | 448.7 | | |
| Motor Carrier | | 143.7 | |
| 61819 | | 305 | SKF |
| **Wheel Carrier Assembly** | 805.12 | | |
| Wheel Carrier | | 537.12 | |
| 61818 | | 268 | SKF |
| **Common Shaft Assembly** | 260.02 | | |
| Shaft | | 25.86 | |
| P1 Gear | | 176.73 | |
| P2 Gear | | 53.43 | |
| Needle Bearings | | 4 | SKF |
| **Total** | 2955.8 | | Circlips, Motor Plate and Fasteners Excluded |

From the measurement the wheel carrier is the heaviest component and has the greatest potential to be optimised. The mass of the 2024 rear wheel assembly is not documented and cannot be compared, however other teams were able to achieve a mass of 3400 g [32]. The mass of the wheel assembly designed will be higher when used on a vehicle due to the additional mounting points required but shows a reasonable base line to build upon.

# 6 Design Validation

To test the gearbox under running conditions it must be put under load. These load requirements are the typical and estimated nominal conditions which have been found in previous chapters, at 8,000 RPM and 8 Nm output from the motor. The conditions will be tested for the approximate length of an endurance race (22 km) as well as an exorbitant amount of testing, assumed to be four endurance lengths. An estimate of 110 km per year is predicted.

Ideally, the AMK motor would have been used for testing, however, no suitable controller capable of interfacing with the EnDat encoder system was available. As a result, the decision was made to utilise the Emrax 228 motor, which was both available and suitable for the application. An additional benefit of this approach is that the test setup can also function as a dynamometer for the testing and characterisation of the Emrax 228 motor currently used by the team, for which no such equipment is presently available.

## 6.1 Testing Rig Design

To validate the gearbox, a testing rig must be designed, developed and manufactured, as no suitable preexisting structure is present and usable. The first design decision is the dynamometer to be used as this will dictate the structure and loading conditions. A common characteristic among the dynamometers assessed the literature review was the need for a higher output speed than produced by the gearbox. With exception of the mechanical loading, this method was avoided due to the high torque output of the gear box and the amount of heat generated from friction would be sufficient. As well as a large torque will be unable to stall in an emergency, requiring either an alternative solution or a speed increasing gearbox. It was decided to use a speed increasing gearbox to provide the required rotational speed. While using a planetary gearbox would be a compact and effective way to increase the speed it is an expensive off the shelf component and as previously discovered, a large undertaking to manufacture.

While electrical, electromagnetic induction and water loading are all viable for the applicable. A water brake was selected due to the availability of a Dynomite 7” within the school. Beyond the availability a water brake required no complex control system beyond control of the flow which can be achieved with a simple ball valve, reducing the complexity of system integration.

The speed required is dictated by the specific water brake and its absorbing capacity provided by charts. Figure 63 shows the capacity of the Dynomite 7” with the required 6.7 kW (9 hp) equating to a minimum rotation speed required of ~2,000 RPM. Due to this graph being the full absorber capacity under these conditions it will turn cold water directly into steam. Therefore, ideally operating under the curve to prevent this and just having hot water, which is easier to contain, and safer, as it remains a liquid.

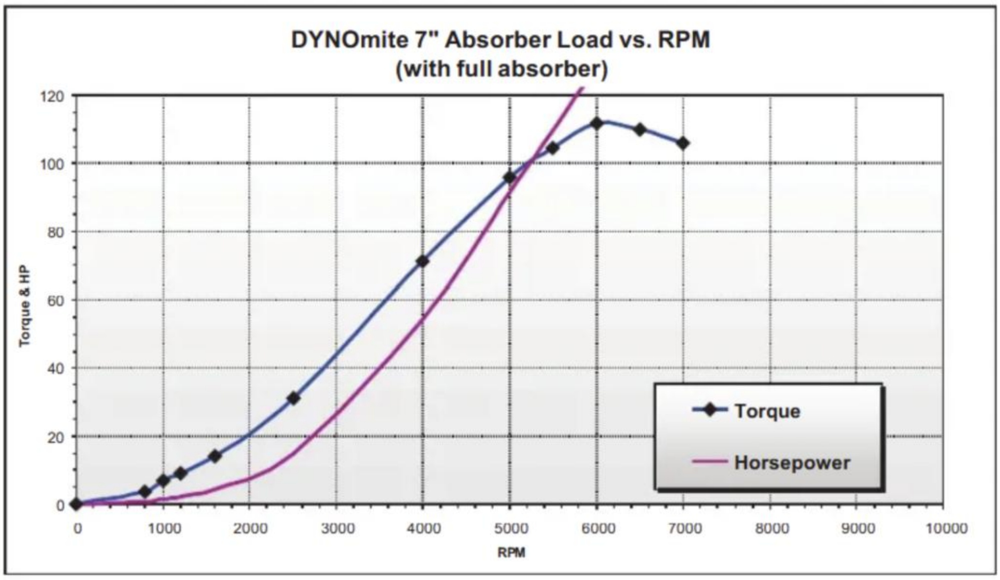


*Figure 63. Dynomite Absorber 7" [73]*

As the nominal testing speed for the motor is 8,000 RPM, with the output of the gearbox at 571 RPM requiring a ratio of at least 3.5. Due to the use of the Emrax the rotational speed available is much lower, with an estimated motor speed of 2,000 RPM. Therefore, a gear ratio to ~10:1 would be required. By using a two-stage chain drive it allows for this while also giving the opportunity to switch sprockets for different use cases such as using the Emrax motor independently, or other motors or future gearboxes with different requirements. While this could also be accomplished with gears such as within a lathe and their change gears it is out of scope for the project requiring much more development. By considering the available sprockets from local suppliers and SKF chain strength catalogues a ratio of 10.7:1 is accomplished. A high-level architecture of the testing rig is presented below in Figure 64 this details the specific sprockets used and how each component interacts, it also shows the general layout of the final testing rig specifically with each chain sprocket.

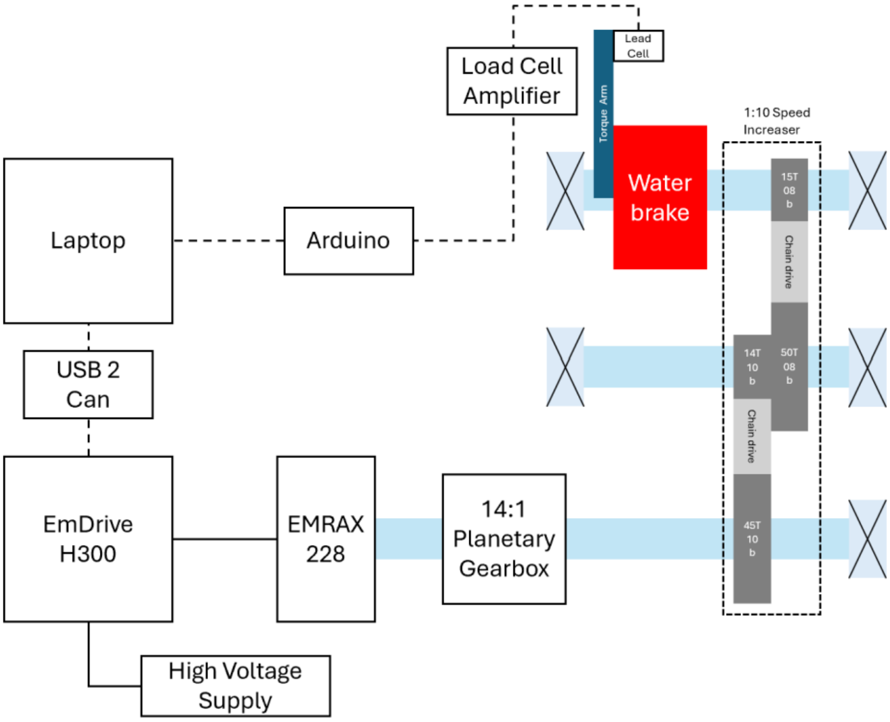


*Figure 64. Testing Rig Architecture*

The testing rig was designed to be an adaptable and compact to allow for testing of other parameters or motors within the workshop environment. Being able to conduct tests on a benchtop model was important for the future of the team.

The design underwent several changes at various stages of development due to the changes in motor, motor controller and power supply. The initial concept was based on the AMK DD5 motor, which mounts directly to the gearbox. Due to this there would be no requirement for motor mounting within the frame. Additionally, the initial motor controller was of much smaller capacity. The intent was a fully encapsulated rig with no need for external components. Ultimately this had to be revised due to the changes present, resulting a much larger motor and motor controller and the use of large batteries. While this increases the overall systems size, it did not introduce constraints beyond storage while not in use.

From the initial desire to restrict size the centre distance between sprockets were minimised to reduce the total volume and height. Although the centre distance is shorter than recommended the wrap angle around the PCD was measured as it should be over 120° [74]. Each angle was measured in CAD and found where the pinion on each stage gear and was found to be 131° and 145° for stage two and stage one respectively. Indicating sufficient tooth engagement on both pinons. Therefore, the reduced centre distance was considered acceptable and did not require change.

The construction of the frame utilises the use of extruded aluminium profiles, utilising T-slots. This approach was selected due to the on-hand supply of lengths as well as the ability to adjust easily and the modularity. The T-slot profile allows for flexibility of components such as bearings, mountings and the motor to be repositioned or altered with only the use of basic hand tools. The use of T nuts allows for greater ease to install additional components once the frame has already been manufactured, such as steel plates on the side for protection, or allowing for any adjustments required. The use of aluminium extrusion also allows for the frame to be lighter compared to a steel alternative. Additionally, an aluminium extrusion frame eliminates the need for welding and thus any thermal distortion.

Pillow block bearings are used to support the shafts holding the sprockets. Using 25mm ID bearings give sufficient material to sustain the forces expected in both bearings and shafts. Mounting the bearings on the aluminium extrusion allows for fine adjustment of the centre distance by allowing movement along the length, effectively creating a zigzag pattern when viewing the chains from the face of the sprockets. This would allow for tension to be applied without the use of a dedicated tensioner. Likewise, more coarse adjustment could be created by altering the placement of the bearing mounting bar via the aluminium extrusion profile. This gives the testing rig much greater usability in the case of other motors, sprockets, and gearboxes for future projects and testing. Offsetting each shaft has the additional effect of increasing the length of the torque arm of the water brake, increasing the reaction arm reduces the amount of force experienced by the frame. Reducing stresses within the structural member.

Each sprocket was given a four-bolt pattern at a specific PCD suited to its hub diameter. Allowing for a flange welded to a shaft to connect. This approach was selected over a standard keyed approach due to the variation in shaft bore sizes, either requiring machining to the appropriate same size or a stepped shaft. A keyed approach would also require additional hardware to prevent axial movement of the sprockets on the shaft. Using a bolted flange interface allows for the sprockets to be changed easily, significantly increasing the adaptability of rig for future consideration.

The flange was welded to the shaft creating a permanent fixture to transmit torque, this process introduces the potential for distortion. Portions of the distortion is likely from imperfect fit of the flange onto the shaft during fixturing for welding. To mitigate this effect each shaft is machined to ensure the mounting face is perpendicular to the shaft axis and ensure proper alignment.

Due to the change in motor a dedicated motor mount is required within the frame. The motor mounting system was used to allow for movement of each axis independently. Allowing for alignment between the motor and gearbox one axis at a time, this is required due to the weight of the motor at over 13 kg, making fine adjustment difficult. The alignment is critical to avoid any unnecessary vibrations or premature wear. The motor was mounted on a series of additional aluminium extrusion fixed to the main frame which allows for adjustment.

While all shafts were able to remain the required 25mm for the bearing the water brake imposes a restriction, having an internal bore of only 19mm. As the shaft is required to have a flange to mate with the sprocket on one side this shaft was unable to meet the 25mm required for the bearing. To accommodate a simple sleeve was machined to fit between the bearing and the shaft, allowing the shaft to pass through the water brake and maintain concentricity within the bearing housing. A key was used to transmit the torque between the final shaft and the internal scalloped dish within the water brake assembly.

To transmit the power between the motor and the planetary gearbox a custom coupling was created for the motor, which the drawing can be found within Appendix D. Whereas the sun gear welded to its own shaft, both using a keyed shaft which would allow for a jaw coupling to be used to absorb small vibrations and accommodate slight misalignment.

Due to the AMK motor not being used the motor plate would instead have to be adapted to create a seal between the shaft and the sun gear shaft. As the motor plate no longer needs to support the weight of the motor, for simplicity it was manufactured from a laser cut acrylic piece of the same outside profile. A thin section small radial seal was incorporated and pressed in place. Using a second piece of acrylic one with a smaller hole to act as a shoulder provides axial support. These would then be glued together and create a single piece. This gives the added benefit of being able to see the oil level, and visual sight of the oil flow against the acrylic plate during operation as the carrier rotates. As the sun gear was no longer held in an axial location due to the motor spline, it required periodic inspection to ensure it had not axially displaced and disengaged from the planet gears.

Major details outlined above can be found within the Figure 65 below where components are highlighted.

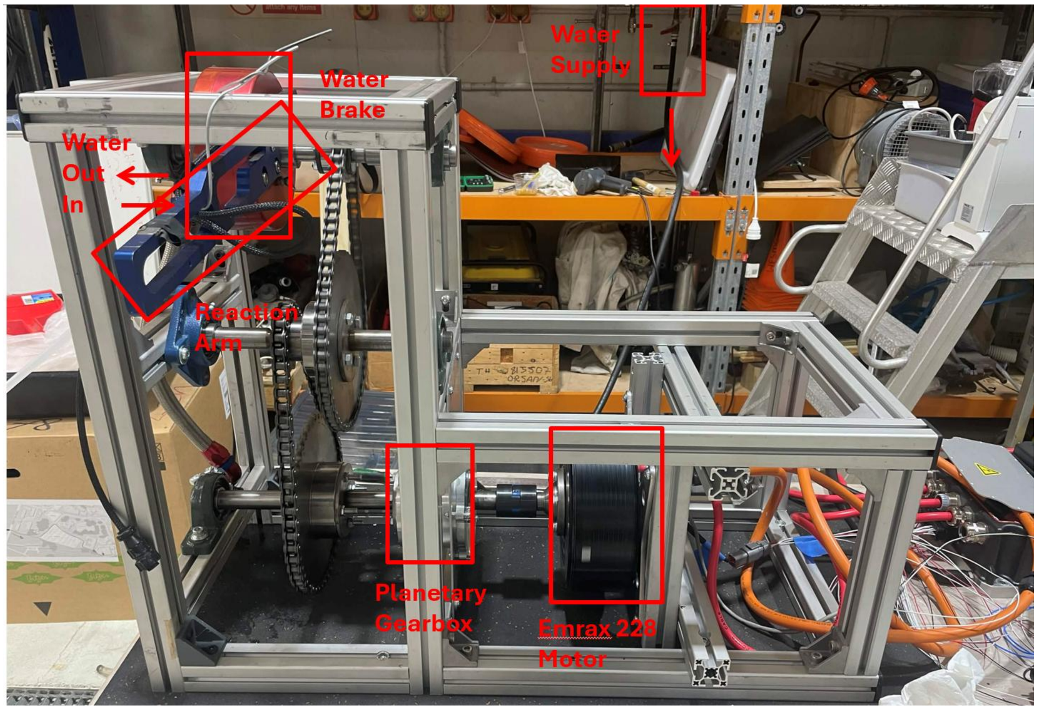


*Figure 65. Testing Rig Side Profile*

Additional components were assessed and were part of the initial conceptual stage but were not implemented into the final design due to the changes throughout the process. A closed loop cooling system for the water brake was considered and components picked but ended up not being used to the change in architecture and power requirements due to the output of the systems and time restrictions. Similarly, the Arduino and load cell measurements were not included due to the loading criteria the input load, the input load can be measured based on the current sent to the motor and allows for a more accurate measurement rather than measuring the efficiency of the planetary gearbox and the chain speed increaser system combined.

## 6.2 Testing Process

During the testing process the motor was placed into speed control mode, this would allow for a continuous speed target from the motor, and the torque could be altered via flow of water using the ball valve on the water supply line.

A vibration analysis tool known as CoCo was used to measure the vibrations of the gearbox. The probe was secured with a piece of adhesive putty to the top of the housing. This may have some dampening effects but is ignored for this process as it will be present in all the data sets. The probe is shown in Figure 66, which also illustrates the direction of each axis. The Y axis runs parallel to the axis of revolution of the gearbox, the X axis measures any sideways acceleration, and the Z axis measures the vertical acceleration.

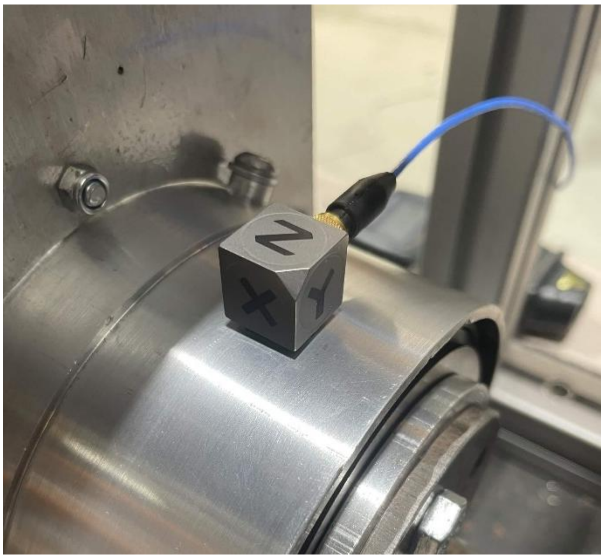


*Figure 66. Vibration Analysis Probe Axis*

The vibration probe was left on the gearbox for the duration of the test to prevent movement from introducing error into the data. Due to the length of tests, the vibrations were recorded at 30-minute intervals for approximately one minute at a time. This could be used to show the vibrations at the time and compare to previous data points and check for an increase in vibrations.

Motor temperature was monitored with a thermocouple probe secured to the side of the housing, to estimate the temperature within the gearbox. An additional thermocouple was placed on a separate piece of aluminium to gain a reference with the changing ambient temperature through the test duration. Each temperature measurement was taken as a discrete value with a 15-minute interval.

The motor controller was configured for closed loop speed control such that the motor torque is automatically varied in response to the applied load to maintain a constant rotational velocity. The load was applied to the motor with a water brake, slowly increasing the flow of water until the torque output of the motor matches the testing conditions.

### 6.2.1 Limitations

The testing process was unable to recreate the expected loading conditions, both applied torque and motor speed was under the desired values. This was due to the limitations of both the power source and motor operating range.

Due to the alternative motor selection, the rotational speed was limited. Both the Golden Motor and Emrax max operating speed fell short of the required. While a speed increasing gearbox could be used the time restrictions made this unfeasible.

Likewise, the change in the power supply operating 80 V, 60 A supplied by wall power was rendered unusable due to external circumstances and thus remains unusable. As a result an alternative battery pack operating at 52 V was to be used. This can with the effect of reducing the maximum rotational speed of the motor.

With the major set backs the motor was only about to reach a maximum no load speed of 1080 RPM and 670 RPM under load.

Due to the low rotational speed of the output, even with the higher ratio of the testing rig the output of the gearbox remains lower than the water brake is required to reach a load of 8 Nm. The maximum load was estimated as 5.5 Nm during testing.

A clamp ammeter was used to estimate the torque output of the motor. By power matching the output power of the battery using Equation (40) and solving for the torque output of the motor with Equation (41).

$$P = VI \tag{40}$$

$$P = \tau\omega \tag{41}$$

This assumes an 100% efficiency between the motor controller and motor, this is a false statement but remains as a limitation. The motor efficiency is likely to be much less than expected due to the low operating speed.

The inclusion of the load cell between the frame and the reaction arm would provide an additional data point to validate the measured output of the gearbox. This is recommended for future testing.

### 6.2.2 Data

After some initial testing to ensure the rig is working correctly and able to load the motor, through a variability of speeds and torques an endurance run test could be started.

Due to the voltage issues discussed in the limitations the test would run at the maximum conditions available. This was at 670 RPM and 5.4 Nm or 380 W, significantly less than initially considered. While the speed is lower the torque is like the 8 Nm, as torque is the driving factor for the stresses applied to a gear the test is still representative and deemed a valid test.

Similarly, because of the voltage the speed target was set higher and the motor was able to reach a steady state for the amount of load.

Due to the slow speed the decision was made to reduce the test time to a single endurance period of 22km. With the rotational velocity of the motor this would equate to ~6 hours of running.

Figure 67 and Figure 68 show the battery voltage and rotational speed over time of the test. Each shows a consistent value with a slight decrease towards the end of the test. Also, can be seen is a portion of the speed increasing. This was due to a motor controller overheating issue. A cooling method was applied for the remaining of the test to prevent this from occurring again. as the speed target was set higher this allowed for the climb. Also present is a stop during the test, due to the gearbox output shaft weld shearing. This was promptly repaired and test continued, the data collection was paused however, the repair took approximately 40 minutes. The effect on the data of this failure is present within the temperature of the gearbox as it allowed time to cool.

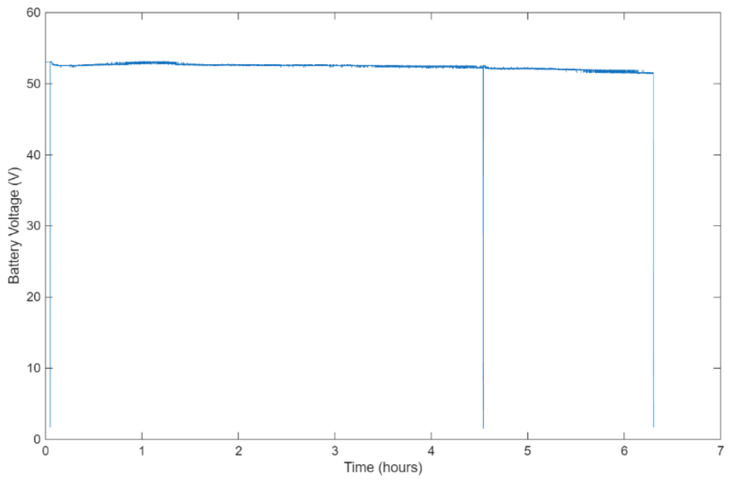


*Figure 67. Battery Voltage 52 V*

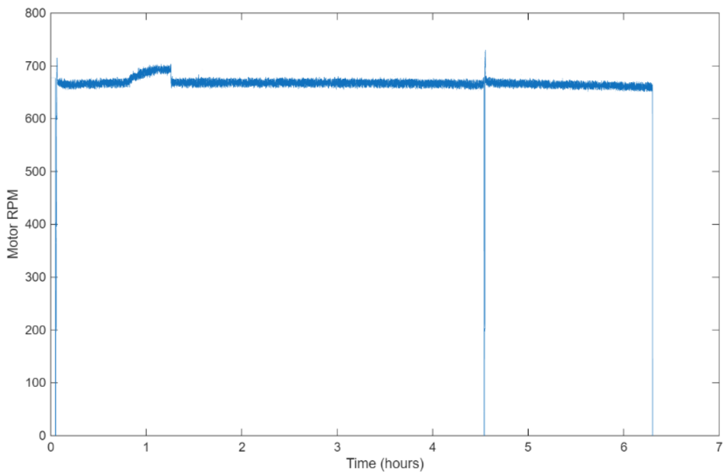


*Figure 68. Motor RPM 52 V*

Based on the voltage output and rotational speed graphs a constant value was deemed to be reasonable. In addition to current, electrical power of the battery can be found as a constant, similarly the constant rotational speed with constant power means a constant torque based on the current.

Figure 69 shows the current output of the batteries throughout the test, showing a constant output except for the two data points due to the motor controller thermal management issue, and limiting the current. The torque can be found using the power matching method in Equations (40) and (41), similarly Emrax provides a Nm/Amp value of 0.75 which aligns closely with an error of 1.2% [75].

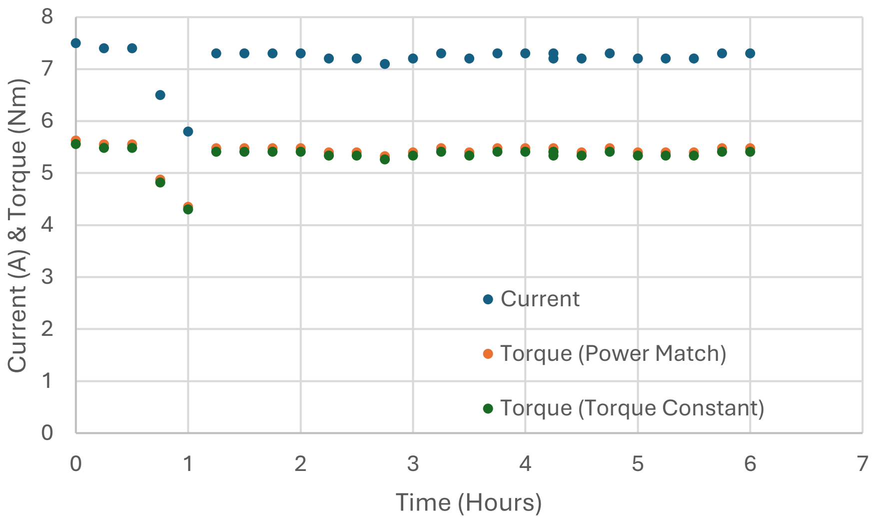


*Figure 69. Current and Torque 52 V*

The temperature was monitored and reached a steady state value of 28°C after 2 hours of running, shown in Figure 70. While only the housing is measured and the internal temperatures will be higher, no significant concern or inefficiencies are present, and the gearbox was not operating at or near its thermal limits.

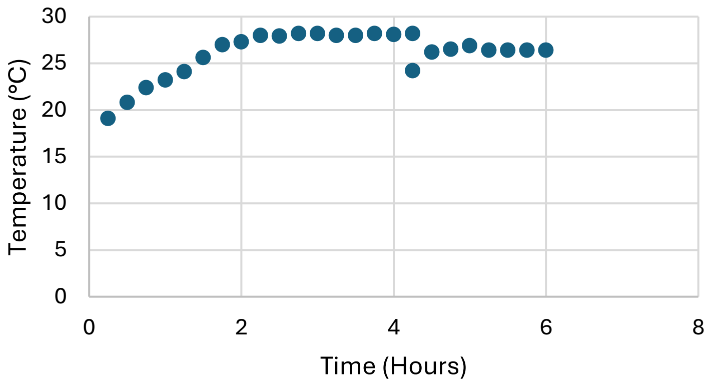


*Figure 70. Gearbox Housing Temperature 52 V*

By running the gearbox under these conditions showed no sign of operational fatigue failure during the time and with addition of the other test can then be taken apart to inspect the components for any additional data.

The vibration response for the test is shown below in Figure 71, taken as a resultant and plotted against time. The data represents a consistent pattern for each time the vibration response is logged, showing a repeated maximum magnitude, except for the final data section which shows a slightly higher peak in acceleration. This increase is likely from the test rig presented by the failure and discussed further along. A gap is present in the data due to a corrupt data file.

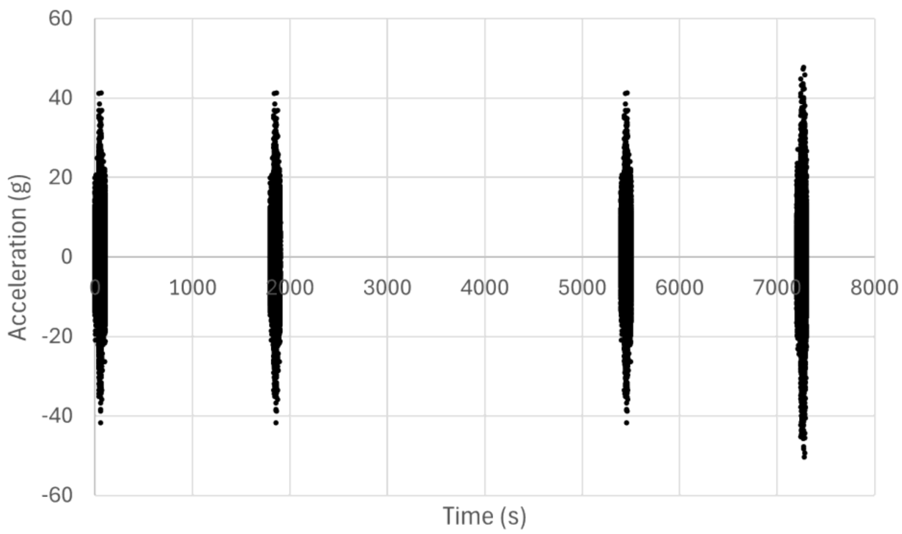


*Figure 71. Vibration Response*

Due to the low voltage supply additional batteries were acquired, doubling the voltage to a 104 V, this would allow the rotational speed to increase and apply a greater load, due to the increase in speed to the water brake. The voltage and rotational speed of the motor can be seen in Figure 72 and Figure 73, showing the constant values present.

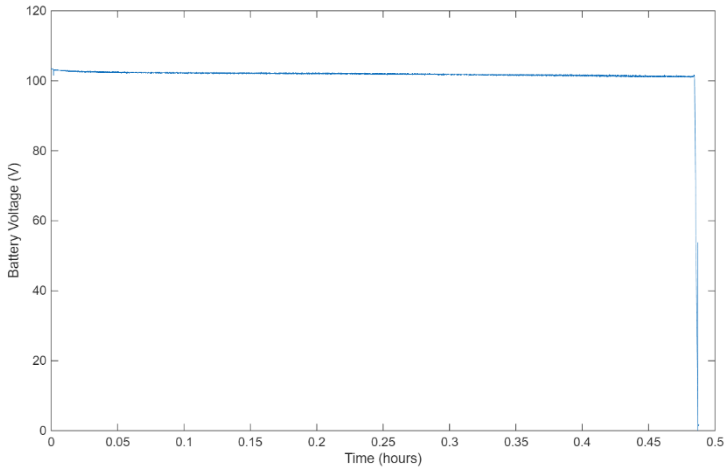


*Figure 72. Battery Voltage 104 V*

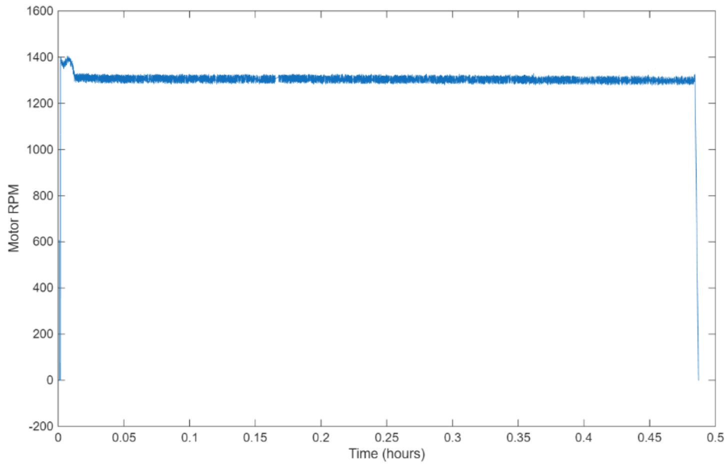


*Figure 73. Motor RPM 104 V*

The test was cut short due to a failure within the rig, where similar to the previous test a shaft and flange weld interface failed, an example of the failure can be seen in Figure 74, where the flange still bolted to the sprocket has separated from the shaft. Due to the situations this could not be repaired, and the test was called short. These failures indicate a fatigue limit within the test rig due to the manufacturing process, likely as this portion was not designed and developed to the same scrutiny as the gearbox.

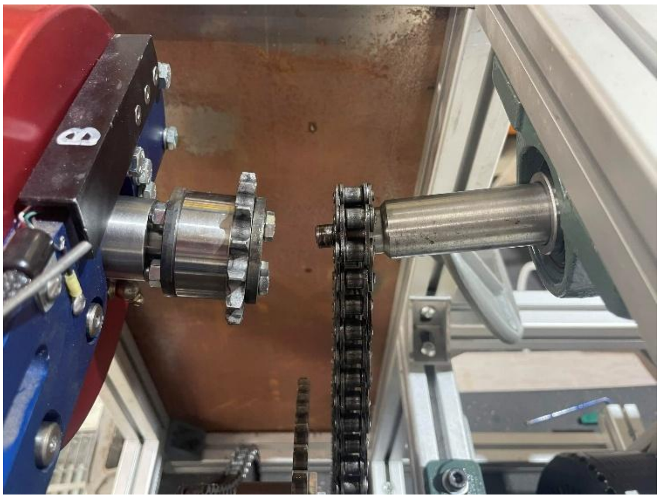

*Figure 74. Testing Rig Shaft Failure*

With the increase in speed the current was able to increase and provide greater torque. With the increase in voltage the target of 8 Nm was able to be reached, as shown in Figure 75. Providing the nominal operating conditions expected. A gap exists as the beginning of the test was measuring data 10 minutes apart but was changed while the test was occurring.

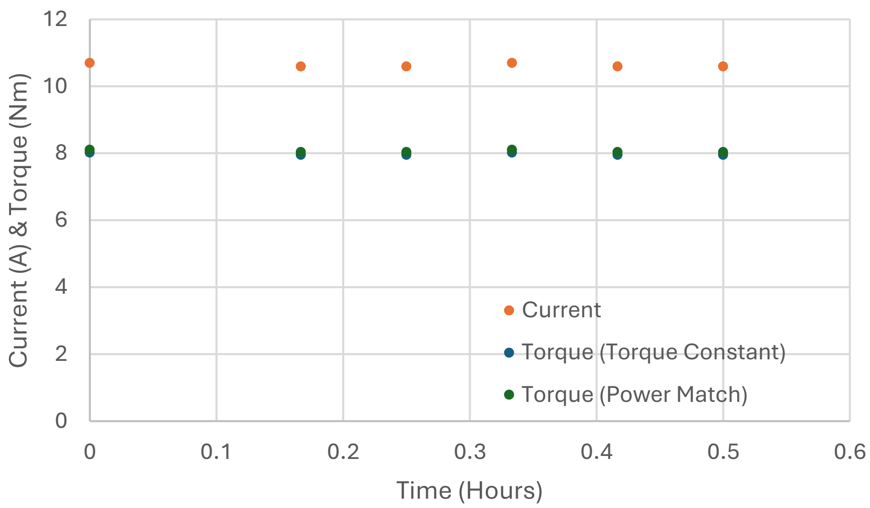


*Figure 75. Current and Torque 104 V*

Due to the time restrictions of the project a full endurance test would not be able to be completed. Therefore, the shortened 30-minute test would provide partial validation. This will not ensure the full fatigue life of the gearbox at higher loads, but due to the higher speeds the test was able to complete a theoretical distance of 3.5km, enough to complete previous dynamic events.

Due to the short test time the gearbox did not reach a steady state value, however the temperatures present where higher than the lower power test, reaching a peak of 31°C this can be observed during a full test and determine the thermal operating conditions. Once the test had finished the input shaft of the sun gear was noticed to be hot to the touch, measuring at 45°C. This allows for an inferred estimate of the internal temperature to be found. Planetary gearboxes can have internal temperatures of 40°C-95°C under typical operating conditions [76]. The gearbox over the short test is therefore not operating near a thermal limit and would require further data to reach a steady state value for the input power. The gearbox does not include any cooling method, like ram air that would be expected as the vehicle is driving. A similar vibration analysis was completed for the second round of testing and presented comparable results to the full endurance run.

## 6.3 Disassembly

After the conclusion of the test the gearbox was disassembled and have an post-test inspection completed. This was to inform of any design decisions that may require change or show any evidence of wear.

After removal of the face plate and any oil drained through the face and drain plug, which is drained into a clean container for examination. This oil was heavily discoloured showing as a deep grey. The oil exhibited a glistening nature, indicating suspended metallic particles likely to be from wear. However, when rubbed between fingers the oil retained a smooth feeling, implying the particles were very fine.

The particles in the oil are suspected from initial wear, as the initial gears before testing showed a slight roughness. This claim is supported by the inspection of the gears, shown in Figure 76. While the face still shows some roughness it is noticeably smoother to the touch, compared to the small off colour portion at the tip which did not mesh with the ring gear due to the slight increase in face width to the planet gear. This smoothing effect could be seen on the sun gear when removed which show polished teeth.

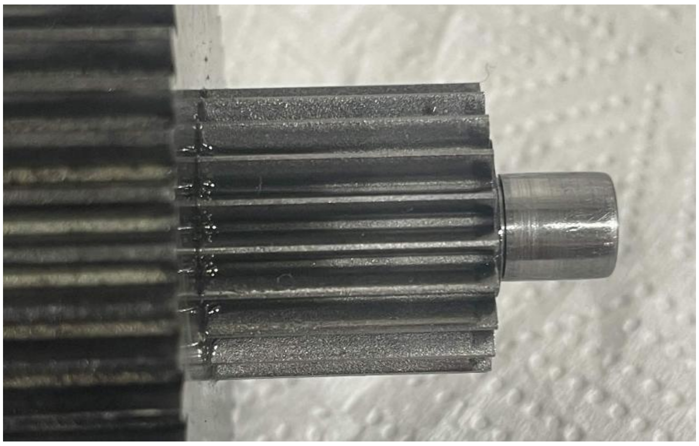

*Figure 76. Planet Gear Face Post Testing*

The use of a heat gun for softening the Loctite bearing retaining compound was efficient, allowing for clean separation of the carriers out of the housing without the need of force or damage. Each piece was disassembled to its single piece, except for the bearing and the pressed planet gears. This was done to prevent any damage from separating these pieces and allow the gearbox to be reassembled easily in future for any testing the team might want to do. Inspection of the pieces combined would still be possible.

Removal of the bearing retaining plate shows a build up of residue around planet shaft one, this can be seen in Figure 77. Despite this accumulation no visible wear or distortion is present on shaft one, or the bore where the two components interface. Each other shaft and bores were checked. The residue build up is likely of made of the same material as present in the oil.

*Figure 77. Residue Around Shaft 1*

Removal of the planets from the shaft shows slight wear on the shaft where bearings were running, each show the same feature as seen in Figure 78. The wear can be seen at either side of the shaft between the circlip groove and shoulder features, compared to the centre of this same area which is smooth as the entire shaft began as. Although the surface finish is altered a micrometre was used and no measurable difference was made at each three locations.

*Figure 78. Shaft Inspection*

With inspection of the planets and ring gear faces showed some striations, these are seen in Figure 79 and Figure 80. The striations are only present on a single planet gear, specifically shaft two. They show surface level markings which are not indicated of any further damage, with no damage to the gear teeth on either the ring or planet.

*Figure 79. Ring Gear Striations*

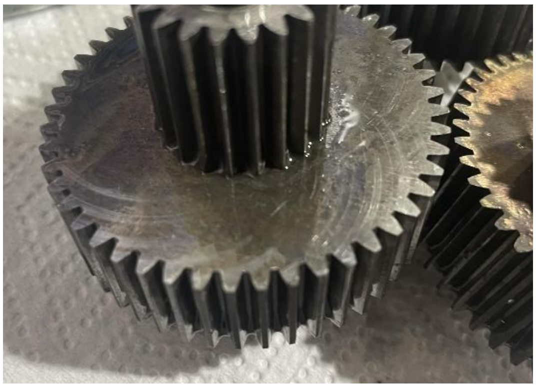

*Figure 80. Planet Gear Striations*

A likely cause of these features is too much allowable axial displacement, from either the circlip on the shaft allowing the gears to move slightly more than allowable or the entire shaft axially displacing further towards the wheel due to slightly too deep of a shaft hole within the carrier. Despite the markings present no major damage is shown but must be checked to ensure no further damage occurs in further testing.

The final major component is the bearings, as the deep groove ball bearings remain pressed into their respective carrier they were spun as an assembly. Rotation remained smooth with no irregularities, binding, roughness or hard points. Suggesting the bearings were not impacted by any misalignment or debris through the testing conditions. The needle bearings were also inspected and also showed no display of any irregular performance.

Overall, the disassembly resulted in minor wear within meshing gears. Additional testing with fresh oil would confirm if this was recurring wear or just bedding in wear but remains out of scope for the testing process within this project. No evidence of any distortion, structural damage or component issues presented themselves. The gearbox can be reassembled and placed back on the test bench if required by future members wanting to explore a planetary gearbox.

# 7 Conclusions

The objective of the project was to design, manufacture and test an in-hub motor gearbox setup, with consideration for design for manufacture. The use of a stepped planetary gearbox with a gear ratio of 14:1 was developed based on tyre data, motor characteristics, track data, and simulation tools. The development of the prototype is aimed at creating a validated architecture to support the WESMO team transition to in-hub motors within future years and support improved flexibility for components within the primary structure.

Experimental testing proved that the gearbox could handle a full endurance race under load conditions, without any failure or signs of significant wear, confirming the ability of a stepped planetary gearbox within wheel assemblies.

Beyond the implementation of the manufacture and assembly of a prototype gearbox, this work aims to lay a foundation for future development within the team and other FSAE teams. Expanding on the gear selection process and the design methodology providing a baseline that can be refined and expanded into a fully integrated system.

The prototype remains as an early-stage implementation with clear options for improvement, optimising areas such as mass, efficiency, and thermal performance. Building upon these sections will ensure the greatest performance improvements.

The results validate the feasibility of the system and provide a direction to be built upon and developed ready for full implementation of an in-hub powertrain.

## 7.1 Recommendations

Based on the design, manufacture, and testing and evaluation of the prototype gearbox multiple areas have been identified for improvement. These improvements can provide greater performance, efficiency, system integration, and robustness for the future of the in-hub transition.

Further validations should be sought after under higher speeds, testing at peak conditions to validate the worst-case loading conditions. Testing under these conditions requires a higher voltage power source. Additionally, the introduction of a suitable motor controller to operate the AMK DD5 motor and complete validation with the motor which the gearbox was designed for. This would be used to validate the complete system and introduce the motor coolant loop.

The gears present in the system have not been mass optimised and can be altered, by altering the geometry and removing mass to form a non-solid gear. This is primarily for the sun planets gears as they have a large diameter difference between the ID and OD and leave room for non-structural mass to be removed. Additionally, the ring gear can be reduced, using a spline or similar to transmit torque with an aluminium retaining plate, significantly reducing the mass of the gear. Similarly, the mass of the wheel carrier is significantly higher than other components, allowing for reduction of mass.

Improvements to the lubrication system are recommended. The current straight cut section to remove mass of the wheel bearing may trap oil at higher speeds due to the centrifugal forces, reducing the amount present at the meshing gear teeth. This straight cut feature could be removed, either completely or with a cap, or introducing a taper to the section to promote oil flow back towards the gears. A complete dynamic simulation may be required for complete understanding. Additionally, integration of the wheel bearing into the flooded portion of the system while relocating the rotary seal to the outer edge, allowing for the removal of the bearing seals and a decrease in friction on said bearing.

Finally, improvements to the testing rig setup can be made, improving the experimental accuracy. Proper integration of the load cell and cooling setup creating a more complete self contained operation. In the event of continued use of the Emrax a fine adjustment mechanism for the height adjustment due to the weight of the motor. As well as greater precision of the shaft manufacture to allow for truer rotation and less vibration.

# References

[1] “History of Formula Student.” Accessed: Mar. 27, 2026. [Online]. Available: https://www.imeche.org/events/formula-student/about-formula-student/history-of-formula-student

[2] Society of Automotive Engineers, “SAE Australia Past Results.” [Online]. Available: https://www.saea.com.au/fsaea-past-results

[3] Formula Student Austria, “FSG Announcements & the Future of FSA.” [Online]. Available: https://fsaustria.at/fsg-announcements-the-future-of-fsa/

[4] EMRAX, “228 Datasheet.”

[5] Monash Motor Sport, “M17-M18.” [Online]. Available: https://www.monashmotorsport.com/m17-m18

[6] “KA-RaceIng e.V. on Instagram: ‘Engineered for performance, proven on track ✨ #karaceing #formulastudent #motorsport #racecar #teamwork,’” Instagram. Accessed: May 04, 2026. [Online]. Available: https://www.instagram.com/karaceing/reel/DWErd-7DD0w/

[7] C. J. Tragakis, “What Are Sprung and Unsprung Weight?” [Online]. Available: https://www.cjponyparts.com/resources/sprung-vs-unsprung-weight#:~:text=Sprung%20weight%20is%20the%20weight%20of%20anything,against%20the%20suspension%20*%20Is%20mostly%20beneficial

[8] W. F. Milliken and D. L. Milliken, *Race Car Vehicle Dynamics*.

[9] T. D. Gillespie, *Fundamentals of Vehicle Dynamics*.

[10] V. Marciano, “MUR Blog - Electric Drivetrain… A New Beginning.” [Online]. Available: https://murmotorsports.eng.unimelb.edu.au/news-and-events/news-and-events/mur-blog-electric-drivetrain-a-new-beginning?utm_source=chatgpt.com

[11] T. Tran, “FSAE Planetary Gearbox.” [Online]. Available: https://thanhvtran.com/portfolio/fsae-gearbox/

[12] D. Mikle and M. Bat’a, “Torque Vectoring for an Electric All-wheel Drive Vehicle”.

[13] H. De Carvalho Pinheiro, M. Carello, and E. Punta, “Torque Vectoring Control Strategies Comparison for Hybrid Vehicles with Two Rear Electric Motors,” *Appl. Sci.*, vol. 13, no. 14, p. 8109, Jul. 2023, doi: 10.3390/app13148109.

[14] Society of Automotive Engineers, “Formula SAE Rules 2025,” 2024.

[15] E. D. Owen, “The Benefits of Four-Wheel Drive for a High-Performance FSAE Electric Racecar”.

[16] “UQ Racing on Instagram: ‘Our planetary gearbox is one of the pivotal changes for EV22, requiring a more advanced powertrain design than ever before. This task has been made easier by KISSsoft! KISSsoft is the modular software that helps design and analyse gears, shafts, and bearings. They’ve made the gear calculations, internal geometry, and shaft-hub connections a breeze!,’” Instagram. Accessed: May 04, 2026. [Online]. Available: https://www.instagram.com/uqracing/p/CgmBVH4r7cB/

[17] G. White, G. Cunningham, and D. Doyle, “Design of an Electric Drive Transmission for a Formula Student Race Car,” *SAE Int. J. Adv. Curr. Pract. Mobil.*, vol. 01, no. 3, pp. 1345–1351, Apr. 2019, doi: 10.4271/2019-01-1295.

[18] “Planetary Gearbox: How It Works and the Advantages?” Accessed: Apr. 27, 2026. [Online]. Available: https://assunmotor.com/blog/planetary-gearbox/

[19] M. Babin, E. DuConge, G. Veigas Marques, and H. Rabin, “Design of an in-wheel powertrain system for a Formula Student race car.”

[20] A. Dynamics, “A planetary gearbox is a gearbox with the input shaft and the output shaft aligned.,” Apex Dynamics. Accessed: Apr. 27, 2026. [Online]. Available: https://www.apexdyna.nl/en/gearboxes/planetary-gearbox-introduction

[21] S.-J. Tsai and Q.-Y. Zhuang, “Design and analysis of compound stepped planetary gear drives for better transmission performances,” *Forsch. Im Ingenieurwesen*, vol. 87, no. 3, pp. 1037–1056, Sep. 2023, doi: 10.1007/s10010-023-00702-6.

[22] “Compound Planetary Gear - Planetary gear train with stepped planet gear set - MATLAB.” Accessed: Apr. 27, 2026. [Online]. Available: https://www.mathworks.com/help/sdl/ref/compoundplanetarygear.html

[23] C. W. Bowen, C. E. Braddock, and R. D. Walker, *Installation of a High Reduction-Ratio Transmission in the UH-1 Helicopter*. 1969.

[24] "Gear Systems | KHK Gear Manufacturer." Accessed: Apr. 27, 2026. [Online]. Available: https://khkgears.net/new/gear_knowledge/gear_technical_reference/gear_systems.html

[25] MECHTEX, "How Does a Planetary Gearbox Work?," MECHTEX. Accessed: Apr. 27, 2026. [Online]. Available: https://mechtex.com/blog/how-does-a-planetary-gearbox-work

[26] "Planetary Gears for heavy-duty Operation - tunnel." Accessed: Apr. 27, 2026. [Online]. Available: https://www.tunnel-online.info/en/artikel/planetary-gears-for-heavy-duty-operation-3313768.html

[27] B. Maruoka, J. Fine, B. Wong, and M. Kai, "development of planetary drive system for formula sae electric race car".

[28] T. Patel, A. Dubey, and L. Bhaskara Rao, "Design and Analysis of an Epicyclic Gearbox for an Electric Drivetrain," *Int. J. Recent Technol. Eng. IJRTE*, vol. 8, no. 3, pp. 6834–6842, Sep. 2019, doi: 10.35940/ijrte.C5787.098319.

[29] School of Engineering, University of Warwick, "The Conceptualisation, Development, Design and Optimisation of an Integrated In-Hub Planetary Gearbox System for a Formula Student Race Car."

[30] O. Makkonen, "Design of a Planetary Gear System for Formula Student Hybrid Drivetrain".

[31] T. Beernaert, "Gear transmission design and in-wheel packaging for a Formula Student race car".

[32] E. Alexsson, E. Henrikson, C. Lund, and C. Tsobanoglou, "Design of a Weight-Optimized Gearbox for a Formula Student Car".

[33] "DANotes: Spur gears: Gear meshing." Accessed: Apr. 16, 2026. [Online]. Available: https://www-mdp.eng.cam.ac.uk/web/library/enginfo/textbooks_dvd_only/DAN/gears/meshing/meshing.html

[34] "The Role of Pressure Angle in Gear Design," www.pairgears.com. Accessed: Apr. 16, 2026. [Online]. Available: http://www.pairgears.com/blog/The-Role-of-Pressure-Angle-in-Gear-Design_b2397

[35] S. P. Radzevich, *Dudley's Handbook of Practical Gear Design and Manufacture*.

[36] R. G. Budynas, J. K. Nisbett, and J. E. Shigley, *Shigley's mechanical engineering design*, Tenth edition. in Mcgraw-Hill series in mechanical engineering. New York, NY: McGraw-Hill Education, 2015.

[37] "Contact Ratio | Gear Nomenclature | KHK." Accessed: Apr. 16, 2026. [Online]. Available: https://khkgears.net/new/gear_knowledge/gear-nomenclature/contact-ratio.html

[38] "How Does Helix Angle Affect Your Gear Design?," https://okdor.com/. Accessed: Apr. 16, 2026. [Online]. Available: https://okdor.com/helix-angle/

[39] "Comparing Spur Gears & Helical Gears | WM Berg." Accessed: Apr. 16, 2026. [Online]. Available: https://www.wmberg.com/resources/blogs/spur-gears-vs-helical-gears

[40] "Undercut | Gear Nomenclature | KHK." Accessed: Apr. 27, 2026. [Online]. Available: https://khkgears.net/new/gear_knowledge/gear-nomenclature/undercut.html

[41] "Profile Shifted Gears | KHK." Accessed: Apr. 27, 2026. [Online]. Available: https://khkgears.net/new/gear_knowledge/introduction_to_gears/profile_shifted_gears.html

[42] L. Tan *et al.*, "Dynamic characteristics analysis of profile-shifted planetary gears considering friction," *Meccanica*, vol. 59, no. 2, pp. 193–215, Feb. 2024, doi: 10.1007/s11012-023-01746-2.

[43] "Case Hardening Explained - How It Works, Benefits & Types," Fractory. Accessed: May 01, 2026. [Online]. Available: https://fractory.com/case-hardening-explained/

[44] "Lubrication of Gears | KHK." Accessed: May 01, 2026. [Online]. Available: https://khkgears.net/new/gear_knowledge/gear_technical_reference/lubrication-of-gears.html

[45] A. Smiley and G. H. Consulting, "Cavitation or Aeration? How to Tell the Difference." Accessed: May 01, 2026. [Online]. Available: https://www.machinerylubrication.com/Read/30768/cavitation-or-aeration

[46] "Dynamometer | Engine, Torque & Power | Britannica." Accessed: May 02, 2026. [Online]. Available: https://www.britannica.com/technology/dynamometer

[47] "A Comprehensive Guide to Dynamometers:," Data Acquisition | Test and Measurement Solutions. Accessed: May 02, 2026. [Online]. Available: https://dewesoft.com/blog/dynamometers-guide

[48] N. Piebenga, “Effect of drivetrain set up on acceleration, torque, shifting and track times,” University of Waikato, 2021.

[49] C. Cross-Reference-Chart, “Comparison Chart of Hoosier Racing Tire Compounds”.

[50] L. Kopf, “Dynamic Analysis Of The WESMO FSAE Car’s Suspension,” 2020.

[51] WESMO FSAE Team, “E25 WESMO Spec Sheet 2024.” Unpublished.

[52] AMK, “Motor-Datenblatt.” 2018.

[53] EMRAX, “118 Datasheet.”

[54] NeuMotors, “44xx Series Datasheet.” 2023.

[55] “Electric motors in Formula Student - a high-speed success story,” Fischer Elektromotoren. Accessed: Apr. 22, 2026. [Online]. Available: https://fischer-elektromotoren.de/en/company/formula-student/

[56] “M024,” FSAE47. Accessed: Apr. 22, 2026. [Online]. Available: https://www.fsae.co.nz/cars-ev/m024

[57] “M025,” FSAE47. Accessed: Mar. 30, 2026. [Online]. Available: https://www.fsae.co.nz/cars-ev/m025

[58] M. Hies, “Electric Drivetrain in an FSAE Vehicle and the Clamping Force of a Friction Retained Differential.”

[59] S. Schumacher, S. Schmid, P. Wieser, R. Stetter, and M. Till, “Design, Simulation and Optimization of an Electrical Drive-Train,” *Vehicles*, vol. 3, no. 3, pp. 390–405, Jul. 2021, doi: 10.3390/vehicles3030024.

[60] J. He, “1.6587 Steel: 18CrNiMo7-6 Case hardening Steels to EN 10084,” Otai Special Steel. Accessed: Apr. 23, 2026. [Online]. Available: https://www.astmsteel.com/product/1-6587-steel/

[61] “ASM Material Data Sheet.” Accessed: Apr. 30, 2026. [Online]. Available: https://asm.matweb.com/search/specificmaterial.asp?bassnum=ma6061t6

[62] Easy Steel, “Special Steels Catalouge.”

[63] “Free Online Beam Calculator | Reactions, Shear Force, etc.” Accessed: Apr. 26, 2026. [Online]. Available: https://skyciv.com/free-beam-calculator/

[64] J. Smith, “The University of Waikato”.

[65] “61819 - Deep groove ball bearings | SKF.” Accessed: Mar. 31, 2026. [Online]. Available: https://www.skf.com/my/products/rolling-bearings/ball-bearings/deep-groove-ball-bearings/productid-61819

[66] “61818 - Deep groove ball bearings | SKF.” Accessed: Mar. 31, 2026. [Online]. Available: https://www.skf.com/undefined/products/rolling-bearings/ball-bearings/deep-groove-ball-bearings/productid-61818

[67] tec-science, “Derivation of Willis equation (fundamental equation of planetary gears) | tec-science.” Accessed: Apr. 19, 2026. [Online]. Available: https://www.tec-science.com/mechanical-power-transmission/planetary-gear/fundamental-equation-of-planetary-gears-willis-equation/

[68] “O-ring Calculator,” Ceetak. Accessed: Apr. 19, 2026. [Online]. Available: https://ceetak.com/o-ring-calculator/

[69] “Selecting fits | SKF.” Accessed: Apr. 25, 2026. [Online]. Available: https://www.skf.com/group/products/rolling-bearings/principles-of-rolling-bearing-selection/bearing-selection-process/bearing-interfaces/selecting-fits

[70] “Seat tolerances for standard conditions | SKF.” Accessed: Apr. 25, 2026. [Online]. Available: https://www.skf.com/uk/products/rolling-bearings/principles-of-rolling-bearing-selection/bearing-selection-process/bearing-interfaces/seat-tolerances-for-standard-conditions

[71] “ISO Limits and Fits Table - The right fits and clearance for bearings and seals.” Accessed: Apr. 25, 2026. [Online]. Available: https://simplybearings.co.uk/shop/Info-Pages-ISO-Limits/c4746_4779/index.html?srsltid=AfmBOooFMEFG8onQHdjzb_g-0HQLgc9LjqFyhDGgomL4bLHAw9AY1N4S

[72] “General bearing specifications | SKF.” Accessed: Apr. 25, 2026. [Online]. Available: https://www.skf.com/group/products/rolling-bearings/roller-bearings/needle-roller-bearings/needle-roller-and-cage-assemblies/general-bearing-specifications

[73] Land and Sea, “Dynomite Owner’s Manual.” Sep. 01, 2012.

[74] Agricultural Machinery Testing and Evaluation, *Center Distance Between Sprockets*.

[75] EMRAX, “EMRAX 228 Techincal Data.”

[76] J. Shen *et al.*, “Thermal Behavior and Operation Characteristic of the Planetary Gear for Cutting Reducers,” *Appl. Sci.*, vol. 15, no. 24, p. 13219, Dec. 2025, doi: 10.3390/app152413219.

## Appendix A

## TTC Tyre Curves

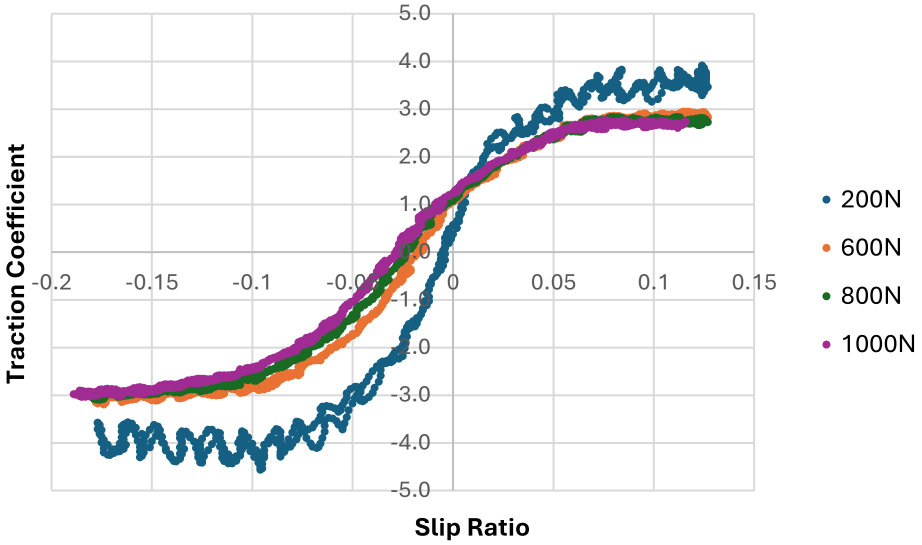


Figure A.1 18x7.5-10 R25B Slip Ratio Traction Coefficient, Averaged

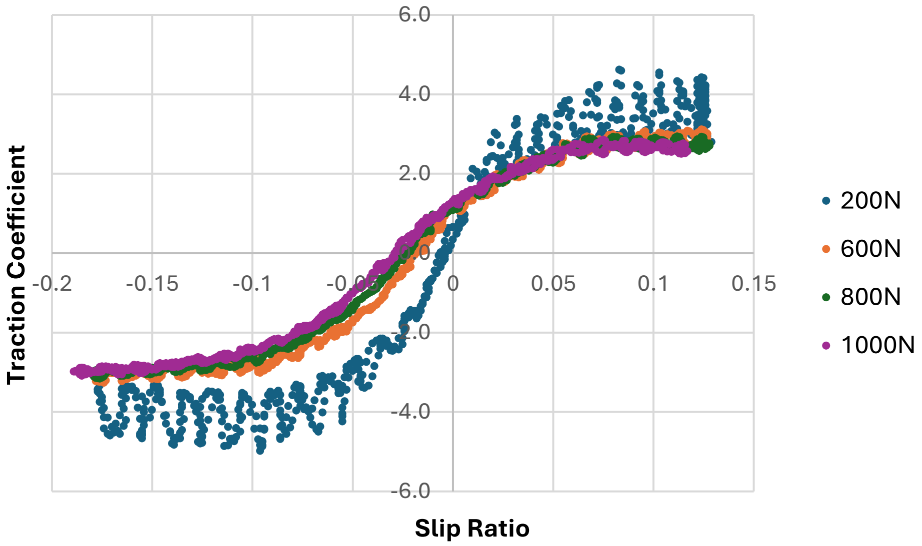


Figure A.2 18x7.5-10 R25B Slip Ratio Traction Coefficient, Raw

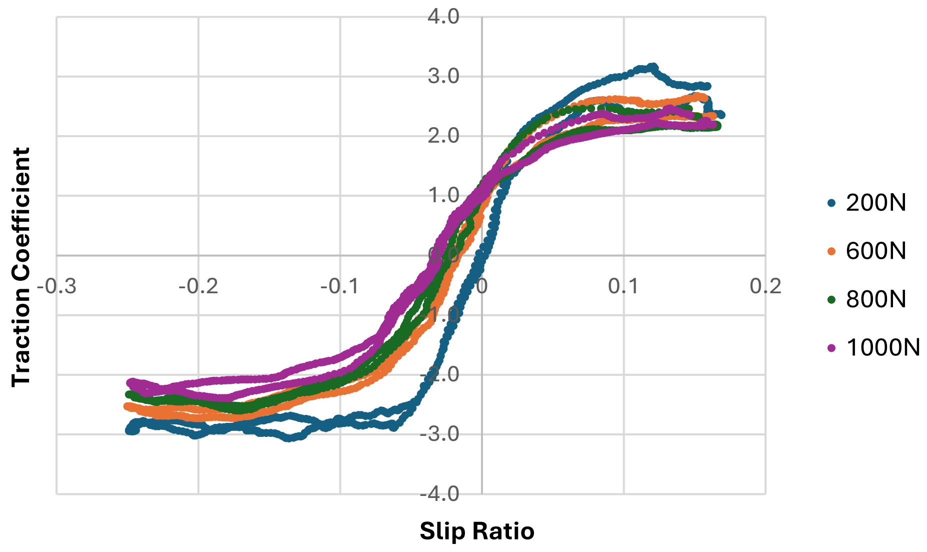


Figure A.3 18x6.0-10 LC0 Slip Ratio Traction Coefficient, Averaged

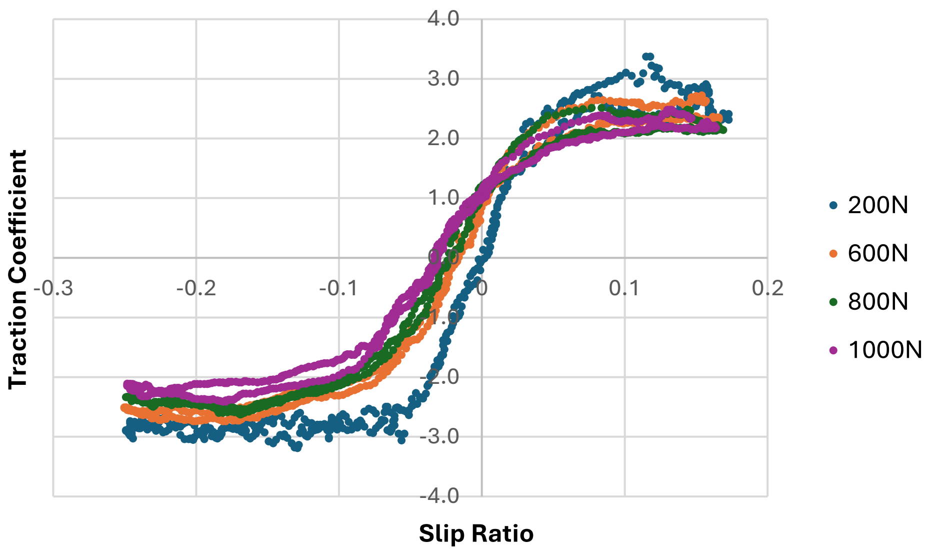


Figure A.4 18x6.0-10 LC0 Slip Ratio Traction Coefficient, Raw

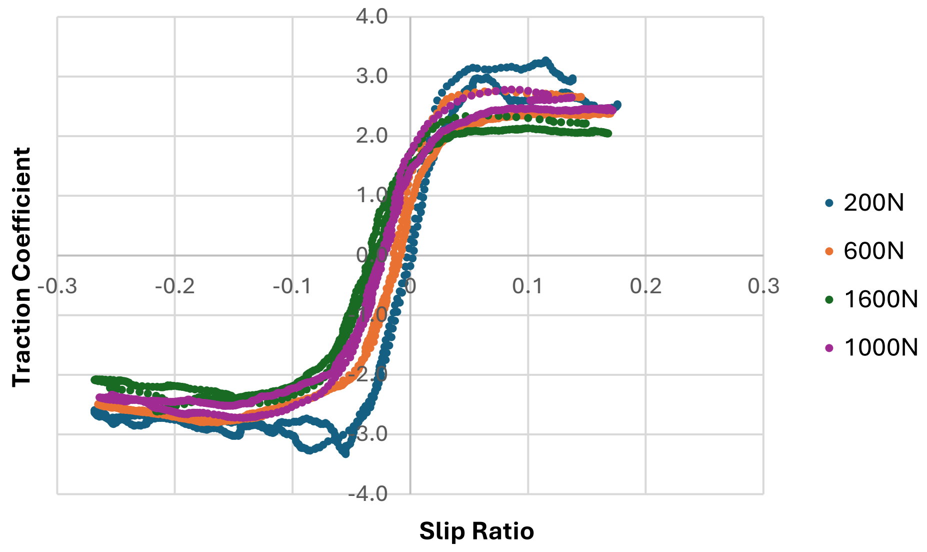


Figure A.5 20x7.5-13 R25B Slip Ratio Traction Coefficient, Averaged

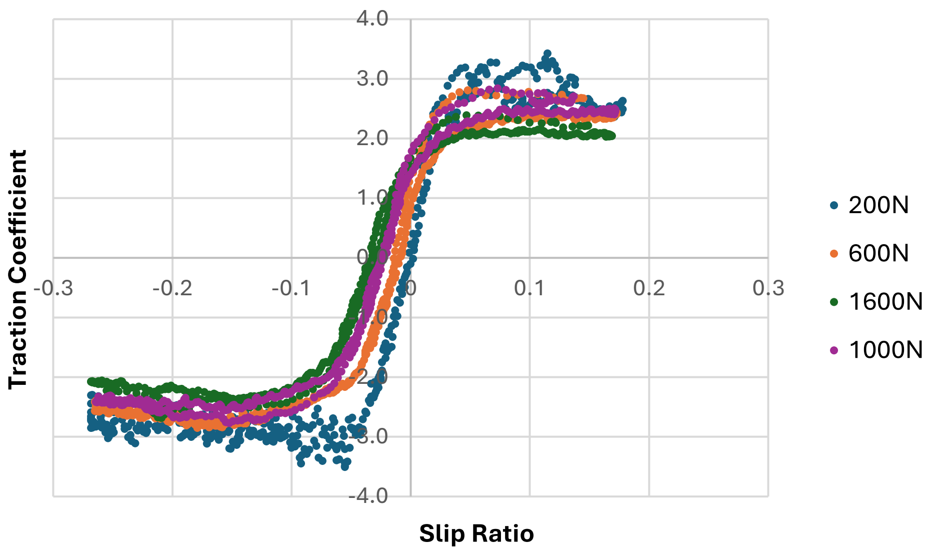


Figure A.6 20x7.5-13 R25B Slip Ratio Traction Coefficient, Raw

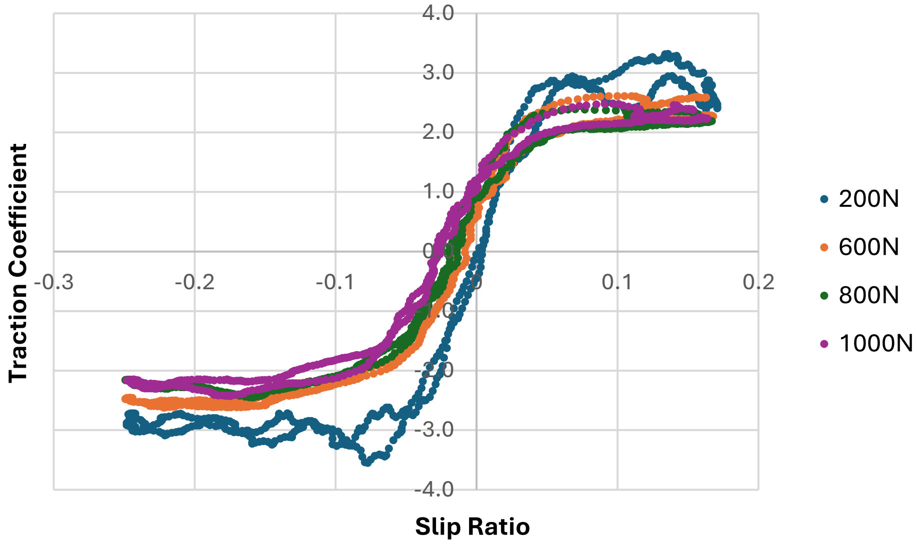


Figure A.7 18x6.0-10 R25B Slip Ratio Traction Coefficient, Averaged

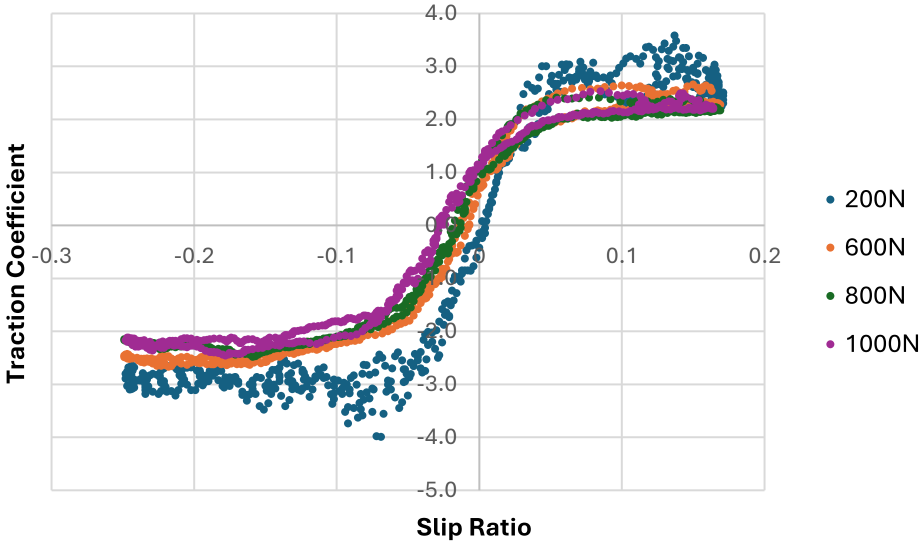


Figure A.8 18x6.0-10 R25B Slip Ratio Traction Coefficient, Raw

Appendix B

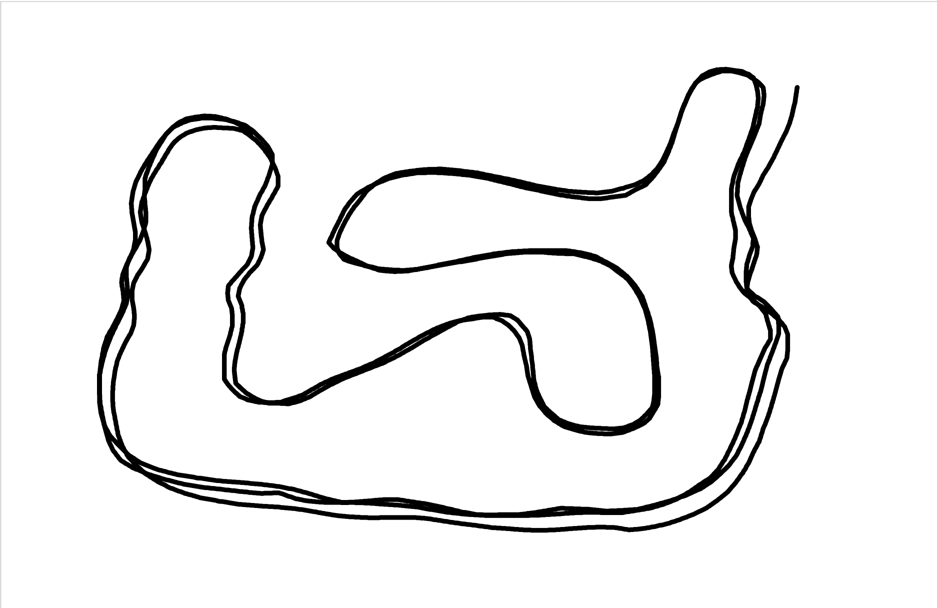

Figure B.1 Oakleigh GoKart Track Map

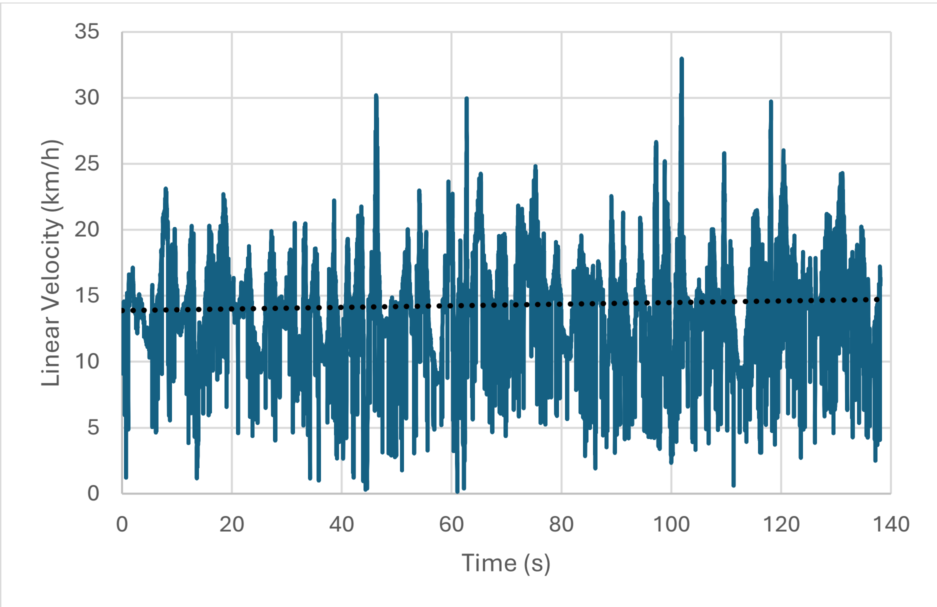


Figure B.2 Oakleigh GoKart Track Linear Velocity

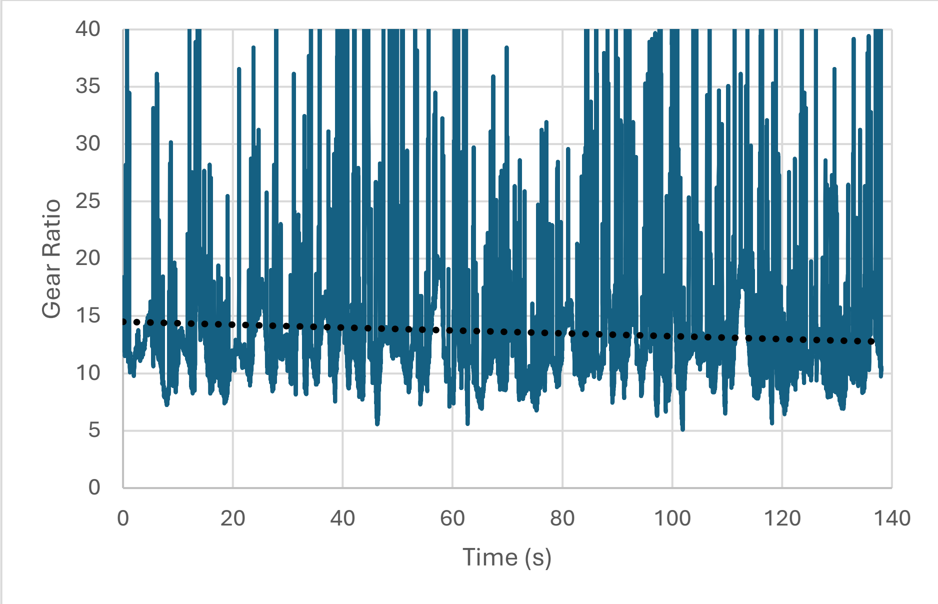


Figure B.3 Oakleigh GoKart Track Gear Ratio

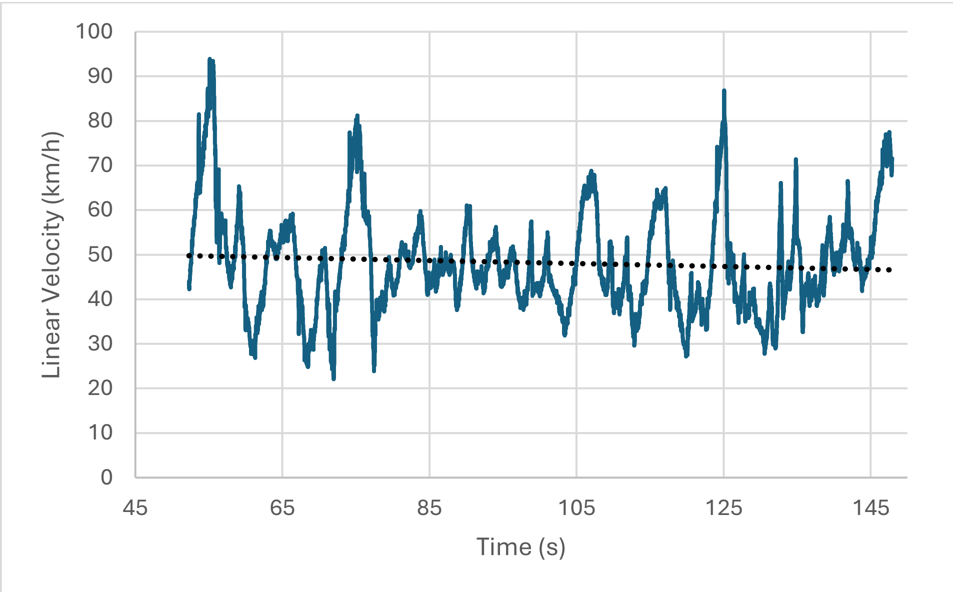


Figure B.4 Winton Autocross Lap 3 Linear Velocity

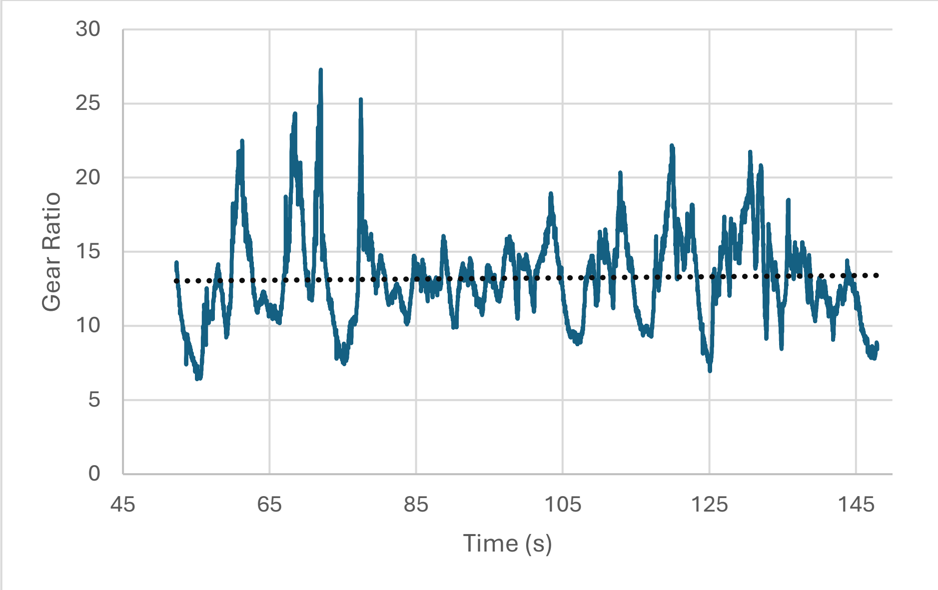


Figure B.5 Winton Autocross Lap 3 Gear Ratio

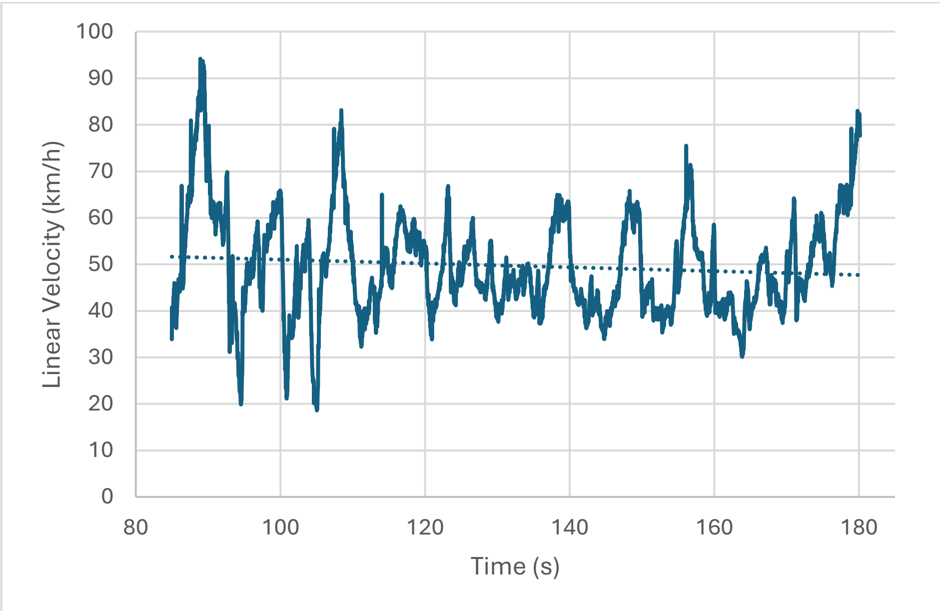


Figure B.6 Winton Autocross Lap 4 Linear Velocity

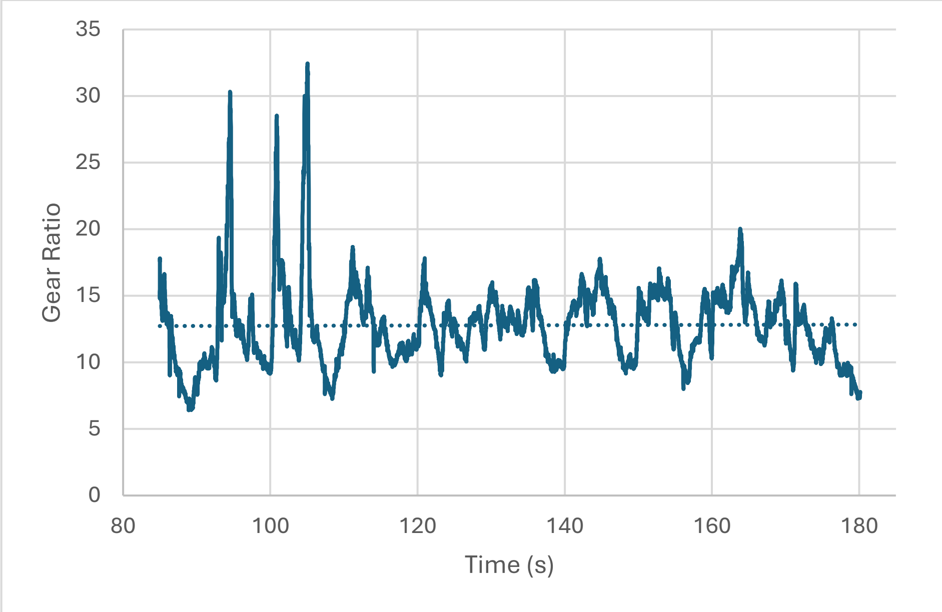


Figure B.7 Winton Autocross Lap 4 Gear Ratio

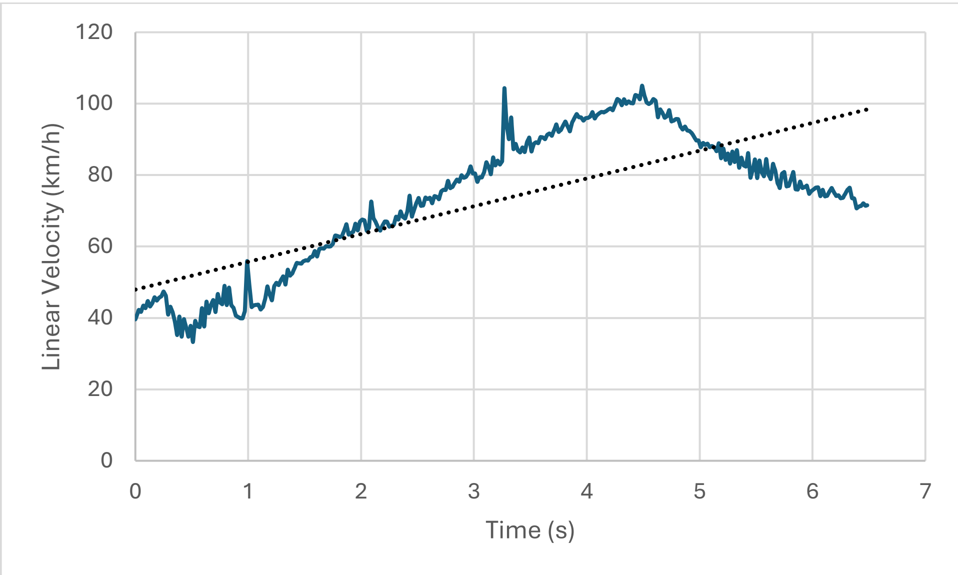


Figure B.8 Acceleration Linear Velocity

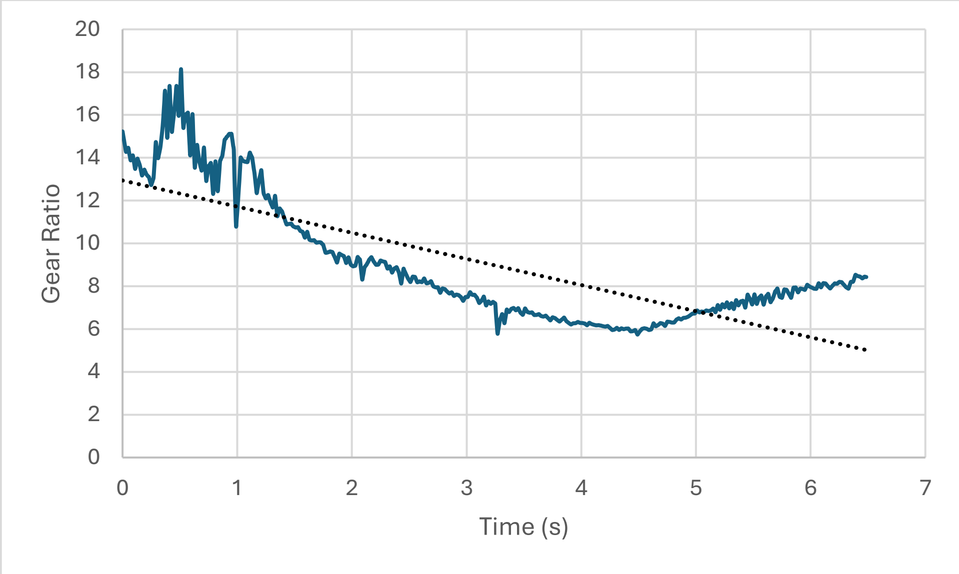


Figure B.9 Acceleration Gear Ratio

# Appendix C

## Shaft Calculations

Reaction Forces

$$\Sigma M_b = 0$$

$$\Sigma M_b = 916(8.6) + 2323(27.2) - R_b(40) = 0$$

$$R_b = \frac{916(8.6) + 2323(27.2)}{40} = 1777N$$

$$\Sigma Fy = 0$$

$$916 + 2323 - 1777 = R_a = 1462N$$

Shear Force and Bending Moment

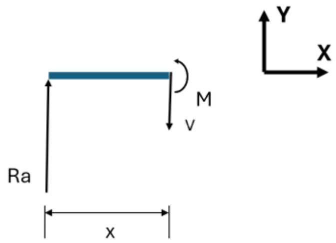


Figure C.1 Shear Force FBD 1

When $0 < x \leq 8.6$

Shear Force

$$\Sigma Fy = 0$$

$$R_a - V = 0$$

$$R_a = V = 1462N$$

Bending Moment

$$\Sigma M_{cut} = 0$$

$$M - R_a(x) = 0$$

$$M = R_a(x)$$

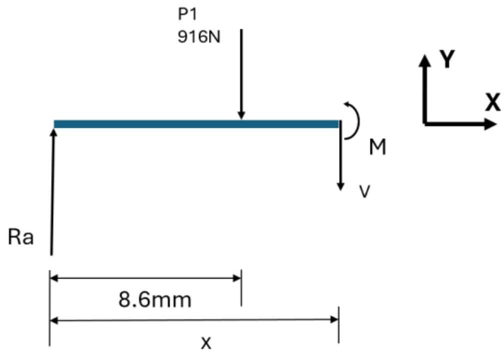


Figure C.2 Shear Force FBD 2

When $8.6 < x \leq 27.2$

Shear Force

$$\Sigma Fy = 0$$

$$R_a - 916 - V = 0$$

$$R_a - 916 = V = 546N$$

Bending Moment

$$\Sigma M_{cut} = 0$$

$$M - R_a(x) + 916(x - 8.6) = 0$$

$$M = R_a(x) - 916(x - 8.6)$$

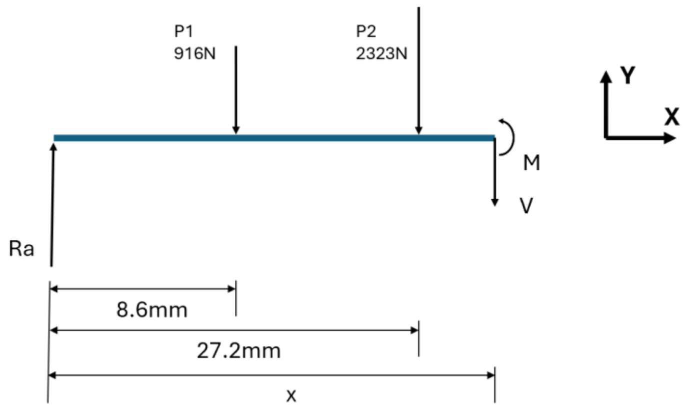


Figure C.3 Shear Force FBD 3

When $27.2 < x \leq 40$

Shear Force

$$\Sigma Fy = 0$$

$$R_a - 916 - 2323 - V = 0$$

$$R_a - 916 - 2323 = V = -1777N$$

Bending Moment

$$\Sigma M_{cut} = 0$$

$$M - R_a(x) + 916(x - 8.6) + 2323(x - 27.2) = 0$$

$$M = R_a(x) - 916(x - 8.6) - 2323(x - 27.2)$$

# Appendix D

## Engineering Drawings

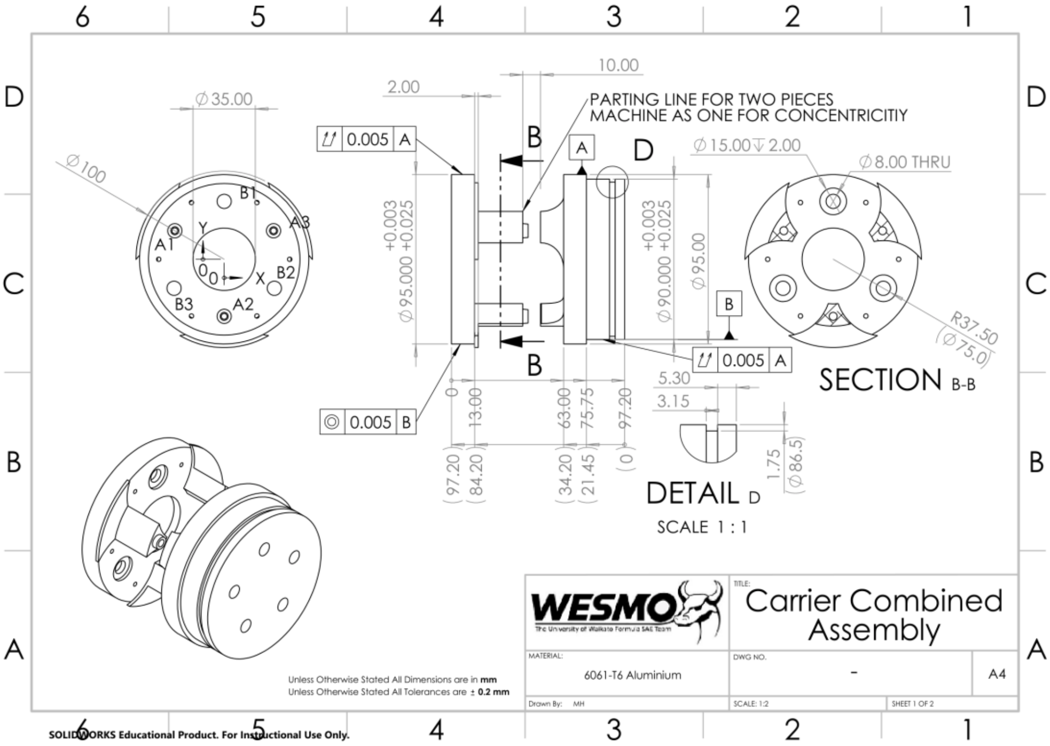


Figure D.1 Carrier Combined Assembly Drawing 1

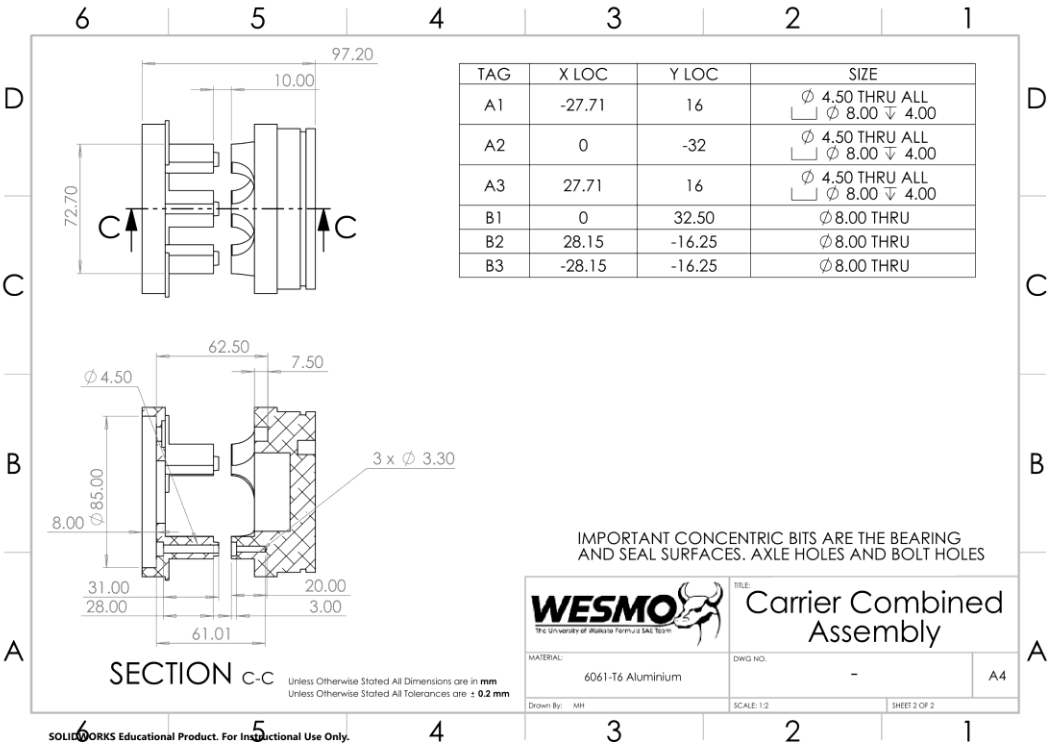


Figure D.2 Combined Carrier Assembly Drawing 2

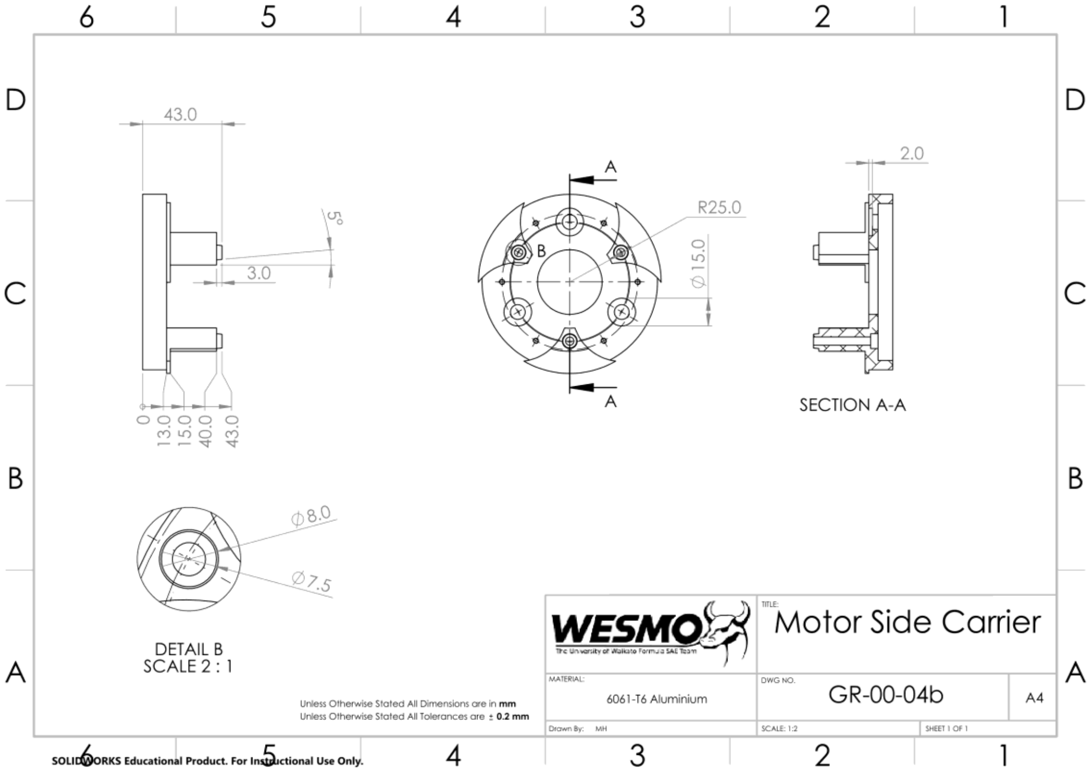


Figure D.3 Motor Side Carrier Drawing

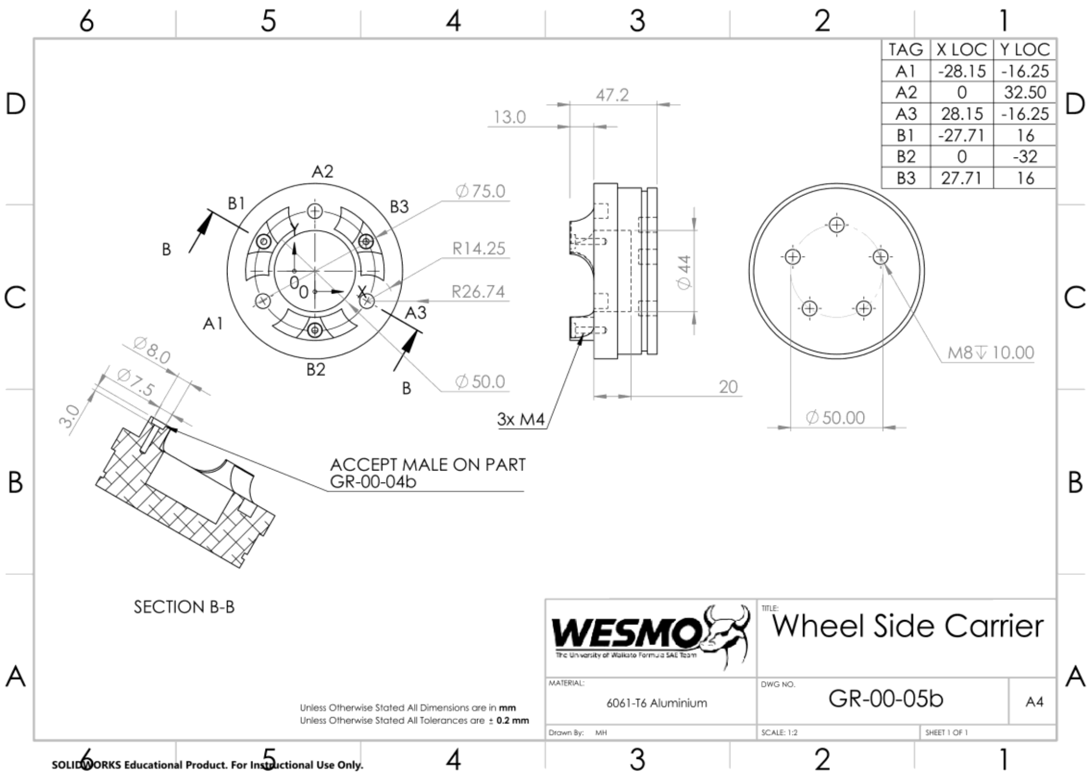


Figure D.4 Wheel Side Carrier Drawing

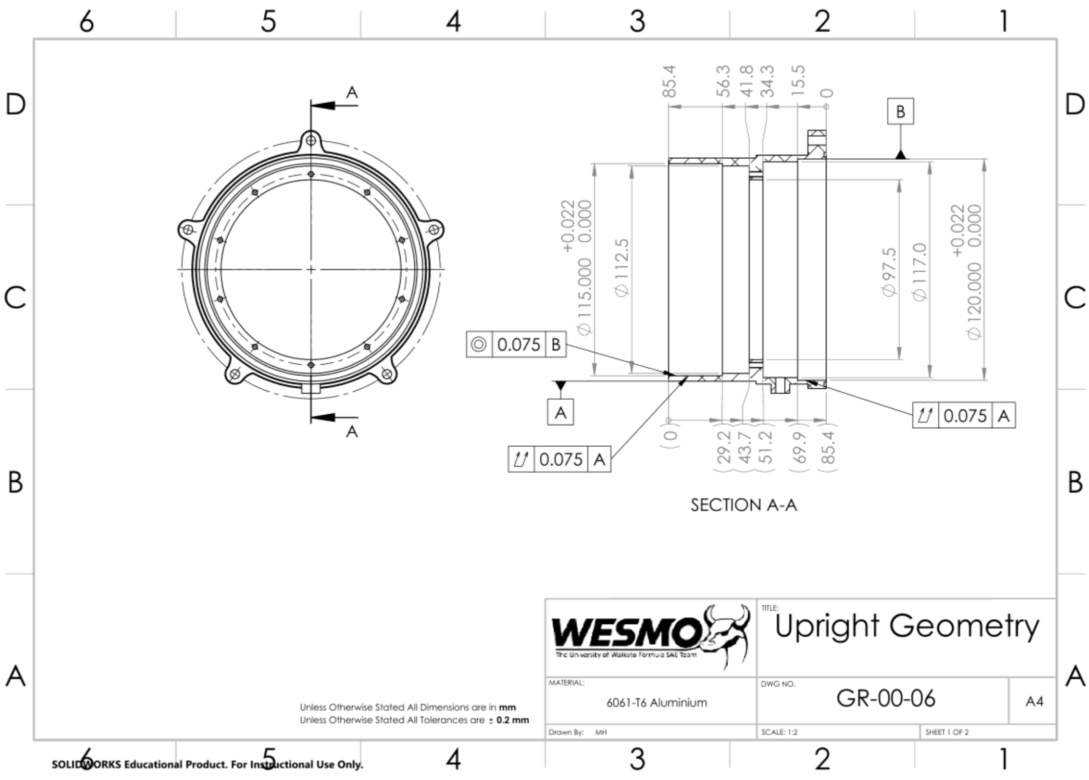


Figure D.5 Upright Geometry Drawing 1

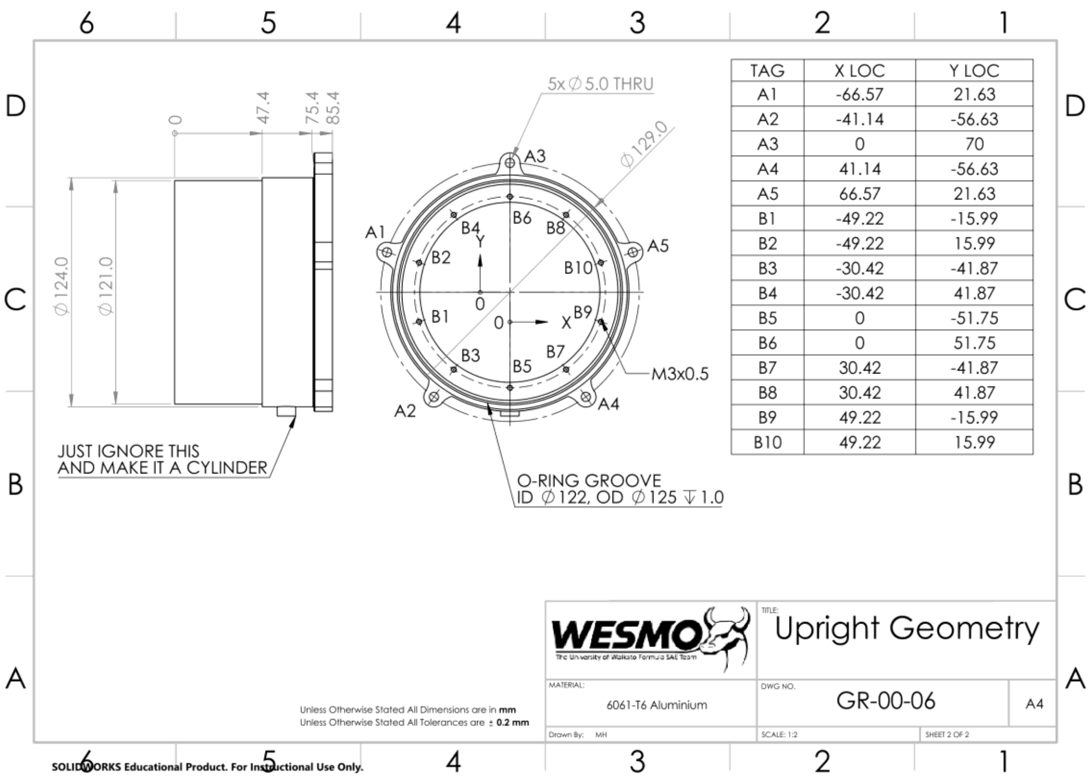


| TAG | X LOC | Y LOC |
|---|---|---|
| A1 | -66.57 | 21.63 |
| A2 | -41.14 | -56.63 |
| A3 | 0 | 70 |
| A4 | 41.14 | -56.63 |
| A5 | 66.57 | 21.63 |
| B1 | -49.22 | -15.99 |
| B2 | -49.22 | 15.99 |
| B3 | -30.42 | -41.87 |
| B4 | -30.42 | 41.87 |
| B5 | 0 | -51.75 |
| B6 | 0 | 51.75 |
| B7 | 30.42 | -41.87 |
| B8 | 30.42 | 41.87 |
| B9 | 49.22 | -15.99 |
| B10 | 49.22 | 15.99 |

Figure D.6 Upright Geometry Drawing 2

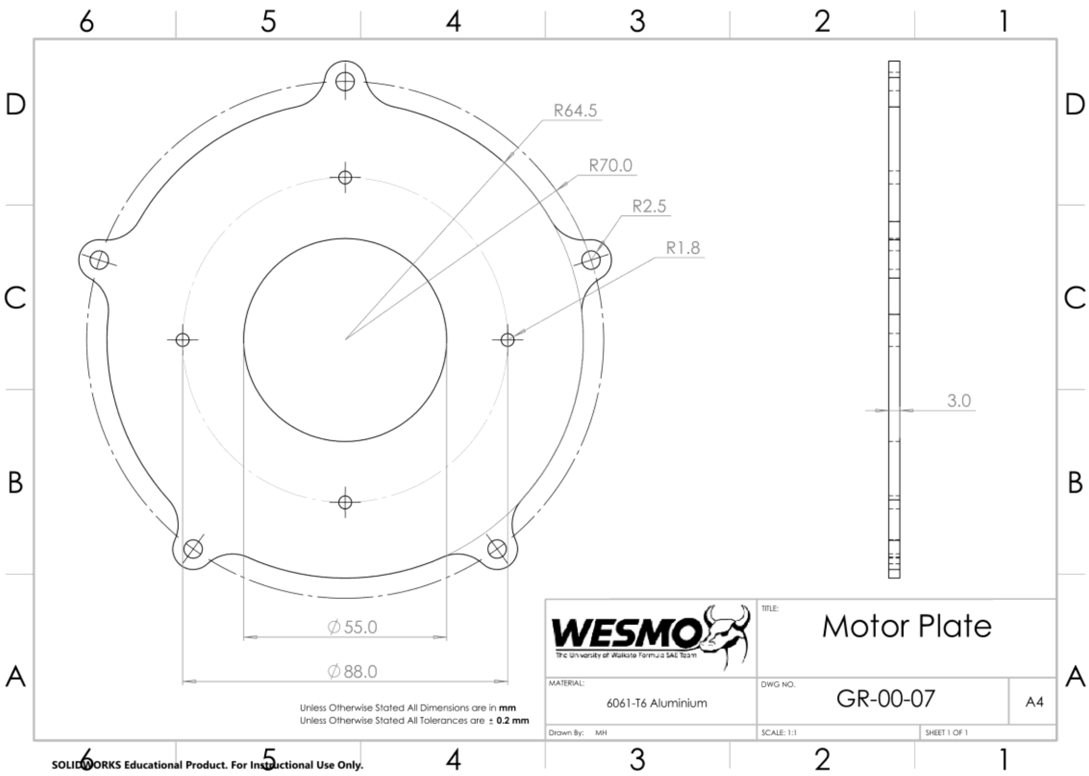


Figure D.7 Motor Plate Drawing

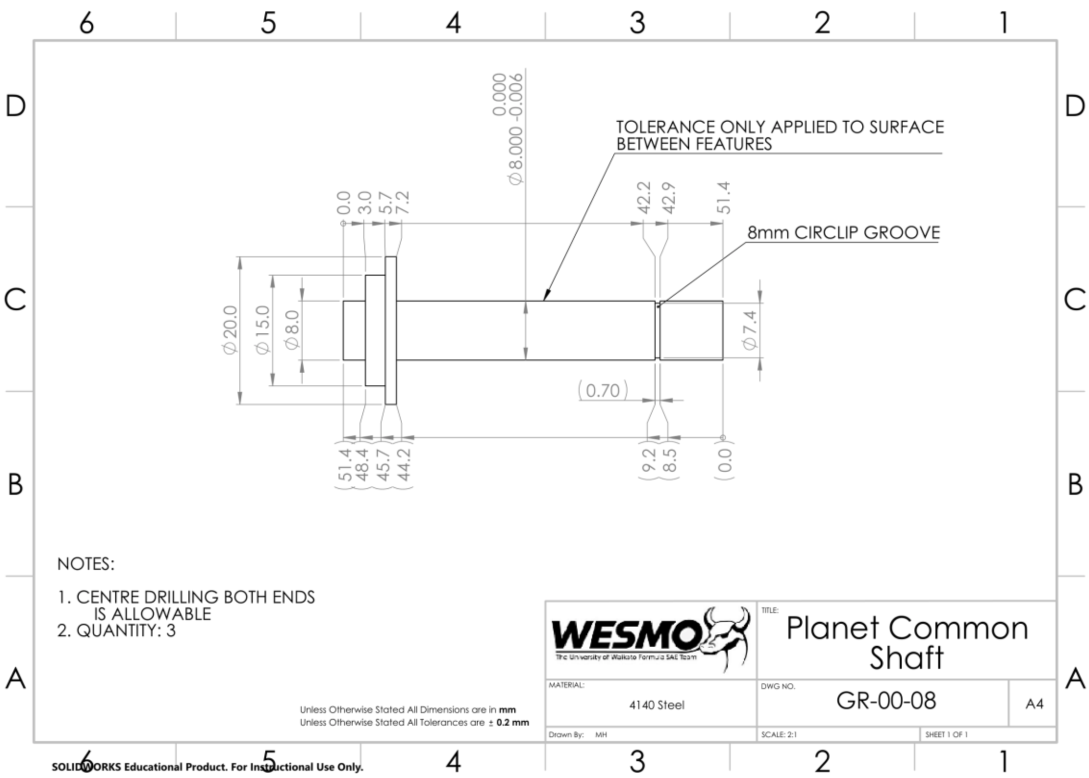


Figure D.8 Planet Common Shaft Drawing

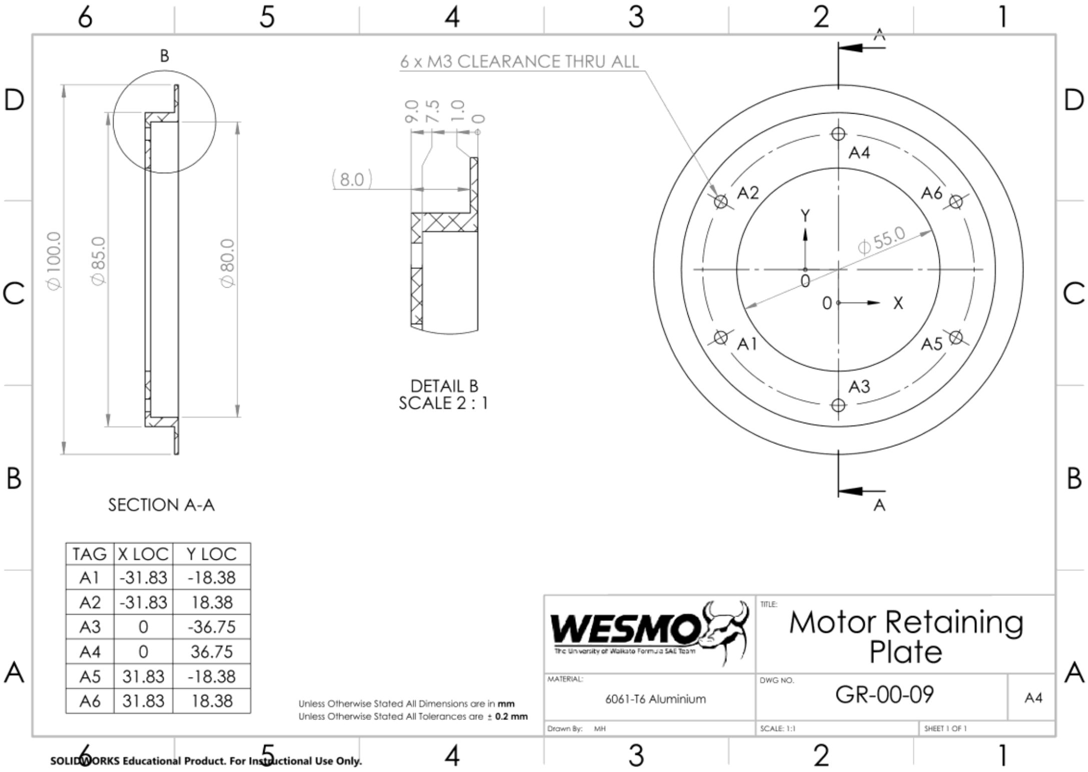


| TAG | X LOC | Y LOC |
|---|---|---|
| A1 | -31.83 | -18.38 |
| A2 | -31.83 | 18.38 |
| A3 | 0 | -36.75 |
| A4 | 0 | 36.75 |
| A5 | 31.83 | -18.38 |
| A6 | 31.83 | 18.38 |

Figure D.9 Motor Bearing Retaining Plate Drawing

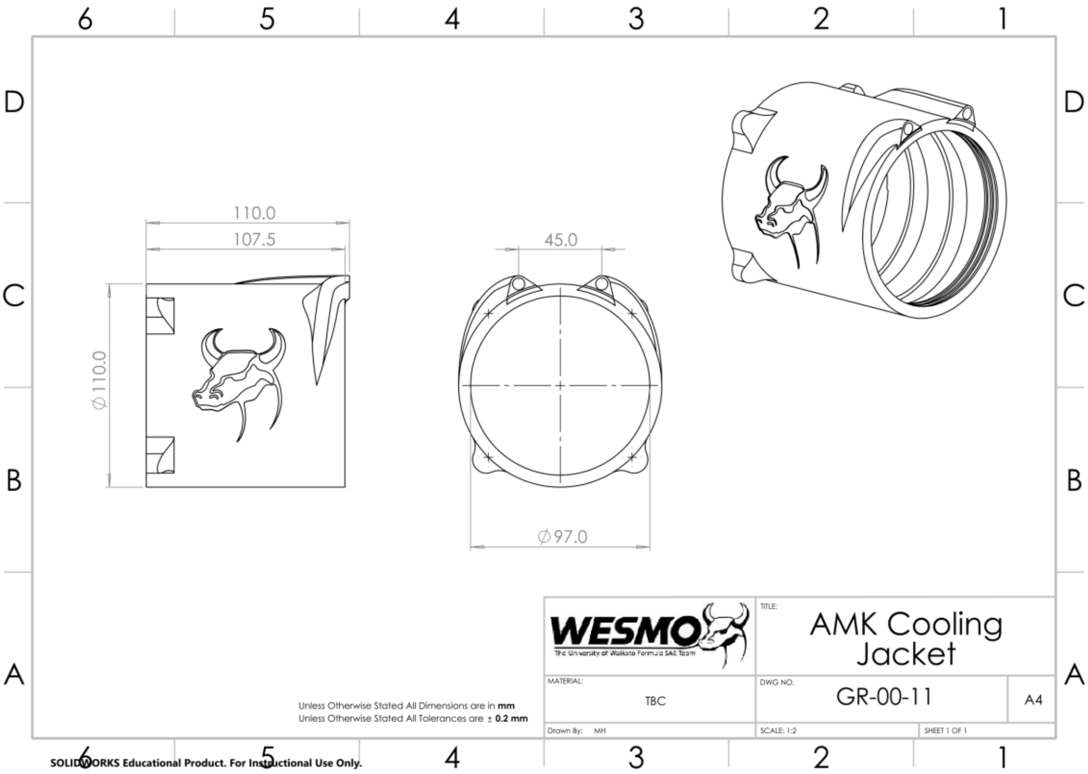


Figure D.10 AMK Cooling Jacket Drawing

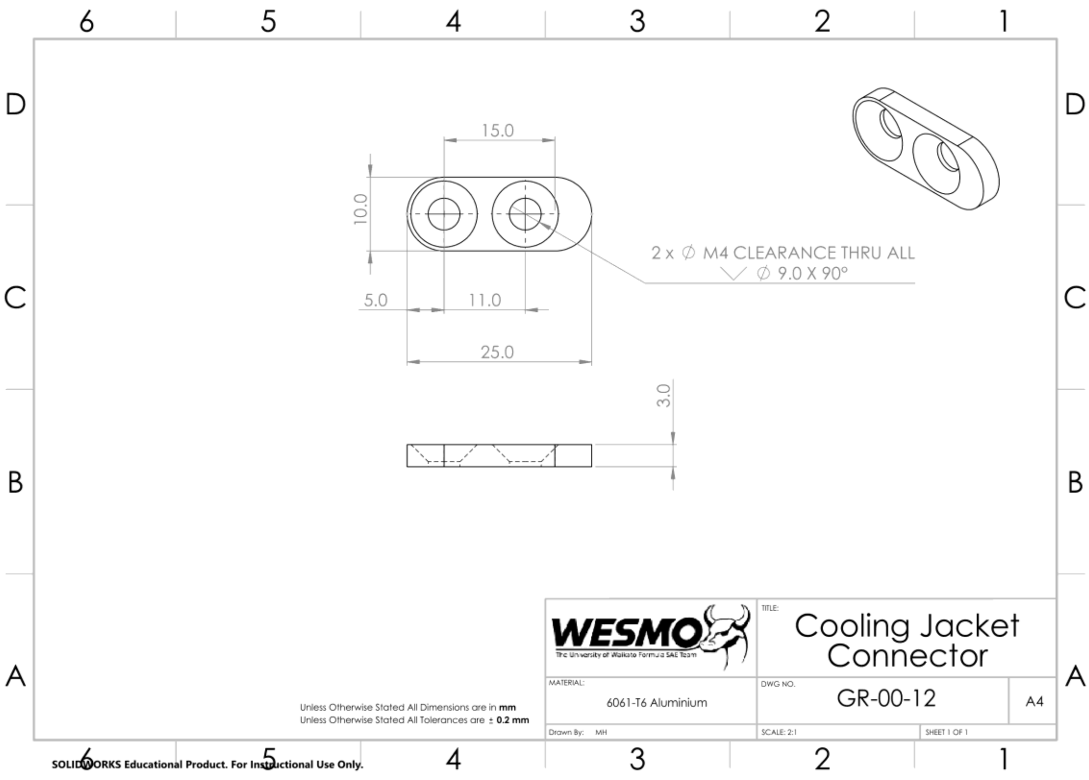


Figure D.11 Cooling Jacket Connector Drawing

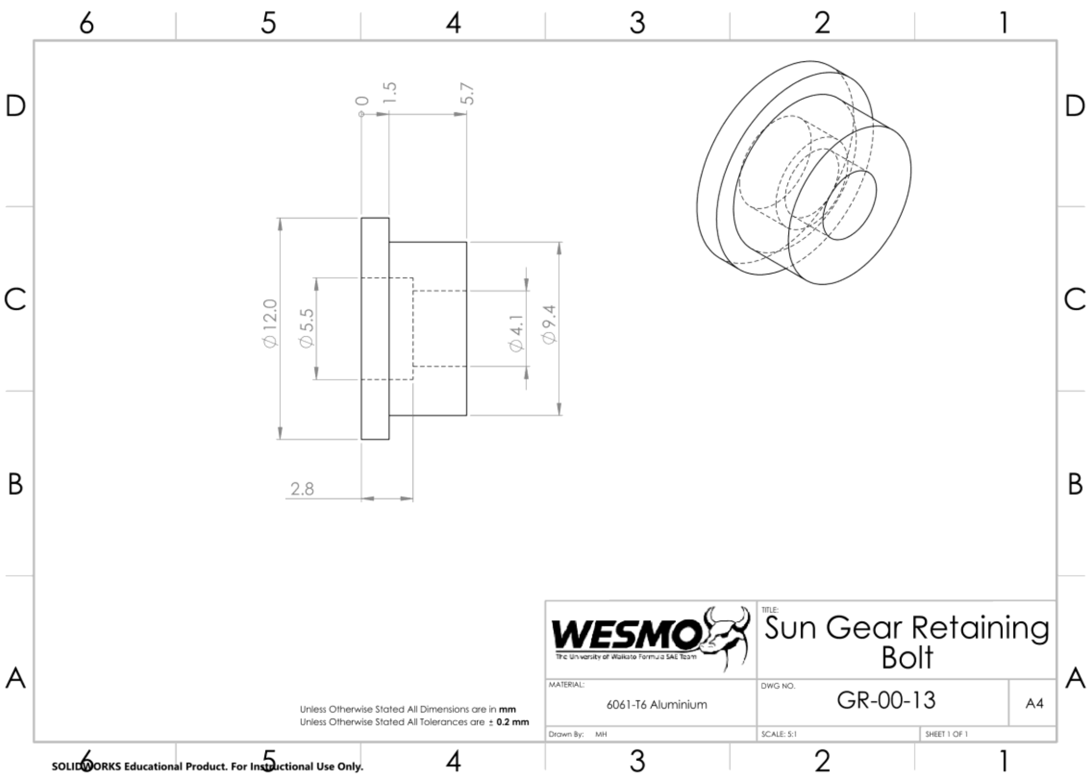


Figure D.12 Sun Gear Retaining Bolt

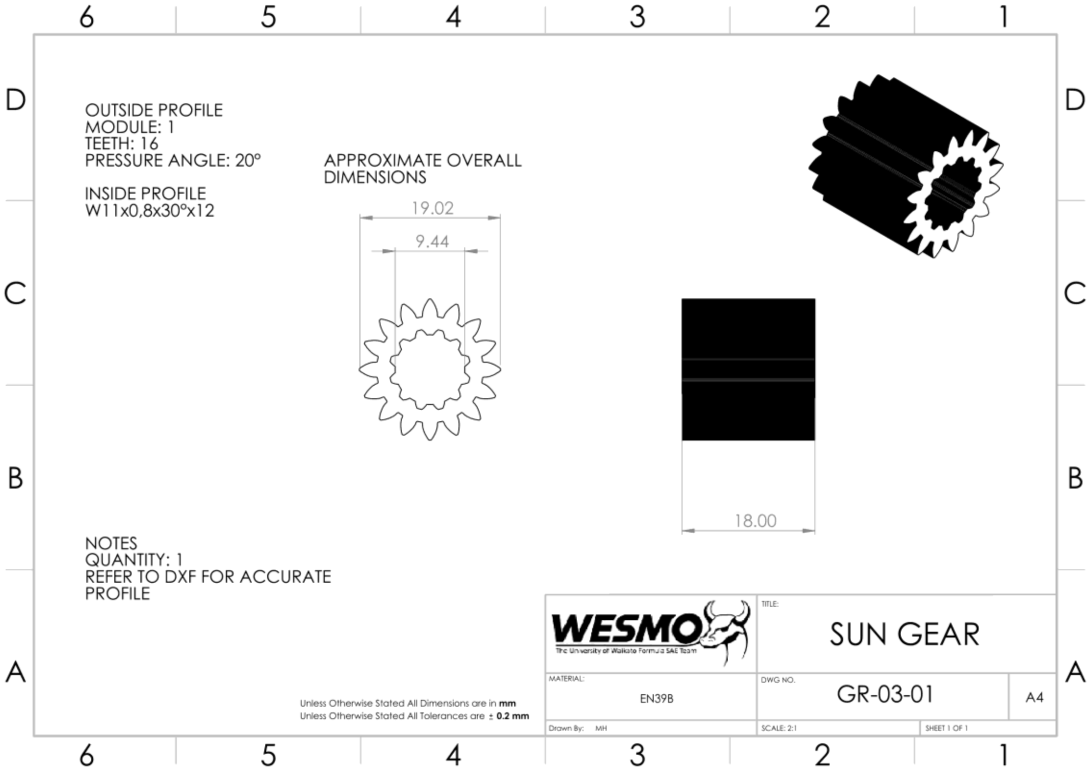


Figure D.13 Sun Gear Drawing

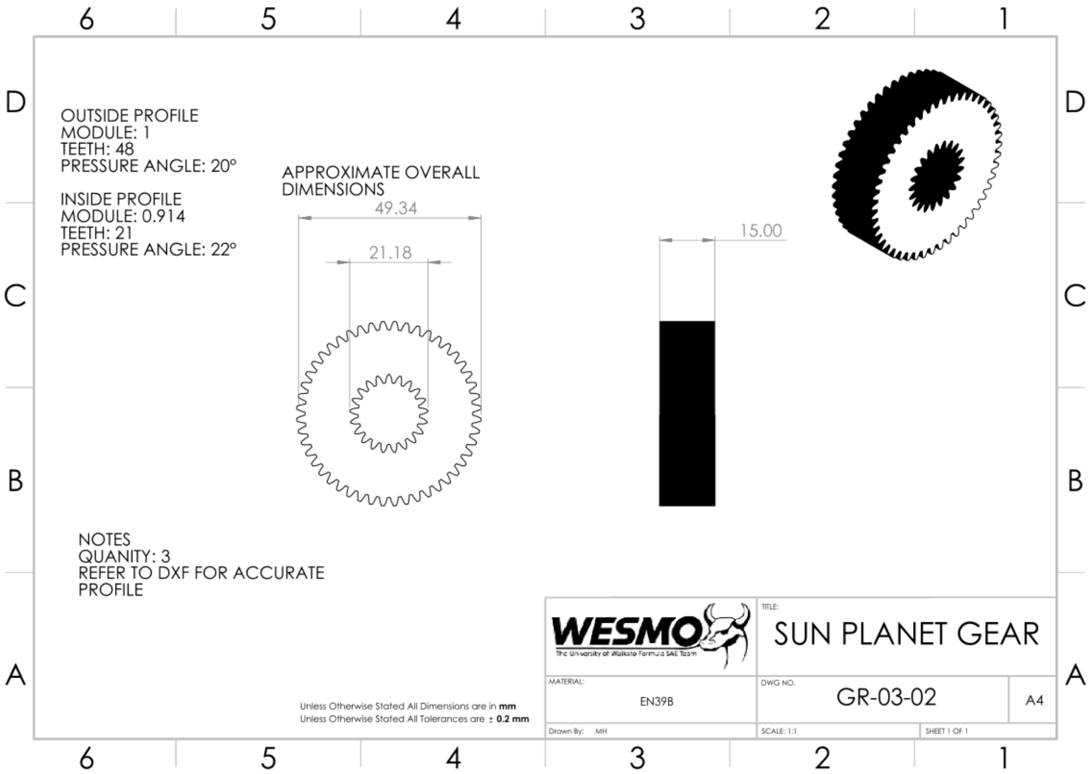


Figure D.14 Sun Planet Gear Drawing

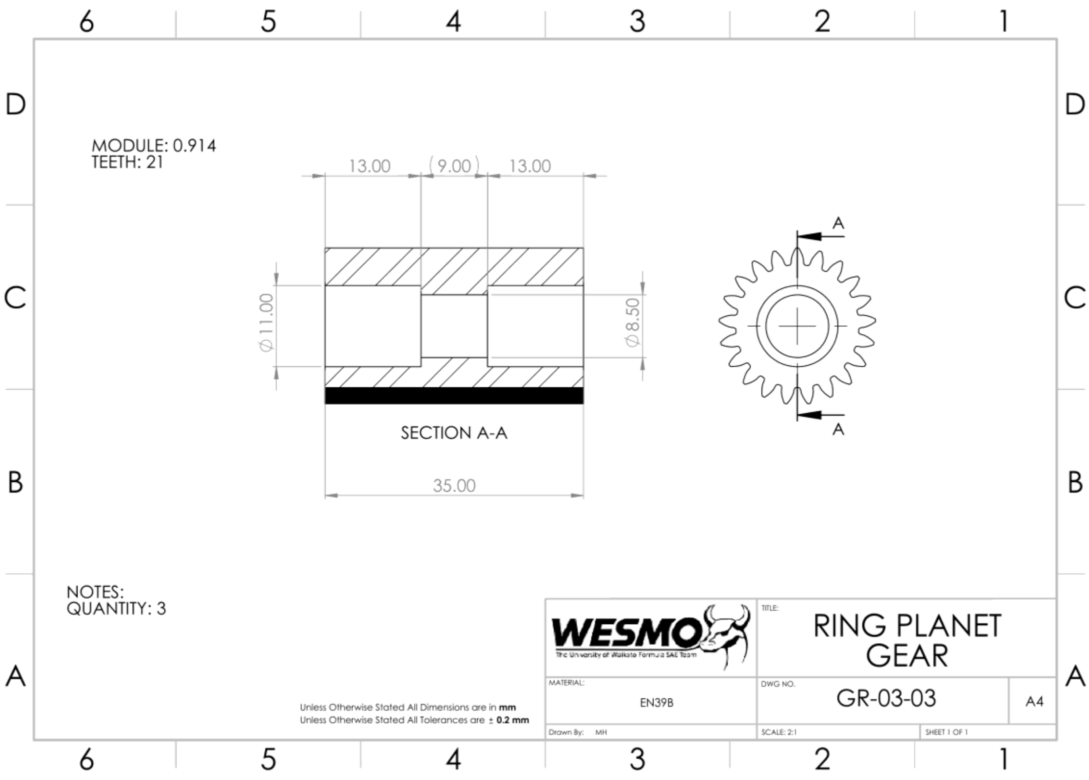


Figure D.15 Ring Gear Planet Drawing

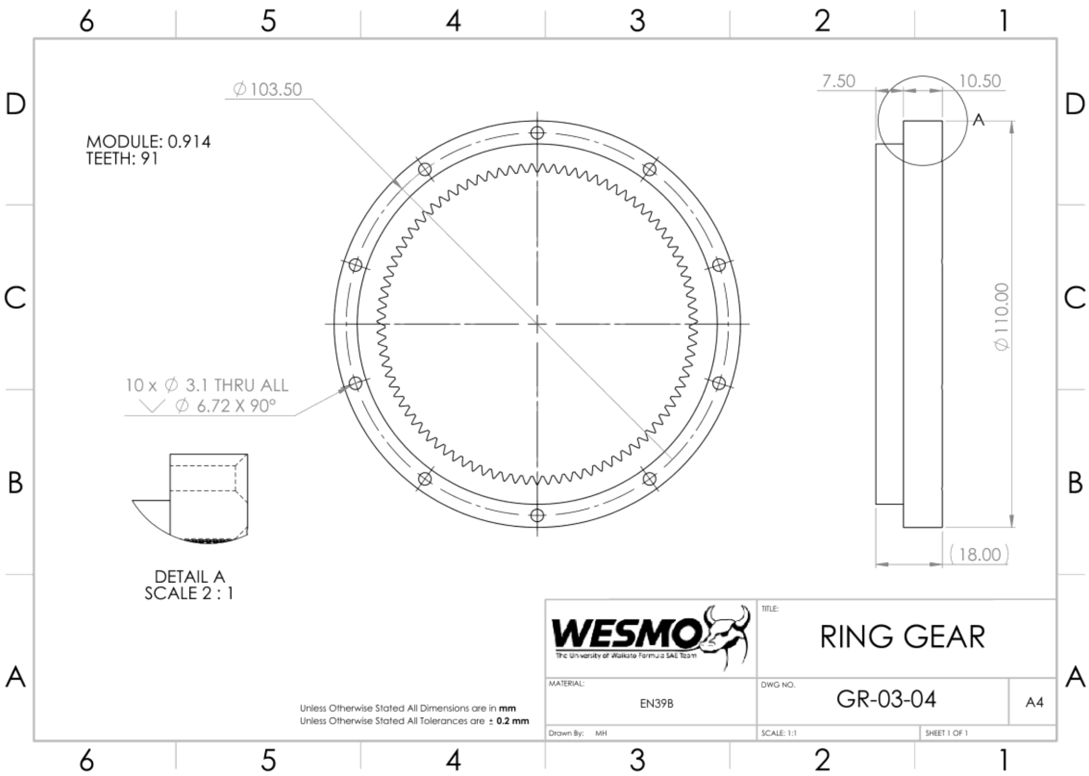


Figure D.16 Ring Gear Drawing

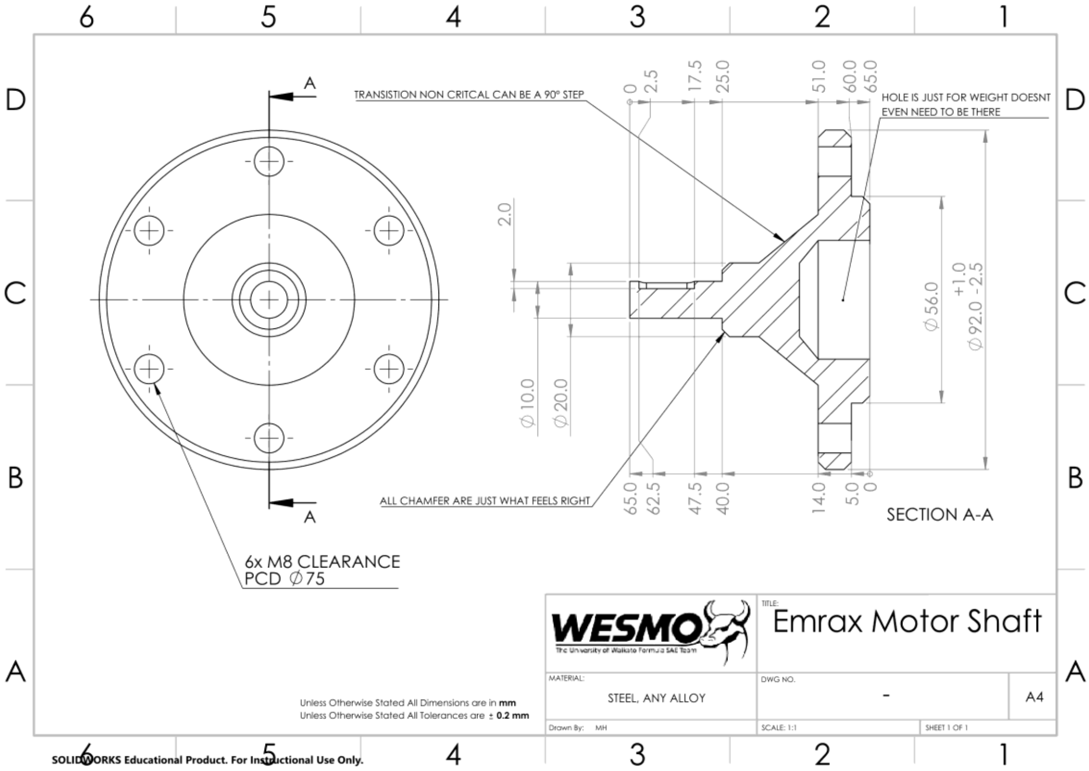


Figure D.17 Emrax Motor Shaft Adapter